FLOODPLAIN VEGETATION DYNAMICS OF SIPSEY RIVER, ALABAMA

by

DEEPA GURUNG

SARAH PRASKIEVICZ, COMMITTEE CHAIR
LUOHENG HAN
CARLA L. ATKINSON

A THESIS

Submitted in partial fulfillment of the requirements
for the degree of Master of Science
in the Department of Geography
in the Graduate School of
The University of Alabama

TUSCALOOSA, ALABAMA

2018

ABSTRACT

The Sipsey River creates Alabama's one of the free-flowing freshwater floodplain forest and supports a high diversity of flora and fauna. This study evaluated the effects of local climate and inundation frequency on the floodplain dynamics for the period between 1990 and 2013, using a combination of remote sensing and GIS approaches. Normalized Difference Vegetation Index was used as a proxy of vegetation productivity. Vegetation types were identified by two methods- unsupervised classification and Seasonality Index. Three dominant vegetation types identified were-hardwood swamp, bottomland hardwoods and pinelands. Elevation and seasonality were found to play an important role in maintaining the distribution of the vegetation types. Change detection from 1990 to 2008 by both the methods identified a decrease in hardwood swamps and increase in bottomland hardwoods and pineland trees.

Temporal variability in NDVI of two vegetation types, hardwood swamp and bottomland hardwoods, was explained by monthly average temperature as indicated by partial least square regression models. Spatial variability in the NDVI due to different flood magnitudes was assessed by using a 2D hydrodynamic model (Cellular Automaton Evolutionary Slope and River model). Results of linear regression showed no relationship between the flood inundation frequency and NDVI associated with the two vegetation types. The study presents baseline information about the overall floodplain vegetation dynamics of one of the few remaining unregulated rivers in Alabama. The need for higher spatial/ temporal resolution data and longer model simulation is recognized for more in-depth study.

DEDICATION

I dedicate this thesis to Bachchu Gurung and Hari Singh Gurung, who have helped me along at every step in more ways than I can ever thank them for.

LIST OF ABBREVIATIONS

US	United States
AL	Alabama
USGS	United States Geological Survey
NDVI	Normalized Difference Vegetation Index
SI	Seasonality Index
ISODATA	Iterative Self-Organizing Data Analysis Technique
RTK	Real Time Kinematics
TM	Thematic Mapper
ETM	Enhanced Thematic Mapper
AOI	Area of Interest
ERDAS	Earth Resources Data Analysis System
GIS	Geographic Information System
SWIR	Shortwave Infrared
NIR	Near Infrared
R	Red
PLSR	Partial Least square regression
CAESAR	Cellular Automaton Evolutionary Slope and River model
NTY	NDVI for Typical Year
DOY	Day of Year
R^2	Coefficient of determination

ACKNOWLEDGEMENTS

I am honored to have this opportunity to thank my family, friends, and colleagues who have helped make this project possible. I express my most sincere gratitude to the chair of this thesis committee, Dr. Sarah Praskievicz for providing me this opportunity two years ago and for her continuous guidance and encouragement during this research. Thank you to my committee members Dr. Luoheng Han and Dr. Carla Atkinson for all their help and guidance throughout this process, and to all the friends and faculty in the University of Alabama, Department of Geography.

Thank you further most of all to Bachchu Gurung, Hari Singh Gurung, Jay Singh Gurung, Deepesh Gurung for many years of guidance and encouragement, without which none of this would have ever been possible.

CONTENTS

LIST OF TABLES

LIST OF FIGURES

1. INTRODUCTION

Hardwood swamps and bottomland hardwood forests are deciduous forested wetlands found in broad floodplain areas developed by river systems that occur throughout the Central and Southeastern US (Hodges 1997). These systems are predicted to have higher levels of primary productivity than upland terrestrial ecosystems due to high water availability and the effects of flooding (Hillard et al., 2017); however, productivity is temporally variable from the influence of flooding and drying. Floodplain wetlands differ significantly in the spatial context, disturbance regime, hydrology, and ecology (Calzada et al., 2017). Several studies in the past have noted the ecosystem services provided by riverine floodplains such as water quality improvement, flood control, waste filtration, carbon storage, wildlife habitat, and recreation (Brauman et al., 2007). Despite their immense ecological and economic values, floodplain wetlands are threatened by population growth and intensive development worldwide (MEA, 2005).

Riverine floodplain systems are relatively flat, but due to the nature of flooding and sedimentation patterns, small changes in elevation result in significant differences in soil drainage and vegetation distribution (Reid 2013). Floodplains in general store large quantities of organic matter that is slowly decomposed, causing a concentration of nutrients. Flood pulses create vital ecosystem connections and mobilize nutrients (Junk et al., 1989). Further, these nutrients are also washed downstream and support estuarine and marine ecosystems (Apalachicola National Estuarine Research Reserve, 2013). Despite the plethora of ecosystem services, they provide, around 1% of the identified forested wetlands have been lost in the later part of the 20th century and most were lost through direct human activities such as river

diversions (MEA, 2005) and agricultural conversion (Hillard et al., 2017). For example, in vast forested wetlands of the Mississippi River Deltaic Plain, vegetation is declining at roughly 62 $km^2\ yr^{-1}$ in the Mississippi River Delta Complex due to river diversions (Day et al., 2000). Among the rapidly disappearing floodplain wetland types are hardwood swamps, a highly productive, species-rich habitat (Hoeppner et al., 2008). The decline of these ecosystems has been attributed not only to human alteration but also to their high susceptibility to changes in timing and quantity of water that they receive as this affects both the structure and composition of plant communities in these environments (Ernst et al., 2001).

Hydrology is among the most important factors in determining the ecological processes in floodplains (Brinson et al., 1981). A key hydrological characteristic of floodplain wetlands is that they are subject to periodic annual flooding from adjacent rivers (Keddy, 2000). Along lowland rivers, the most common mechanism of floodplain inundation is frequently occurring discharge events that inundate the entire floodplain surface (Calzada et al., 2017). Additionally, the extent, frequency, and timing of overbank flows define hydrological connectivity of the river channel-floodplain system related to the exchange of energy, matter, and organisms (Poff et al., 1997).

Climate variability has large impacts on all ecosystems, and both growing season and total amount of vegetation, are strongly affected by alterations in climatological parameters (Piao et al., 2006; Shen et al., 2015; Thomey et al., 2011; Qi et al., 1999, Wang et al., 2003). Hydrological variability is driven by climate variability and moderated by properties of the catchment (Nemec and Schaake, 1982), including anthropogenic land use and land-atmosphere responses (Calzada et al., 2017). Studies have also found that the annual discharge that spreads through floodplains is greatly influenced by antecedent meteorological conditions (Milzow et al.,

2010). Infiltrated water is lost by transpiration through the vegetation of the assembly of islands that characterize the wetlands/floodplains (Wolski and Savenije, 2006). The hydrology of wetlands is subject to major natural fluctuations at various timescales, induced by the interplay between local and upstream meteorology (Milzow et al., 2010). Studies have found positive feedback mechanisms between a decrease in vegetation cover and a corresponding decrease in precipitation (Barbosa et al., 2006). The possible reasons behind this could be because of increasing albedo, radiative cooling of the air column, and an enhancement of large-scale atmospheric subsidence and desiccation (Barbosa et al., 2006).

Remote sensing techniques offer practical and economic means to study vegetation phenology, monitor long-term vegetation cover and analyze spatiotemporal vegetation changes. Landsat images, covering a long period of time since 1986, have been used to conduct quantitative analyses of vegetation patterns and change all across the world (Xie et al., 2008). The Landsat sensors' temporal coverage, spatial resolution, and data accessibility make them especially useful for monitoring vegetation all across the globe (Shen et al., 2015). The sensors record electromagnetic radiation in different sets of individual bands and are able to produce digital images of Earth's surface. The Landsat TM sensor has seven sets of bands. Each Landsat scene has 30-meter resolution for bands 1, 2, 3, 4, 5, and 7 and 120-meter resolution for band 6. The Landsat ETM+ sensor has eight sets of bands, with 30-meter spatial resolution for bands 1, 2, 3, 4, 5, and 7; 60-meter resolution for band 6; and 15-meter resolution for band 8 (Xie et al., 2008). Each Landsat image covers approximately 185 by 170 kilometers of Earth's surface. The revisit cycle of sensors is sixteen days for a particular area. The USGS Earth explorer is an online search and order tool for satellite data that enables users to easily access and download currently available Landsat 1-5 MSS, Landsat 5 TM, Landsat 7 ETM+ data for free.

Over the last two decades, numerous studies have highlighted the potential key role of Landsat data in analyzing vegetation dynamics based on Normalized Difference Vegetation Index (NDVI) (Lillesand et al., 2000). NDVI is based on the differential reflectance that plants exhibit for different parts of the solar radiation spectrum. NDVI captures the contrast between red and near-infrared reflectance of vegetation and reflects the energy absorption by leaf pigments such as chlorophyll (Linderholm, 2006). While healthy vegetation strongly absorbs photosynthetically active radiation for energy required for photosynthesis, internal mesophyll structures in the leaf scatter radiation in the near–infrared region to prevent overheating of the plant (Bulcock and Jewitt, 2010). NDVI is calculated as the ratio of the difference between visible red and near-infrared bands to the sum of the two and is considered a good indicator of the ability of vegetation to carry out the process of photosynthesis (Otto et al., 2011). It has been widely used to understand the phenology and vegetation growing season from regional to global scales (Piao et al., 2006; Melaas et al., 2013). Growing season refers to the period in a given year that is available for plant growth and biomass accumulation. Changes in phenology that occur during growing and non-growing seasons are explored by using phenology, satellite data, and surface air temperature (Linderholm, 2006). NDVI-based productivity shows clear changes in spring and fall phenology related to temperature and precipitation changes (Shen et al., 2015). For example, an increase in winter and spring temperature leads to earlier green–onset. Similarly, increase in summer and fall temperature delays the timing of leaf drop and reduction in greenness over the Northern Hemisphere (Jeong et al., 2017). Several studies in the past have used NDVI to correlate floodplain vegetation productivity to hydrological and climatological factors (Zhou et al., 2001). NDVI has been utilized as a common metric to monitor changes in

vegetation and land cover, and to investigate the response of vegetation to global and local climate (e.g., Piao et al., 2006, Shen et al., 2015).

Historically, the use of satellite images for long-term observation and monitoring of land-surface vegetation has been well established with NDVI time series (Los et al., 1994). Despite the large body of work using NDVI time series to study vegetation in subtropical climates (Nicholsan et al., 1990), few researchers have assessed the temporal and spatial patterns in detail (Barbosa et al., 2006). Further, documentation of bottomland hardwood forest productivity in relation to local climate is rare. Among very few existing studies, one study has found an increase in growth of black walnut (*Juglans nigra*, a bottomland hardwood species) in Central Ohio with summer temperatures (Dudek et al., 1998). Hence, analyzing the impacts of climate on deciduous vegetation becomes crucial in understanding the dynamics of vegetation driven by environmental conditions.

Studies conducted in northern mid- and high-latitudinal zones have found that NDVI increases with increased temperatures (Ichii et al., 2002; Piao et al., 2003; Piao et al., 2006; Udelhoven et al., 2009). Qi (1999) found that the yearly maximum NDVI was highly correlated with temperature at high latitudes of the northern hemisphere. Accordingly, the southeast US, located in mid-latitude zones, is a region sensitive to temperature rises. Other studies have used NDVI to link the response of vegetation growth to variations in rainfall and air temperature (Frensholt & Rasmussen, 2011). Vegetation response to environmental change is likely lagged (Nicholsan et al., 1990). Tewari et al. (2003) found that temporal variability of NDVI was concurrently linked to the temperature regime, but the relationship with precipitation exhibits a time lag. A study by Wen et al. (2012) in a floodplain ecosystem found that NDVI was most sensitive to the anomalies of rainfall at a 6-month timescale. The effects of warming vary

throughout the spring green-up, due to changing physiological sensitivity during plant development. Warmer air temperatures lead to a lack of moisture and eventually hydrological stress, which could delay leaf development (Wang et al., 2016). During hot days, stomata closure reduces photosynthesis and delays leaf-out (Yousfi et al., 2015). The Southeastern US has ecoregions ranging from coastal zones to mountainous forest and rolling Piedmont. This provides a reason to examine the interactions between seasonal climate variations across ecosystems with full a range of leaf habit from deciduous to evergreen.

In addition, forested wetland systems are susceptible to changes in the timing of flood and quantity of water that they receive. The implications of the timing and frequency of flooding cannot be fully understood without quantification of its most essential component: inundation. Inundation dynamics is defined as a temporal and spatial pattern of floodplain inundation, such as occurs continuously within a year and over many years (Benke et al., 2000). For example, tree genera such as *Taxodium* and *Nyssa* require late fall to winter floods for dispersing their buoyant seeds to potential sites (Schneider and Shritz, 1988). Inundation depends on discharge and delineation of floodplain areas and cannot be explained in absence of any of these (Tronstad, et al., 2005). At lower discharge rates, rivers flow in well-defined channels but, at higher water discharges in natural systems, wide floodplains are recurrently inundated (Junk, et al., 1989). Naturally, flooded area is typical of the bald cypress and water tupelo swamps in the floodplain forests, where poor drainage and frequent long inundation are common (Kroschel et al., 2016). Flooding affects the growth of adult trees and seedling mortality; it also affects the time of seed germination and survival (Hoeppner et al., 2011).

Community changes occur because of variance in the flood tolerance capability and the effects of flooding on growth rates (Megonigal et al., 1992). Variation among species arises from

the difference in the number of adaptations used to counteract flood stress; for example, increased soil moisture can cause an increase in plant growth over large areas, but reduced growth vigor and plant mortality could take place in areas with high flood frequency or with prolonged inundation (Tronstad et al., 2015).

Previous research has found that natural regeneration of bald cypress is affected by flooded conditions; seedlings may be adversely affected by prolonged flooding (Pezeshki, 1994). De Steven and Sharitz (1997) found that under slow-moving water, seeds are carried away from parent trees to germinate and establish in open area once water recedes. At the other extreme, excessive flooding reduces the trapping of buoyant seeds and results in net transport of seeds and eventually affects associated productivity (Schneider and Sharitz 1988). My study identified different types of vegetation in the Sipsey River floodplain in Alabama and explored how local climatic parameters have been affecting their productivity over thirty years from 1986 to 2016. I used two-dimensional flood modeling to explore how the frequency of inundation of big and small floods affects the vegetation productivity.

Analyzing the spatial and temporal dynamics of these ecosystems is important for proper resource management and for ensuring the viability of these habitats. My research utilized satellite images to analyze the spatial and temporal dynamics of vegetation along the forested wetlands created by the Sipsey River. The overall objectives of this study are:

1. Identify vegetation class by using an unsupervised classification method and Seasonality Index and assess the difference between two methods and study floodplain dynamics for the study period.

2. Assess temporal variability in NDVI by analyzing climatological and hydrological controls on NDVI for identified vegetation classes using statistics such as Spearman's rho correlation and partial least square regression.
3. Assess the spatial variability in NDVI by analyzing impacts of inundation frequency via use of 2D hydrodynamic flood modelling (CAESAR) for floods of different magnitudes.

2. MATERIALS AND METHODS

2.1. Study site and datasets used in the study

2.1. a. Study site

The focal area of the study is located at 33° 15.183' N latitude and 87° 47.343'W longitude, covering 54.5 km^2 of area. The site lies in floodplains created by the Sipsey River (Figure 1). It is a 5th-order river located in western Alabama, US that is a tributary of the Tombigbee River. It begins near the Marion and Fayette county lines and travels through Fayette, Tuscaloosa, Pickens, and Greene counties, covering a total length of 148 km. Its watershed contains two physiographic provinces and five eco-sub-regions. The northern headwaters of the Sipsey River start in the Cumberland Plateau physiographic province at the confluence of the New and Little New Rivers (Duncan et.al, 2005). Shortly after, the Sipsey River enters the lower-gradient East Gulf Coastal Plain physiographic province, first joining the Fall Line Hills and then the Southeastern Floodplain sub-regions (Figure 1). The lower gradient and relatively uniform topography of the Southeastern Floodplain region increase the sinuosity of the river in this area. This area has many dissected pools and oxbow lakes (Tronstad et al., 2005) and an extensive alluvial floodplain (Hopper et al., 2012). The Sipsey River is located within a Cfa (Humid subtropical) Köppen-classified climate region. On average, March receives the most rainfall (157.5 mm), and October receives the least (76.2 mm).

Most reaches in the Sipsey watershed have an extensive (1-3 km wide) bottomland hardwood forested floodplain with dense canopies (Hopper et al., 2012). In the middle reaches of the Sipsey River, there are pine plantations used for timber harvest, but marginal wetlands

throughout these reaches serve as a buffer to most of the adverse effects due to logging (Haag et al., 2010). The lower reaches of the Sipsey River have large areas of swamp forest, composed mainly of *Nyssa aquatica* L. (water tupelo) and *Taxodium distichum* (L.) Rich (bald cypress) (Hopper et al., 2012). Both these species lose their leaves in winter and grow in low, saturated, and seasonally inundated soils (Cecilia et al., 2016). Bald cypress usually achieves dominance competing with water tupelo. Water tupelo requires more stringent wet conditions to be competitive at the seedling stage and is less shade-tolerant (Hook 1984). Reduced inundation periods and varying ground elevation characterize drier conditions and a diverse mosaic of habitats is produced, allowing many trees to thrive. Here bottomland hardwood forests are present (Cecelia et al., 2016). In the study area, the vegetation consists of mostly deciduous trees, such as water hickory (*Carya aquatica*), overcup oak (*Quercus lirata*), and sweetgum (*Liquidambar styraciflua*) (Kirkman et al., 2007). A transition habitat from hydric to mesic is present that supports mixed wetland forest where bottomland hardwoods, hardwood swamp, and pines are present in equal number. Finally, the pineland forests present in the area are dominated by loblolly pines (*Pinus taeda*).

The Sipsey River is identified as a high-quality river and worthy of federal protection according to the Nationwide River Inventory (Benke, 1990). It retains exceptional assemblages of freshwater species due to the lack of human modifications along the river, including 42 species of freshwater mussels (McCullagh et al., 2002), 12 native species of crayfish (Hopper et al., 2012), and over 100 species of fish (ADCNR 2012). The Sipsey also has invertebrates within the floodplain ecosystem, including sandflies, midges, beetles, and micro-crustaceans (Tronstad et al., 2005).

2.1. b. Satellite data and LiDAR DEM

Temporal variability in vegetation indices and classes were determined based on the analysis of Landsat 5 TM and Landsat 7 ETM images collected between 1990 and 2013 (WRS2 scenes: path 21, row 37). Landsat 7 ETM images were used in this study, even though on May 31, 2003, the Scan Line Corrector (SLC) that compensates for the forward motion of Landsat 7 failed. This was because the study area lies in the middle of the Landsat image and was unaffected by the scan line corrector failure (Figure 2). Table 1 provides the details of bands for each of these sensors (Landsat 5 TM and Landsat 7 ETM). These images were provided by USGS as Landsat surface reflectance data already atmospherically corrected by the National Aeronautics and Space Administration's (NASA) Landsat Ecosystem Disturbance Adaptive Processing System (LEDAPS) algorithm (Cissell et al., 2018). I omitted images with greater than 10% cloud cover; Table 2A shows a list of images used in the study. Presence of clouds significantly reduced the number of available images (i.e. 110 out of 720). However, this timespan was sufficient to characterize the yearly dynamics in the floodplain area.

All the images were processed in Earth Resources Data Analysis System (ERDAS) Imagine version 2015 (Hexagon Inc, Las Vegas, NV). ERDAS Imagine is the digital image processing software, used to process the Landsat TM and ETM data. Each image was first clipped by an Area of Interest (AOI) polygon and NDVI was obtained from the clipped study area. Figure 3 displays the original Landsat TM scenes and the subset of the area used in the study for the years 1990 and 2008.

A LiDAR-derived DEM for the area of interest was obtained from the Open Topography High-Resolution Data, University of California at San Diego. The LiDAR DEM was resampled to the 30-m pixel size of the Landsat images using the standard bilinear interpolation

implemented in ArcMap, which uses the four nearest cells. To characterize the vegetation cover, I used the Normalized Difference Vegetation Index (NDVI), as a proxy for vegetation productivity, which is defined as:

$$\mathrm{NDVI} = \frac{\mathrm{NIR} - \mathrm{RED}}{\mathrm{NIR} + \mathrm{RED}} \qquad \text{eq. (1)}$$

where NIR and RED are surface reflectance of the near infrared band (Landsat Band 4) and the red band (Landsat Band 3). NDVI values range between -1 and 1 (Cecilia et al., 2016); vegetation has NDVI values generally above 0.3, while both wet and non-vegetated areas have NDVI either negative or close to 0. Figure 4 displays images downloaded for summer and winter months and their NDVI in the study area.

2.1.c. Hydrological and meteorological data

Annual peak flow data to calculate flood recurrence interval; daily average flow data required for the inputs of the CAESAR model (1979-2013); seasonal and annual water level data for the Man Kendall test were downloaded from the Elrod gaging station (02446500), installed in the Sipsey River (https://waterdata.usgs.gov/nwis/dv/?referred_module=sw.). The gaging station is located within a kilometer of the study area. Gridded climatological datasets were downloaded from the Northwest Alliance of Computational Science and Engineering PRISM Climate Group for monthly precipitation and average, minimum, and maximum temperature (http://prism.oregonstate.edu/).

2.2. Application of Unsupervised classification and Seasonality Index to study the vegetation dynamics in the study area

This section describes the methodology to use to achieve first objective i.e. identify vegetation class by using unsupervised classification and Seasonality Index and study their dynamics for the study period

The study uses two methods of vegetation classification: unsupervised classification and an alternate method of Seasonality Index (SI). The purpose of using both techniques was to assess if an alternative method of SI has the potential of being used as a classification technique of vegetation and in what way are the two methods different. The assessment was done by comparing the accuracy assessments of the two techniques. This comparison provided an idea about which vegetation classes could be better identified by the two techniques.

2.2. a. Vegetation classification using unsupervised classification

Unsupervised classification or clustering is an effective method of partitioning remote sensor image data in multispectral feature space and extracting land- cover information (Jensen, 2016). It is the process whereby numerical operations are performed that search for natural groupings of the spectral properties of pixels, as examined in multispectral feature space.
The clustering process results in classification of number of spectral classes (Jensen, 2016). The analyst then transforms the spectral class into thematic information classes of interest (e.g. forest, agriculture, urban) (Huang et al., 2007). Among several clustering algorithms developed so far (Jensen, 2016), this study uses ISODATA (Self Organizing Data Analysis technique) clustering algorithms. It is iterative because it repeatedly performs an entire classification (outputting a thematic raster layer) and recalculates statistics. "Self-Organizing" refers to the way in which it locates the clusters that are inherent in the data (Rajan et al., 2015). Clusters are merged if either

the number of pixel in a cluster is less than a certain threshold or if the centers of two clusters are closer than a certain threshold (Anchang et al., 2016). Clusters are split into two different clusters if the cluster standard deviation exceeds a predefined value and the number of pixels is twice the threshold for the minim number of members (Anchang et al., 2016). Each time the clustering repeats, the means of these clusters are shifted. The new cluster means are used for the next iteration (Rajan et al., 2015).

To implement unsupervised classification, it was necessary to identify images that fall 30 days of within one another. Every year was divided into summer (May to August) and winter seasons (December to February) with images being within a window of 1 month. Due to the availability of images for exact one-month window (during summer season), I chose two years to conduct this classification: 1990 and 2008 (Table 2B).

An unsupervised classification using the Iterative Self-Organizing Data Analysis Technique (ISODATA) algorithm (Pasher and King 2010) was performed on the clipped area of two summer images from the years 1990 and 2008. For each image, the blue, green, red, and near-infrared bands and both shortwave infrared bands – Bands 1 through 5 and 7 for the Landsat 5 TM image – were included in the unsupervised classification procedure (Jones et al. 2014). Each unsupervised classification was run with 10 iterations and identified 10 spectral classes, which were assigned to one of the following four information classes (Jensen 2015): hardwood swamp, bottomland hardwood, pinelands, and unclassified or water (Long and Giri 2011).

2.2. b. Field survey for vegetation identification

Vegetation identification by field survey was done in August of 2017. This field survey was done for two purposes. First, was to identify the vegetation in area. Second, to train myself to better interpret the visual elements of Google Earth image. Visualization of the Google Earth

images of August 2017 before and after the field visit were practiced. The insights and knowledge developed from this visualization were used to interpret visual elements in the reference image (Google Earth image, 2006) while conducting accuracy assessments of classification.

A 3 km long reach across the river channel was selected to note the vegetation coordinates. Coordinates were noted at space of every 100 meter on either side of the road. Altogether, 60 vegetation coordinates (30 on each side) were recorded. Real time kinematics (RTK) positioning system was used to collect the coordinates of these 60 points. The base of RTK positioning system was installed on the road as it needs an open sky to give and receive the signals from the rover. The rover of RTK system was carried and the coordinates were recorded. Moving beyond 500m away from the RTK base, into the forest led to the rover losing signal from its base and therefore, trees were only identified within 500m on either side of the road. At each coordinate, a circular transact of 30 feet radius was measured and all the trees falling within this radius were identified using Kirkman et al., (2007).

2.2.c. Accuracy assessment of unsupervised classification

An accuracy assessment was performed on the 2008 image classifications in Earth Resources Data Analysis System (ERDAS) Imagine version 2015 (Hexagon Inc, Las Vegas, NV) (Figure 5A). Accuracy assessment could not be performed on the 1990 image due to the unavailability of a reference image (Google Earth image), from 1990 to 1997. Reference image for the year 2008 was high resolution (1m) Google Earth image obtained on May 2006 (Cornejo et al., 2005; Kovas et al., 2001; Cissell et al., 2018). This image was the only nearest available image during growing season. There was no available image between May 2006 and 2010 during the growing season. To conduct the accuracy assessment, a stratified random sampling option

was selected as the method to add random points on the classified image and 500 points were generated, which ensured that each information class was represented proportionally in the sample set relative to that information class's relative coverage of the study area (Jensen 2015). Control points in each classified map were referenced to high spatial resolution Google Earth imagery from corresponding dates (Morissette et al. 2005).

Overall accuracy is the probability that a point classified on the map accurately represents that category in the reference image. It is determined by dividing the total number of classified points (that is, the sum of the diagonal in the error matrix) by the total number of sampling points (Jensen, 2015). Further, accuracy was determined by the number of correct sampling points in a class divided by the total number of points that were actually classified in that category (Jensen, 2016). Similarly, producer's accuracy was determined by the total number of correct points in a class divided by the total number of points of that class as determined from the reference image (Google Earth image in this study) (Jensen, 2016). Finally, the Kappa coefficient of agreement (K) is a measured, which is the measure of agreement or accuracy between the remote-sensing-derived classification on the map and the reference image was determined. If the K value is greater than 80%, it represents strong agreement or accuracy between the classification map and reference image. K values between 40% and 80% represent moderate agreement and less than 40% represent poor agreement (Jensen, 2016).

2.2. d. Change detection by unsupervised classification

Per-pixel post-classification comparison change detection was used to quantify change in vegetation cover between 1990 and 2008 (Jensen 2015). In both images, pixels representing hardwood swamp, bottomland hardwood, pinelands, and water were coded with values of 1, 2, 3, and 4, respectively. In the 2008 classified map, pixels representing hardwood swamp,

bottomland hardwood, pinelands, and water were coded with values of 11, 12, and 13, respectively. The pixels in each class were converted to square-km to quantify vegetation cover area and change in the period between 1990 and 2008 (Jensen 2015).

2.2. e. Vegetation identification using Seasonality Index

Seasonality Index was first used to identify the vegetation types in a similar study conducted in the Apalachicola delta of Florida (Cecilia et al., 2016). The Seasonality Index (SI) is the ratio of maximum NDVI calculated in winter months to the maximum NDVI calculated in summer months. To do this, every year was divided into summer (May to August) and winter (December to February). I chose the images which were within a month window; in summer as well as in winter. This avoided the errors that would arise from choosing images from non-anniversary dates. Four years were found to have exact sets of images (during summer and winter) within one-month window; those were - 1990, 1995, 2000 and 2008. Table 2C provides the lists of images that were used to calculate SI for four years. NDVI rasters were obtained from available Landsat images for these months in ERDAS Imagine software. Finally, the raster of Seasonality Index was obtained by using eq. (2) in the raster calculator in Arcmap 10.4. Eventually, vegetation cover was classified into three types based on the values of Seasonality Index derived from these values.

$$SI = \frac{NDVI_w}{NDVI_s} \qquad \text{eq. (2)}$$

Where $NDVI_w$ is NDVI of winter month and $NDVI_s$ is NDVI in summer month.

2.2. f. Accuracy assessment of vegetation types identified by SI

Accuracy assessment of vegetation identification by SI in the year 2008 was performed in ArcMap 10.4 (Figure 5B). The reference image for this assessment was the image obtained on

May 2006, from Google Earth. This date was used as the reference because this was the only nearest available image during the growing season (May 2006).

First, the classified raster was reclassified using reclassify tool –as water/unclassified (1), hardwood swamp (2), bottomland hardwood (3), and pineland (4). By using the create random points tool, 500 random points were generated on this reclassified raster. Secondly, this shapefile was converted into kml file and loaded on google Earth to see how points aligned with vegetation type. Then, in ArcMap, a new field was added and named as Ground/Google. Under this field ground Reference classes were to be added as, (11) water/unclassified, (22) hardwood swamp, (33) bottomland hardwood, (44) pineland. This was done by toggling back and forth to Google Earth image in ArcMap. In this way, all the values for ground truth class values were created. Then, I added the identified vegetation type as a next field in the attribute table. This was done by using the extract to value tool- which extracted all the values of the vegetation types that were reclassified in the beginning as 1 for water/unclassified, 2 for hardwood swamp, 3 for bottomland hardwood and 4 for pineland. Finally, this attribute table containing the code for reference image and code SI identified vegetation types was then exported into Excel sheet to create an error matrix.

2.2 g. Change detection using SI identification.

Change detection in each of the vegetation types identified from SI for these four years was analyzed in Arcmap 10.4. The number of pixels under each vegetation type was multiplied by 900 (pixels area 30*30) and then converted into square kilometers.

2.2 h. Mann Kendall test to analyze trend in water level

The Man Kendall test was performed to determine if there was any trend in water level that may have an impact on change in vegetation cover. For this monthly water level data

between 1977-2008 were obtained from United State Geological Survey. These data were then categorized into annual, summer (May to August) and winter (December to February) water levels. For summer, average values of summer months were taken and for winter, average values of winter months were taken. For the annual water level, average of all the months were taken.

There are several approaches for detecting the trend in the time series. Trends take various forms, such as increasing, decreasing and cyclic (Fiester et al., 2008). The most popularly used test for detecting trend in the time series is the Man Kendall test. The advantage of using this test is that it does not require the data to be normally distributed (distribution of normal variables as a symmetrical bell-shaped curve) (Tabari et al., 2011). According to this test, the null hypothesis H_0 assumes that there is no trend (the data is independent and randomly ordered) and this is tested against the alternative hypothesis H_1, which assumes that there is a trend (Onoz and Bayazit 2003). The basic principle of test is based on statistics S and is computed as follows:

$$S = \sum_{k=1}^{n-1} \sum_{j=k+1}^{n} sign(x_i - x_k)$$

eq. (3)

Where S = Mann Kendall test value

X_j and X_k-= Sequential data values; k and n = length of data

S value is assumed to be 0 (no trend). A very high positive value of S indicates an increasing trend and a very low negative value indicates a decreasing trend. In this test, it is assumed that when n is greater or equal to 8, the test statistics S is approximately normally distributed with mean and variance as follows:

$$E(S) = 0$$

$$Var(s) = \frac{1}{18}[n(n-1)(2n+5) - \sum_{i=1}^{m} t_i\ (t_i - 1)(2t_i + 5)] \qquad \text{eq. (4, 5)}$$

Where m is the number of tied groups and t_t is the size of ith t group.

If the significance level α (alpha) is 0.05 then a p-value greater than 0.05 should accept the null hypothesis (no trend). I hypothesized that there is no trend in the seasonal and annual water level over thirty years period (1977-2008). Mann Kendall test was performed in XLSTAT version 2017.5 (Addinsoft, Paris, France) using significance threshold of 0.05.

2.3. Comparison of the two methods

Comparisons were done in two ways. First, comparison of the accuracy assessments and change detection was done to see which method performed well in identifying the different classes. Second, SI identification was compared with respect to unsupervised classification to see when the SI differed the most with unsupervised classification and was named as SI versus unsupervised classification. It was calculated by subtracting the values (area of vegetation coverage) obtained via SI cover from values obtained via unsupervised classification. The percent difference from unsupervised classification was then calculated. Percentage different from unsupervised classification was calculated for areal coverage of vegetation types in the year 1990 and 2008. Percentage different from unsupervised classification was also calculated for the change detection from 1990 to 2008.

2.4. Temporal and spatial distribution of NDVI of vegetation types in the study area

2.4. a. Preparation of NDVI datasets for each vegetation types

Temporal and spatial distribution of the NDVI values for each vegetation types was analyzed for the period between 1990 and 2013. The first step was to get the datasets of NDVI for three vegetation types for all the months in this time. Since Seasonality index was found have better (this will be discussed later in detail) delineated the hardwood swamp and bottomland

hardwood, the polygons derived from this method were used to extract the NDVI values of vegetation types for all the images that fall between 1990 and 2013.

After obtaining the SI raster for the year 1990, it was reclassified to single integer values and converted into polygon shapefiles in ArcMap 10.4. These polygons were then overlaid on the NDVI raster for the rest of the months in 1990. By using the extract to values tool, NDVI values were obtained for two shapefiles (for two vegetation types - hardwood swamp and bottomland hardwood). This step added an extra table in the shapefile attribute with NDVI values in each cell. Finally, running the zonal statistics tool, mean NDVI was obtained for each shapefile. Assuming the vegetation type pixels do not change much within five to eight years, the polygons derived for the year 1990 were used to extract the NDVI from all the images available from 1990 to 1994 following the same method.

Similarly, the polygons obtained from 1995 were used to extract the information from images available from 1995 to 1999; polygons obtained from 2000 were used to extract information from images available from 2000 to 2008; and polygons obtained from 2008 were used to extract the information from images available from 2008 to 2013 (Table 2A).

2.4.b. Temporal distribution of NDVI of vegetation types over the day of year

Using these NDVI values obtained from above for three vegetation types, their distribution over the year was analyzed. I gave a name to this plot as NDVI typical year (NTY) plot for each vegetation type. The significance of using this plot was to see how does NDVI associated with vegetation types change along days of the year (out of 365). Firstly, the dates were arranged between 1 and 365 (number of days in one year or DOY) in a column in Excel. For example, NDVI value of date 1/1/1990 would be in the row of 1 (DOY); similarly, NDVI value of date 1/2/1990, would be in the row of 32 (DOY). In this way, all the NDVI values for

all three vegetation types were placed according to the DOY. This was done for all three vegetation types for 23 years. These were then plotted as scatter plots in Excel.

2.4. c. Spatial distribution of NDVI along different elevation

SI for the year 2008 was used to see how elevation plays a role in distributing the vegetation in space. To do this, SI raster was reclassified into three classes, and overlaid on the LiDAR DEM. By using the extract to values tool in ArcMap, elevation was extracted for each pixel. The attribute table was then exported as an Excel file and a box and whisker plot was made using SPSS software.

2.5. Temporal variability in NDVI by partial least square regression model

Here I assessed temporal variability in NDVI by analyzing combination of climatological and hydrological variables on NDVI for identified vegetation classes using statistics such as Spearman's rho correlation and partial least square regression (PLSR model). These analyses were also performed for the period between 1990 and 2013. In this analysis, response variables were NDVI associated with the vegetation types (as obtained in section 2.4.a) and predictor variables were hydrological and climatological datasets.

2.5. a. Preparing climatological and hydrological data as predictor variables for PLSR modeling

Vegetation response to environmental changes (e.g., rainfall and temperature) has been found to be lagged in several studies in the past (Nischolsan et al., 1990). A study conducted by Maxwell and Knapp (2009) found that growth of *Nyssa ogeche* (hardwood swamp species) is more sensitive to the amount of rainfall from the previous summer than the recent winter rainfall. Therefore, I searched for the most appropriate timescale for each image for the explanatory variables. I took a moving average of climatological as well as hydrological variables. For each

image, I took monthly moving average of antecedent two months, antecedent three months up to moving average of antecedent six months for climatological variables (minimum, maximum and average; rainfall) (Table 3).

Similarly, hydrological data have also been found to have similar lagged effects. Previous studies have stated that vegetation recovery positively responds after two weeks of daily stream flows (Wen at al., 2012, Townsend 2001). Therefore, I took weekly, two-, three-, four-, five- and six-weekly moving averages of daily streamflow data (Table 3).

PLSR modeling was carried out on two vegetation types: hardwood swamp and bottomland hardwood. The third vegetation cover type, pineland forest, was not included in PLSR, since it was found to be situated along higher elevation and would be unaffected by the hydrological variables (Cecilia et al., 2016).

2.5.b. Pre-processing of response variable (NDVI) and predictor variables (climatological and hydrological data)

Descriptive statistics were calculated for all the response (NDVI) and predictor variables (climatological and hydrological variables) in SPSS software. Spearman's rho correlation coefficient test was conducted to analyze the strength of the relationship between the response (NDVI) and predictor variables (climate and hydrological) mentioned in Table 4. For these, monthly climate and hydrological variables associated with the monthly NDVI values were considered.

2.5. c. PLSR model and its setup

The partial least-square regression (PLSR) method was used to construct the models, and was conducted in software, JMP statistics package version 14.0.1 (SAS Institute Inc. Cary, NC):

$X = TPT + E$

$$Y = UQT + F \quad \text{eq. (6)}$$

where X is an n x m matrix of predictors; Y is an n x p matrix of responses; T and U are n x l matrices that are projections of X and Y; P and Q are, respectively, m x l and p x l orthogonal loading matrices; and matrices E and F are the error terms (Praskievicz, 2016). The method generates orthogonal latent variables (components) that are linear combinations of standardized predictor variables (Mevik et al., 2007). The loadings are the regression coefficients, or relative weights, of each of the original predictor variables in the new component (Asner and Martin 2008). PLSR has been designed to confront the situation of many, possibly correlated, predictor variables (Martens 2001). PLSR has been proven to be a good collinearity reduction technique for time series analyses and has been successfully applied with multi-temporal satellite images such as MODIS and Landsat and the indices derived from them (Normalized Difference Vegetation Index, Enhanced Vegetation Index, Leaf Area Index) (Darvishzadeh et al., 2008; Lazaridi et al., 2011, Praskievicz et al., 2016).

A cross-validation method was used to determine the number of significant PLSR components needed to obtain the most reliable prediction model for NDVI in each vegetation types. Q^2 (the fraction of total variation of the dependent variables that can be predicted by a component) and Q^2_{cum} (the cumulative Q^2 over all the selected PLSR components) were computed using the following equations:

$$Q^2 = 1 - \frac{PRESS}{SS} \quad \text{eq. (7)}$$

$$Q^2_{cum} = \frac{PRESS}{SS} a \quad \text{eq. (8)}$$

where (a = 1, 2……m),

PRESS is the predictive residual sum of squares, SS is the residual sum of squares, and m is the number of PLSR components. When Q^2_{cum} is greater than 0.5, the model is considered to have a good predictive ability.

As stated earlier, not all climatological and hydrological variables need to be included in the PLSR model (Shi et al., 2013) as redundant variables can lead to PLSR models with low statistical significance. Hence, the following procedure was followed that gave an optimal model. First, simulation of PSLR models was performed with all the predictor variables. Next, a series of simulations of new PLSR models was performed with variables eliminated. This elimination of the predictor variables was based on the value of VIPs greater than 0.8. Eventually, optimal model was selected based on the regression coefficient with lowest PRESS; largest coefficients of determination (R^2) and largest value of Q^2_{cum}.

The best model was selected based on the regression coefficient with the lowest PRESS (Yeniay and Goktas 2002). In the PLSR modeling, the importance of predictors for dependent variables is given by the importance of the projection (VIP) and, therefore, variables with large VIP values (greater than 0.8) are the most relevant for explaining the dependent variables (Shi et al, 2013).

2.6. Assessing spatial variability in NDVI using 2D flood modeling (CAESAR)

This section describes the methodology to achieve third objective i.e. to assess the spatial variability in NDVI by analyzing impacts of inundation frequency via use of 2D hydrodynamic flood modelling (CAESAR) for floods of different magnitudes.

This analysis was also carried out on two vegetation types: hardwood swamp and bottomland hardwood. The third vegetation type, pineland forest, was not included, since it was

found to be situated along higher elevation and would be unaffected by the hydrological variables (Cecilia et al., 2016).

Floodplain inundation occurs at least annually, often for an extended time (weeks to months) during the winter-spring period in the Sipsey River. I studied the impact of inundation frequency due to different flood recurrence interval on spatial variability of NDVI. Inundation frequency is the number of times the area was inundated by a flood (Huang et al., 2014). For this analysis, 2D flood modeling program; CAESAR (Cellular Automaton Evolutionary Slope and River model) was used. I chose this model because it is well-documented, is based on cellular automata, and performs the simulation pixel-by-pixel, benefitting all levels of heights provided by the DEM.

2.6. a. Data preparation for CAESAR modeling

To conduct this analysis, the first task was to identify floods of various recurrence intervals. Streamflow recurrence intervals are based solely on magnitude of the annual peak flow and indicate the probability that a given flood will be equaled or exceeded in any given year (https://water.usgs.gov/edu/100yearflood.html). To calculate flood recurrence interval, the method described by Dalrymple (1960) was followed and are outlined below.

Long-term peak flow records (1929 to 2016) were downloaded from USGS. These yearly peak flows were ranked, and recurrence intervals were calculated using eq. (9)

$$R = \frac{N}{M + 1} \qquad \text{eq. (9)}$$

where R = recurrence interval; N = number of records; and M = rank of the peak flow.

In this way, floods of various recurrence intervals were determined and were found to range from 1 to 37 years.

Bankfull discharge at a river cross-section is the flow that just fills the channel to the tops of the banks and marks the conditions of incipient flooding (William, 1978). In this study area, the 1.5-year recurrence-interval flood was considered as a bankfull discharge (William, 1978), and had a value of 197 m^3s^{-1}.

Among all floods of various recurrence intervals, three floods (5-year, 10-year, and 37-year floods) were selected for 20 days' simulations in CAESAR. I chose a 20-day simulation because of computationally intensive nature of the CAESAR model (Coulthard et al., 2001).

2.6. b. CAESAR model

Floodplain inundation modeling was performed using the Cellular Automaton Evolutionary Slope and River (CAESAR) model. Recent studies done by Zellou (2017) have suggested that CAESAR entails relatively simple cellular representation of water within the reduced-complexity landscape evolution model (LEM) framework, which enables replication of channel and floodplain dynamics with good precision. CAESAR can accurately quantify the magnitude of inundation required across the significantly disturbed floodplains of such a naturally wet surface. Therefore, CAESAR could be an appropriate tool for dealing with flood inundation with the situation of rapid wetting and drying, as it allows visualization of the area that will be inundated first and those that remain submerged even when the flood recession begins.

CAESAR has four main parts: the hydrological model, fluvial erosion, deposition and slope processes, and the flow model (Coulthard et al., 2001). This research only used the flow model. The CAESAR landscape evolution model simulates landscape development by moving water across the regular grid cells and changing cell elevations per the erosion and deposition from fluvial and slope processes. CAESAR operates in two modes, basin and reach (Coulthard et

al., 1998). In reach mode, it uses sources of discharge (both water and sediment). The flow model of CAESAR uses a "flow-sweeping algorithm" (Coulthard, et al., 2002), which calculates a steady-state, uniform flow approximation of the flow field. Discharge is distributed to all cells within 2-5 cells range in front of a cell per the difference in the water-surface elevations of the contributing cell and bed elevation of receiving cells. If there is an obstruction, then the discharge remains in contributing cells to be distributed in subsequent steps (possibly in different directions) during the same scan. Flow depth and velocity are calculated by Manning's equation. The flow-sweeping algorithm in CAESAR is a simplification of the full shallow-water equations applied in x and y directions to simulate 2-D flow over a raster grid (Bates et al. 2010). The flow between cells is calculated by using eq. (6):

$$Q = \frac{q - gh_{flow}\Delta t\frac{\Delta(h+z)}{\Delta x}}{(1+\frac{gh_{flow}\Delta tn^2q}{h_{flow}^{\frac{10}{3}}})}\Delta x$$

eq. (10)

where Q is the discharge (m^3s^{-1}), q is the flux between cells from the previous iteration ($m^2\ s^{-1}$), g is acceleration due to gravity (ms^{-1}), n is Manning's coefficient (dimensionless), h is cell water depth (m), z is elevation (m), t is time (s), x is the grid cell width (m), and flow is the maximum depth of flow between cells. The cell water depth (h) is updated, after establishing the discharge across all four boundaries of a cell, using eq. (7):

$$\left(\frac{\Delta h^{i,j}}{\Delta t}\right)^n = \frac{Q_x^{i-1j} - Q_x^{ij} + Q_y^{ij-1} - Q_y^{ij}}{\Delta x^2}$$

where i and j are cell coordinates. eq. (11)

2.6. c. CAESAR model setup, outputs and analysis

The input parameters for the CAESAR model included LiDAR-derived DEM (resolution-10 m) and daily discharge corresponding to three floods.

The output of the model produced forty-five to sixty ASCII files of water depth, which were then converted into rasters (spatial resolution = 10m) and were resampled to a 30-meter resolution. A Python code was written in Pycharm to calculate the inundation frequency. This code converts all the rasters into binary version based on the threshold of water level. The threshold was decided to be 0.02 meters. The threshold was determined based on water depth in the floodplain (25 meter from the main channel) during the 5- year flood; which indicated that if a 5-year flood could bring 2 centimeters of inundation in the floodplain area; that area would be inundated during larger floods as well. Assigning greater threshold than 2 cm missed most of the floodplains. Therefore, this threshold was obtained from series of trials, which delineated maximum extent of the floodplain. This threshold of water depth was kept constant for all the flood considered in this study. The binary rasters were added on top of each other to produce a single final raster. This final raster displayed the flood raster with pixel values of inundation frequency. The inundation frequency maps were then georeferenced in ArcMap 10.4 and overlaid on the NDVI rasters. Finally, by using tools such as Extract Values to Points, Raster Calculator, and Select by Attribute in ArcMap 10.4, the NDVIs corresponding to different vegetation types were extracted. The attribute tables were then exported to Excel and the linear regression was performed for NDVI for the two vegetation types.

3. RESULTS

3.1 Application of Unsupervised classification and Seasonality Index to study the vegetation dynamics in the study area

3.1. a. Dominant vegetation types identified by two methods (unsupervised classification and SI) and their accuracy assessments

Unsupervised classification classified the study area into four classes: hardwood swamp, bottomland hardwoods, pineland, and water or unclassified for the year 1990 and 2008 (Figure 6).

An accuracy assessment performed on the unsupervised classification for the year 2008 showed that the overall accuracy of the unsupervised classification was 60% with the kappa statistic of 0.47, which means that the classification was moderately accurate (Table 4). Among the four classes, the highest accuracy was obtained for the water/unclassified pixel of producer's (71%) and user's accuracy (87%); followed by pineland trees of 61% for producer's accuracy and 75% for user's accuracy); followed by bottomland hardwood of 52% (producer's accuracy) and 57% (user's accuracy); followed by hardwood swamp of 58% (producer's accuracy) and 40% (user's accuracy).

The SI also identified three vegetation types, Pine trees ($SI \approx 1$), bottomland hardwood ($SI \approx 0.5$), and hardwood swamp ($SI \approx 0.3$) (Figure 7). Pine trees had SI close to 1 since NDVI is similar during the year for evergreen species. Bottomland hardwood and hardwood swamp had lower SI.

The accuracy assessment showed an overall accuracy of 71.2% and kappa statistics of 0.59 (Table 5). Accuracies percentage were- for water/unclassified-user's accuracy of 35% and producers accuracy of 40%; for hardwood swamp, user's accuracy of 86% and producer's accuracy of 82%; for bottomland hardwoods, user's accuracy of 74% and producers accuracy of 79%; for pineland, users accuracy of 60% and producer's accuracy of 54%.

In the filed survey, out of total 60 locations, 25 locations were identified as hardwood swamp, 20 locations were identified as bottomland hardwoods and 15 locations were identified as pinelands (Table 6, Figure 8). The most common tree species (Table 6) of the hardwood swamps in the study area were water tupelo (*Nyssa aquatica*) and bald cypress (*Taxodium distichum*). These trees were found along the investigated segment of the river and in depressions which occur within floodplains and were found to be habitually inundated. Both tree species lose their leaves in winter and grow in low, saturated seasonally inundated soils and in deep swamps (Schneider et al., 1988).

Bottomland hardwood trees were found to be located at relatively higher elevation than the hardwood swamps, where sediments get settled during the overbank flows creating alluvial deposits. These locations were found to be drier, supporting mainly deciduous trees such as southern red oak (Quercus falcata), American elm (*Ulmus americana*), sweetgum (*Liquidambar styraciflua*), yellow poplar (*Liriodendron tulipifera*), and American beech (*Fagus grandifolia*) (Table 6).

Pinelands were found to be located at higher elevations than the other two vegetation types. Except 15 locations across 3 km of the reach selected, most of the pinelands were along the higher elevation and farther from the road access. Out of 15 locations, 8 locations were found

to be mixed, where both bottomland hardwoods as well as pineland were equally present. The pine trees in the study area were dominated by loblolly pine (*Pinus taeda*).

3.1. b. Change detection in vegetation cover types in the study period (1990-2008)

Change detection using unsupervised classification showed that hardwood swamp decreased by 33%; bottomland hardwood increased by 45% and pinelands increased by 26% in the period of eighteen years (Table 7, Figure 9). Similarly, the SI showed that hardwood swamp decreased by 20% while bottomland hardwood and pinelands increased by 15.3% and 60%, respectively (Table 8, Figure 10). Change detection between 1990 and 2008 by both methods showed an expansion of pineland trees along the east, northeast, southwest, and southeast corners of the region (Figure 11).

3.1. c. Mann Kendall test to analyze the trend in water level

The Mann- Kendall test performed on seasonal and annual water level data showed no trend between 1977 and 2008. Though S values were positive for annual (S=6), winter (S=2) and summer (S=4) water level, this increase was not statistically significant (p-values were greater than 0.05). And therefore, it indicated that there was no trend from 1977 to 2008 (Table 9, Figure 12).

3.2. Comparison of two methods

3.2. a. Comparison of accuracy assessments, change detection performed on two techniques

For unsupervised classification, water/unclassified pixels showed highest accuracy (71% as producers and 87% as users); while SI showed lowest accuracy (40% producer's, 35% user's) (Table 10A). Similarly, unsupervised classification for pineland trees showed second highest accuracy (61% for producer's and 75%user's) while SI showed relatively low accuracy

(producer's 54%, 60% user's). Unsupervised classification showed lower accuracy for bottomland hardwoods (as 52% for producer's, 57% user's), while SI showed relatively higher (79% as producer's, 74% user's). Lastly, unsupervised classification showed lowest accuracy for hardwood swamp (58% as producer's, 40% user's), while SI showed relatively higher (82% as producer's, 86% as user's).

3.2. b. SI identification versus unsupervised classification

In the 1990, SI differed 17% in hardwood swamp; 19% in bottomland hardwood; 33% in pineland trees; hence SI differed most in pineland classification from unsupervised classification (Table 10B). Similarly, for the year 2008, it differed by 41% in hardwood swamp; 2% by bottomland hardwood; and 15% in pineland forests; hence SI differed highest in bottomland. For change detection in the areal coverage of the vegetation; it differed by 31% in hardwood swamp; 50% in bottomland hardwood; and 56% in pinelands, hence SI differed most in change detection of pinelands.

3.3. Temporal and Spatial distribution of NDVI for vegetation types

The three vegetation types possessed lowest NDVI signatures during the winter season (starting days of year) and highest NDVI signatures during summer (in the middle of the year) (Figure 13). Among the three, hardwood swamps had the lowest NDVI values during winter but highest variability in a year. Pinelands had highest NDVI values during winter but lowest variability in a year. Bottomland hardwoods possessed medium variability in NDVI values in a year.

The SI derived vegetation types for the year 2008 showed that distribution was driven by differences in elevation (Figure 14). Pineland trees were found along the highest range of elevations (ranged from 60 m to 94 m); bottomland hardwood forests along the medium range of

elevation (ranged from 62 m to 87 m); and hardwood swamps along the lower range of elevation (ranged from 60 m to 73 m). This was also evident during the field survey of vegetation. Hardwood swamps were mainly along the lowest elevation and depressions and pinelands were spread out along the higher elevation in the study area.

3.4. Assessing temporal variability in NDVI

3.4. a. Descriptive statistic of response variables (NDVI) and predictor variables (climatological and hydrological)

During summer, for hardwood swamp, NDVI ranged from 0.47 to 0.8 with a mean of 0.75 and standard deviation of 0.07 (Table 11A). Similarly, for bottomland hardwood, NDVI values ranged from 0.66 to 0.82; with a mean value of 0.77 and standard deviation of 0.04. Maximum monthly temperature ranged from 80.1 °F to 96.8 °F; with mean of 88.8°F and standard deviation of 4.8 °F. Minimum monthly temperature ranged from 54.9°F to 72.25 °F; with a mean of 65.7 °F and standard deviation of 5.17 °F. Average monthly precipitation ranged from 0.12 inches to 10.36 inches with a mean of 3.98 inches and standard deviation of 2.32 inches. Weekly discharge ranged from 1.2 cubic feet per sec to 59.2 cubic feet per sec with a mean of 12.30 cubic feet per sec and standard deviation of 14.68 cubic feet per sec.

During winter, for hardwood swamp, NDVI ranged from 0.38 to 0.79 with a mean of 0.49 and standard deviation of 0.1 (Table 11B). Similarly, for bottomland hardwood, NDVI values ranged from 0.26 to 0.45; with a mean value of 0.35 and standard deviation of 0.05. Maximum monthly temperature ranged from 48.6 °F to 63.05 °F; with a mean of 57.11 °F and standard deviation of 3.62 °F. Minimum monthly temperature ranged from 27.8 °F to 40.65 °F; with a mean of 34.5 °F and standard deviation of 3.46 °F. Average monthly precipitation ranged from 1.09 inches to 10.89 inches with mean of 5.08 inches and standard deviation of 2.37 inches.

Weekly discharge ranged from 3.94 cubic feet per sec to 164.2 cubic feet per sec with a mean of 42.4 cubic feet per sec and standard deviation of 41.57 cubic feet per sec.

The range and standard deviation of NDVI values of hardwood swamps were higher than that of bottomland hardwood during both seasons. The range and the variation of climate variables were higher in summer than in winter.

3.4. b. Correlation analysis between NDVI and hydrological and climatological variables

The NDVI of the forest in the study area demonstrated a high correlation ($0.6 < r < 1$, $p = 0.01$) with climatological parameters (average, maximum, and minimum temperature), while there was a medium negative correlation ($-0.3 < r < -0.6$, $p = 0.01$) with hydrological parameter (weekly streamflow) (Table 12). NDVI of both vegetation types showed a weak negative ($-0.3 < r$, $p = 0.05$) correlation with average monthly precipitation.

Among the predictor variables, maximum monthly temperature showed a strong negative correlation ($r >- 0.6$, $p =0.01$) with streamflow values. Monthly rainfall showed medium positive correlation ($0.6 < r < 1$, $p = 0.05$) with streamflow.

3.4.c. Partial least square regression (PLSR) model to determine temporal variability in NDVI of vegetation types in the study area

The amount of variance explained by the independent variables was greater for hardwood swamps than the bottomland hardwoods (Table 13A). Both vegetation types were found to be regulated by identical climatic variables.

Hardwood swamp:

The PLSR model for hardwood swamp identified two factors as the number of factors that minimized the predicted residual sum of squares (PRESS); the value PRESS was found to be 0.45. This optimal model cumulatively explained 83% of the variance in NDVI of hardwood

swamp with a cumulative Q-square of 0.96; and a negative intercept of -0.38 at statistically significant level ($p<0.001$), (Table 13A). The most significant variables were average monthly temperature (coefficient = 0.009, VIP=1.02); followed by average temperature of the antecedent two months (coefficient = 0.009, VIP=0.99); followed by monthly maximum temperature (coefficient = 0.002, VIP=0.98) and minimum monthly temperature (coefficient= -0.006, VIP=1). NDVI showed a positive correlation with all the variables except with monthly minimum temperature. PLSR model predictions were more accurate when the NDVI values were low (between 0.25 and 0.45) as most of the points lie closer the regression line. PLSR model prediction are less accurate during the higher NDVI values (between 0.6 and 0.9) as few points were farther from the regression line (Figure 15A). The equation of the regression line obtained from the model (eq.12) is as follows:

$$\text{SwampNDVI}_{\text{predicted}} = 0.002 * A_1 + 0.009 * B_1 + 0.009 * B_2 - 0.006 * C_1 - 0.38$$

eq. (12)

Where A_1= Maximum monthly temperature; B_1= Average monthly temperature; B_2= Average monthly temperature of antecedent two months; C_1 = Minimum monthly temperature.

Bottomland hardwoods:

This PLSR model for bottomland hardwoods identified two factors as the number of factors that minimized the predicted residual sum of squares (PRESS); the value for PRESS was found to be 0.71. The optimal model explained 58% of the variability in NDVI, with cumulative Q^2 of 0.53; and a positive intercept of 0.15 at a statistically significant level ($p<0.001$) (Table 13A). As indicated by the coefficients and VIP values, the most important variables were average monthly temperature (coefficient= 0.006, VIP= 1.04); followed by average temperature of the antecedent two months (coefficient= 0.0013, VIP = 0.99); followed

by monthly maximum temperature (coefficient= 0.0005, VIP=0.99); followed monthly minimum temperature (coefficient = -0.0002, VIP=0.98). All the variables were positively correlated except minimum monthly temperature. PLSR model predictions were more accurate when the NDVI values were lower (between 0.4 and 0.55) and higher (between 0.65 and 0.9) as most of the points lie closer to the regression line. Model predictions were less accurate when the NDVI values were of medium values (between 0.55 and 0.65) as the point are farther from the regression line (Figure 15B). The equation of the regression line obtained from the model (eq.13) is as follows:

$$\mathrm{BottomlandNDVI}_{\mathrm{predicted}} = \ 0.002 * \mathrm{A}_1 + 0.009 * \mathrm{B}_1 + 0.009 * \mathrm{B}_2 - 0.0006 * \mathrm{C}_1 + 0.15$$

eq. (13)

Where A_1= Maximum monthly temperature; B_1= Average monthly temperature; B_2= Average monthly temperature of antecedent two months; C_1= Minimum monthly temperature.

PLSR models showed no correlation between NDVI and predictor variables such as average, maximum and minimum monthly temperature during winter and summer seasons. And therefore, no optimal model could be established for either of the vegetation types for summer and winter seasons. For hardwood swamp, during winter, very low R-square values (0.08) with low cumulative Q-square (0.004) were found (Table 13B). For bottomland hardwoods, R-square of (0.08) at cumulative Q-square of 0 was found. For hardwood swamp, during summer, R-square of 0.14 and low cumulative Q-square of 0.11 were found. For bottomland hardwoods, R-square of 0.05 with cumulative Q-square of 0.3 were found (Table 13C).

3.5. Assessing spatial variability in NDVI

3.5. a. 2D flood-inundation modelling

Flood inundation frequency was found to be increasing with increasing magnitude of flood. For the 5-year flood, the maximum inundation frequency was 41 and most of the water remained in the channel and secondary channels (Figure 16A). For the 10-year flood, the maximum inundation frequency was 40 but flow covered a wider (than 5-year) area of the floodplain (Figure 16B). For the 37-year flood, the maximum inundation frequency was 58 as well as flow covered a wider area of the floodplain (Figure 16C). Very few days (2 to 4 days) exceed bank full discharge during each flood. For 5-year flood, only two days exceed bank full discharge (Figure 17A). For 10-year flood, four days exceed bank full discharge (Figure 17B) and for 37-year flood, two days exceed bank full discharge (Figure 17C).

For 5- year flood, NDVI values were associated smallest range of flood inundation frequency that lied between 0 to 25 (Figure 18). For 10-year flood, NDVI values were associated with medium range of inundation frequency that lied between 0 to 40 (Figure 19). For 37-year flood, NDVI values were associated with largest range of flood inundation frequency that lied between 0 to 52 (Figure 20).

Linear regression between inundation frequency and associated NDVI showed no relationship between the two. Coefficients of determination R^2 between inundation frequency and NDVI for hardwood swamp for 5, 10 and 37-year floods were found to be 0.0046 ($p = 0.14$), 0.00026 ($p = 0.2$) and 0.0005 ($p = 0.3$; Table 14A). Similarly, for the bottomland hardwood, the coefficient of determination R^2 for 5-year, 10-year and 37-year floods were found to be 0.012 ($p = 0.37$), 0.002 ($p = 0.06$); 0.002 ($p = 0.2$), respectively (Table 14B).

4. DISCUSSION

4.1. Application of unsupervised classification and SI to assess the vegetation dynamics for the study period

4.1. a. Dominant vegetation types identification by two techniques

Identification of the vegetation types by two methods indicates that remote sensing and GIS techniques offers practical and economical means to discriminate the vegetation types. The successful identification of vegetation by SI indicates that it can also discriminate the vegetation types based on the spectral signatures. SI identification of three vegetation types in this study agrees with the study conducted by Cecilia et al. (2016), where SI was first used to identify three vegetation types as hardwood swamp, bottomland hardwood and pinelands.

While unsupervised classification using Landsat TM, images is among the most common classification technique and has been successfully used earlier by several researches (Harvey and Hill 2001; McCarthy et al. 2005); numerous alternate classification algorithms have been developed in the last few decades (Xie et al., 2008; Coppin et al., 2004). The ratio of winter NDVI to summer NDVI (ratio of NIR-Red / NIR + Red) by SI technique (one of the alternate technique) is based on the idea that vegetation is highly reflective in the near infrared and highly absorptive in the visible red. This makes NDVI and classification techniques that involve the use of NDVI, a good indicator to reflect the dynamic changes of vegetation groups. Besides SI, there are several other published alternative methods of vegetation classification based on modification of NDVI. Few of these are as Modified Normalized Difference Vegetation Index or MNDVI (ratio of Shortwave Infrared + Red / Shortwave Infrared + Red) used by Rouse et al.

(1973), Green Normalized Difference Vegetation Index or GNDVI (ratio of Near Infrared – Green / Near Infrared + Green), used by Gitelson et al. (1996), Transformed NDVI or TNDVI (ratio of Near Infrared + Red / Near Infrared + Red +1) used by Tucker et al. (1979). Like my study, these studies also found that such alternative methods showed higher accuracy in vegetation identification over unsupervised classification. This is discussed in detail in the later sections.

4.1.b. Change detection in vegetation cover types in the study period (1990-2008)

Unsupervised classification and SI identification showed a decrease in hardwood swamps and an increase of pineland and bottomland trees in the period of eighteen years. The increase in pine and bottomland hardwood land cover could be due to the forests management practices such as regrowth of formerly logged areas by mixed forests (pine trees and hardwood trees) for timber production and recreational purposes (ADCNR, 2016). Study area lies within Forever Wild Land Trust program, initiated in the year 1992, under Alabama Department of Conservation and Natural Resources to conserve the public lands and forests of Alabama (ADCNRLD, 2009). While there is no published report associated with the study area but increase in the bottomland hardwoods and pineland forests could be due to the reforestation, which is one of the main activities of the Forever Wild Program.

Pinelands in the study area, were observed to be increasing in the east, northwest, and southeast corners of the study area. The southeastern region of the USA has over 13 million hectares of pines composed of loblolly pine (*Pinus taeda*), slash pine (*Pinus elliottii*), longleaf pine (*Pinus palustris*), and shortleaf pine (*Pinus echinate*) (Nabavi et al., 2018). Among these species, loblolly pine, which is a dominant species in the Sipsey watershed, is known to be the most commercially important species due to its ability to survive in a broad range of sites and its

fast growth (Zhao et al., 2011). It regenerates from wind dissemination, is shade-intolerant and comprises an early stage in forest succession on Coastal Plain sites (Cain et al., 2001). Studies have found that vegetation species which are dispersed by wind such as pine trees are more abundant and widespread as compared to those that are dispersed by water such as bald cypress (Battaglia et al., 2002). Loblolly pine is also planted widely and is subjected to an intense breeding program in the Southeastern US (Farjat et al., 2017). While these are not the only possible reasons for the increase of the pine trees in the study area, further research would be needed to address the exact mechanism.

The loss of hardwood swamp could be due to the massive demand for biomass, commercial plantations, and replacement by other species. Several studies have attributed loss of hardwood swamps to repeated logging for agriculture and timber production (Kellison et al., 1997; Dahl et al., 1991). Another possible explanation could be the difference in the seed dispersal mode. Hardwood swamps are dispersed by water (Reid et al., 2014) and is argued to be less abundant than those that are dispersed by wind such as loblolly pines (Stanturf et al., 2000).

This decline could also be due to the presence of feral hogs that feed on the seedlings and fruits of tupelos. This might have limited the regeneration process of these species in the study area. Despite extensive documentation of hog disturbance in southeastern US forests (Singer et al., 1984; Kaller & Kalso 2006), very few studies have been conducted to quantify their impacts on tree regeneration. Sieman et al (2009) found that feral hogs negatively affected the tree regeneration by feeding the seeds of water tupelo (*Nyssa aquatica*) in the mixed deciduous forest in Texas. The other possible reason could be the influence of insects on seed survival, which is still not fully understood (Kroschel et al., 2016). But a few studies have found that insect parasitism can also restrict the regeneration process of floodplain forests. In a study of *Taxodium*

distichum and *Nyssa aquatica*, Keeland (1995) found that low seed production and low seed viability due to insect parasitism were limiting the regeneration process. Further research is needed to address these decline in the hardwood swamps and increase of the bottomland hardwoods and pinelands in the study area.

4.1.c. Vegetation cover change and water level

The lack of change in river water levels over the study period confirms that the loss of hardwood swamps was not due to change in water level. My results were in contrast with the study conducted by Cecilia et al. (2016) in which they found that a decline in the hardwood swamp and bottomland hardwood vegetation was due to a decline in the water level. Further research would be needed to understand the exact reasons behind this decrease in hardwood swamp as and the increase in pineland vegetation.

4.2. Comparison of two methods

4.2. a. Comparison of accuracy assessments, change detection performed on two techniques

An accuracy assessment performed on vegetation identified by two methods on the 2008 image showed that while the overall accuracy of both were not very high (Kappa coefficient K= 0.47 in unsupervised classification; K= 0.59 for SI); both represented moderate agreement with the reference image (Jensen, 2015). The moderate accuracy of both the techniques suggest that the spectral separability of vegetation species is challenging in the study area. It is challenging because, all vegetation species contain same basic components that contribute to its spectral reflectance, including chlorophyll and other light-absorbing pigments, water, protein, starches, waxes, and structural molecules (Kokaly et al., 2003).

The lower classification accuracy of unsupervised classification could be due to the large number of mixed pixels. From the error matrix produced, it was evident that unsupervised classification misclassified the hardwood swamp pixels with bottomland hardwood pixels and vice versa. Several pixels of bottomland hardwood were also misclassified as pinelands. This is because there are several spots, where the pineland and bottomland hardwoods are present together as observed in field survey.

However, the error matrix obtained for accuracy assessment of the SI indicated that this technique misclassified most of the water/unclassified pixels with pineland pixels. Like the unsupervised classification, it also misclassified bottomland pixel as pineland pixels but not to the same degree as misclassified by unsupervised classification technique.

The high accuracy for classifying water pixels by unsupervised classification over the SI suggested that SI could not identify the water pixels as accurately as unsupervised classification. Higher accuracy of hardwood swamp and bottomland hardwood by SI over the unsupervised classification suggested unsupervised classification could not identify these two vegetation types as accurate as SI. This observation was also found in the study conducted in floodplain wetlands by Cecilia et al. (2016) where the error matrix showed higher accuracy for hardwood swamp and bottomland hardwoods than those for the water pixels derived from SI.

Although there were disagreements between the two methods as stated above in quantifying the vegetation cover over the period, both methods showed a similar trend. For example, hardwood swamp was found to have decreased and pinelands increased in extent according to both methods. Additionally, bottomland hardwoods were also found to have increased in both methods over the period of eighteen years. This strengthens the evidence that

SI has the potential to discriminate between the vegetation types and could be used as a vegetation identification technique.

4.2.b. SI identification versus Unsupervised classification

Different accuracy level by different techniques indicates that even in same area, different method yields different vegetation maps. SI derived vegetation showed highest difference with unsupervised classification in delineating areal coverage of pinelands for the year 1990; and highest difference in hardwood swamp for the year 2008. They also differed highest during the change detection of pineland forests. This difference suggests that even in same area, different approaches yield different change maps. This difference is due to the differences in the classification algorithms used by two methods. Unsupervised classification uses clustering algorithms such as ISODATA (Jensen, 2015) and users decides number of clusters for each class while SI methods uses a ratio of winter to summer NDVI values (Cecilia et al., 2016) and then the user classifies the classes between various ranges of SI values. This highest difference in pineland change detection and higher accuracy of classifying pineland by the unsupervised classification method suggests that further research should be done to identify the techniques in which these two methods could be combined to produce better classification results.

4.3. Temporal and spatial distribution of NDVI of vegetation types

The NDVI for a typical year (NTY) suggests that the NDVI pattern in different vegetation types is driven by change in seasons. As spring (March and April, DOY=1 to 90 to 120) approaches, trees begin reacting to increasingly longer periods of daylight and warming temperatures. This spurs chlorophyll production and photosynthesis in newly developing leaves. As spring moves to summer (May, June, July, and August; DOY = 150 to 230), when daytime temperature continues to rise, the leaves develop more fully and reach maturity. Then as winter

(December, January, and February; DOY= 290 to 365) approaches, temperature begin to cool and plants lower food production via photosynthesis and leaves begin to senescence. This changes the color of leaves due to a lack of chlorophyll and ultimately leads to falling of the leaves (Melaas et al., 2013).

It was evident from the NTY plot that, hardwood swamps, which thrive in the lowest elevation and has been reported to experience annual flooding and higher water permanency (Darst, 2008), reflect not only the lowest values of NDVI signatures, but also highest annual variability with seasons. The high variability in NDVI behavior indicates that trees (mainly hardwood swamps) at the lowest elevation are more sensitive to the season and time of the year; they increase their photosynthetic activity during summer and shed their leaves during winter season. In contrast to this, the middle to the highest elevation were colonized by bottomland hardwoods and pinelands, which are reported to be less flooded (Townsend 2001; Heitmeyer et a l., 1991). Pineland showed the highest NDVI values and the lowest annual variability, showing the unseasonal nature of these forests. Studies in the past have found that pinelands are only affected by extreme events such as extreme dry environmental conditions, suggesting more stable behavior (Cecilia et al., 2016, Marchetti et al., 2016).

The distribution of vegetation types along different range of elevation could be due to the physiological adaptations of hardwood swamp trees such as water tupelo and bald cypress. These species have been documented to possess higher flood tolerance and hence thrive at the lowest elevations that typically get submerged by water (Kroschel, 2016). Their capacity to survive under anoxic and saturated soil conditions limits their competition with other species (Darst, 2008) at these lower elevations. These observations denote that elevation and seasonality are driving the distribution of the vegetation and pattern of NDVI associated with them.

4.4. Assessing temporal variability in NDVI

4.4. a. Descriptive statistics of NDVI and predictor variables

The descriptive statistics of the predictor and response variable showed the difference in their mean values and standard deviation with seasons. Maximum NDVI values during the summer season in both vegetation types indicates that during this period, NDVI is influenced by the canopy foliage, that would maintain high biomass (Ramoelo et al., 2015). This also suggests that leaves turning green and expanding in spring (associated with the onset of photosynthesis) in deciduous canopies tends to be captured well by NDVI from Landsat (Barr et al., 2004).

Meanwhile, NDVI values in both vegetation types were lowest during non-growing or winter seasons (December to February), when deciduous trees drop their canopy foliage (Tomlinson et al., 2013). During both seasons (summer and winter), higher mean, range and standard deviation of NDVI values in hardwood swamps than that of bottomland hardwoods indicates higher NDVI variability in hardwood swamps. This supported my previous results where hardwood swamp exhibited larger variation with day of the year, indicating that they are more influenced by change in seasons.

For climatological variables (minimum, maximum, average temperature and rainfall), larger range and higher standard deviation during summer indicates higher variability of the climate variables in summer than winter. For hydrological variable such as mean weekly streamflow, higher values in winter was found, which is expected, because area receives most of its precipitation during winter, which increases the streamflow in rivers. In addition to this, during the winter season the vegetation undergoes senescence, with little to no evapotranspiration that leads to an increase in streamflow and water level in the river. This

observation supports previous studies where lower evapotranspiration rates due to low tree canopy raises the streamflow and water level in forested streams (Kolka et al., 2000).

4.4. b. Correlation analysis between NDVI and predictor variable (hydrological and climatological)

The strong positive correlation with climate variables and the medium negative correlation with hydrological variables suggests that hydrological variables does not influence the NDVI as much as climate variables in the study area. The negative correlation of NDVI with weekly streamflow values was expected because productivity increases evapotranspiration which results in decreased streamflow. The lack of correlation of NDVI with monthly precipitation suggests that monthly rainfall does not play a significant role in vegetation productivity in the study area. This was contradictory to the idea that rainfall provides sufficient moisture required to conduct the photosynthesis and respiration. Studies have found that rainfall in combination with temperature has a positive impact on vegetation productivity (Marques et al., 1998). While this relation could be stronger in drier regions, in subtropical forests such as my study area, rainfall might not have as pronounced effects as temperature. However, results seen in my study may vary if the time lags of daily rainfall and daily temperature datasets, would be considered, instead of monthly average.

Among the predictor variables, the negative correlation between monthly temperature (average as well as maximum) with streamflow suggests an adverse impact of temperature on streamflow. This is expected because, during growing seasons, warmer temperature leads trees to reach their full foliage which increases evapotranspiration. Increased evapotranspiration eventually lowers streamflow in the streams. During the winter or non-growing season-, little to

no evapotranspiration because of vegetation senescence leads to higher stream flows (Jones and Post 2004; Brooks, 2002).

4.4. c. Partial least square regression (PLSR) model determining temporal variability of NDVI in two vegetation types

The fit of the PLSR model ranged from a cumulative R^2 of 0.58 in bottomland hardwoods to 0.83 in hardwood swamps. Higher cumulative R^2 in PLSR model for hardwood swamps suggest that combination of predictor variables explain more variance in hardwood swamps than in bottomland hardwoods. Two latent factors were retained as factors in PLSR models for hardwood swamp and bottomland hardwoods, which means that there were two dimensions of variance in both vegetation types. Identical climate variables in both models (PLSR models of hardwood swamps and bottomland hardwoods) suggests that variability is influenced by similar climate variables. This could be due to the smaller size of the study area (55 km^2), where the vegetation types might have been behaving in a more homogenous manner with respect to climate variables. The fitted coefficients imply that vegetation productivity in the study area is more dependent on climatological variables instead of hydrological variables such as weekly streamflow (including time lags up to antecedent six weeks of streamflow). This contrasts with previous studies, which have found that that streamflow has positive impacts on bottomland hardwood trees which are less frequently flooded and located at higher elevation (Dudek et al., 1998; Keeland et al., 1995). It is likely possible to see an impact if the analysis could be conducted at a monthly time scale. For example, examining how streamflow affects the NDVI of either of the vegetation types during May, June, September or December.

PLSR models for hardwood swamps and bottomland hardwoods highlight that the monthly average temperature is the most important variable influencing the temporal variability

in NDVI. This is expected because, with an increase in monthly temperature, the vegetation productivity increases. Temperature affects several other aspects of vegetation, such as plant composition and diversity, phenology, and biomass. In subtropical forests of mid latitude regions, such as the one in this study, monthly temperature is strongly correlated with the vegetation productivity (Mao eta la., 2012; Marques et al., 2004; Hasenauer et al., 1999). Piao et al., (2003) found that the monthly average temperature showed highest correlation with vegetation productivity during most of the year, except the months of August and September in mid latitude forests of China. Piao examined the trend at different months of the year while my analysis presents a general scenario about how climatic factors regulate the vegetation productivity but did not examine monthly variability. In addition, to productivity, temperature has also been shown to regulate the evapotranspiration rates in forests (Chen et al., 2018, Zha et al., 2013). While my analysis did not look at how trees drive the stream hydrology, these forests have an important role in regulating the overall watershed ecosystem.

Both models (PLSR models for hardwood swamp and bottomland hardwoods) showed monthly average temperature of the antecedent two months as the second most important variable. This suggests that the monthly variation in temperature does not solely change the underlying pattern in NDVI; instead it is also controlled by the antecedent two-month temperature conditions. This time lag is expected because, plants need enough thermal time for leaf onset, which is regulated by temperature. This time is needed to increase the primary productivity by assimilating carbon after leaf emergence in spring (Chen et al., 2018).

Both models showed a positive correlation with monthly maximum temperature (as the third most important variable in both models). This observation contrasts with the idea that with an increase in maximum temperature above optimal conditions photosynthesis may decline

sharply, and severely affect the carbon balance. Respiration also increases exponentially with increasing temperature, so at some point carbon loss exceeds carbon gain (Seyednasrollaha et al., 2018; Luedeke et al., 1994). In this study area, the higher coefficient of monthly maximum temperature is associated with hardwood swamp. The possible explanation behind this observation could be since roots of hardwood swamps are inundated more often than other vegetation. Higher temperature combined with an adequate amount of moisture throughout the year could increase the plant productivity. However, this phenomenon could vary during different months of the year. Further research is required to analyze during which months of the year the maximum temperature could be most beneficial to vegetation productivity of hardwood swamps.

Both models showed a negative correlation with the monthly minimum temperature, which is expected because with a decrease in temperature the productivity also decreases. This observation is consistent with the other studies, where minimum temperature has been correlated with the leaf fall and reported to negatively affect the vegetation productivity of deciduous forest systems (Marques et al., 2004).

The difference in the coefficients of climate variables among the two models arises due to the difference in the timing between leaf growth/decay, availability of sunlight and temperature, the likely start of photosynthesis, and spring leaf development (Kikuzawa, 2003, Yang et al., 2015). Such differences in response of climatic variables were also found by a study conducted within deciduous forests of Petersham, Massachusetts, using high-resolution aerial photography techniques. This study found a difference of 20 days between leaf color timing of red maple and American beech; indicating phenology varies with the tree species (Klosterman et al., 2018).

The sets of variables were found to be unable to model the NDVI variability in different seasons. The PLSR models with very low R^2 and large number of factor stated that variation in NDVI could not be explained by the combination of the predictor variables taken in this study. This suggested that there could be more factors that might have been playing a role in temporal variability of NDVI during winter and summer seasons in either of the vegetation types. It is also possible that a shorter time lag of 7 days to 10 days in climate variables and their combination might show pronounced effects on the NDVI variability at seasonal scale (winter/summer). Therefore, in the future, incorporating shorter time lags (days instead of months) could help establish the relationship between climate variables and seasonal NDVI.

Significant changes in the temperature might have a profound effect on functional aspects of the ecosystem. The Southeastern US is expected to experience an increase in the rate of warming through the end of the century, with a rise in average temperature of 2.5 to 5°C by the 2080s (Karl et al., 2009). The precipitation trend indicates a decline of 10% to 30% of summer time precipitation (IPCC, 2007). Therefore, it becomes important to study the climate effects on rapidly decreasing swamp vegetation.

This analysis provides a general background about how climate variables affect the vegetation productivity in the forested wetlands. This analysis could not identify the underlying phenomenon at seasonal or inter-annual variability due to several limitations to the study. First, due to limited satellite images, impacts of climatological and hydrological impacts could not be studied at a monthly scale. The number of usable images was relatively small because of the lower temporal resolution (16-day revisit period), in conjunction with frequent cloud cover in subtropical regions. The 110 images for twenty years (1990-2013) suggested that on average only 5 images were available for a year. As a result, establishing a relationship between variables

and NDVI according to each month or season for the 23 years was challenging. It is possible to increase the number of images by using MODIS satellite imagery (1-day revisit period), but its lower spatial resolution (250 m) limits its use in relatively smaller areas such as this (55 km^2). Second, the first-time lag of each climatic variable started by 30 days in my datasets; closer time lags of 10 days or 15 days could enhance or differ the results. Therefore, higher spatial and temporal resolution images, combined with shorter time lag will be required in the future to diagnose the in-depth leaf phenology in more detail. A better understanding is clearly needed to develop more accurate models.

4.5. Assessing spatial variability in NDVI

4.5.a. Spatial variability (due to inundation frequency) of NDVI

This analysis also compared hardwood swamp and bottomland hardwood vegetation types; which are supposed to be seasonally flooded. Pine trees, thriving along the higher elevation areas are supposed to be unaffected by flooding, and therefore, were excluded. Results shows that the range of values of inundation frequency increased with the increasing magnitude of the flood recurrence interval. This was expected because higher magnitude flood would cover larger area of the floodplain. Also, the areas or the pixels nearest to the channel would have highest flood inundation frequency value (during each flood), as that pixel would be more frequently inundated.

However, the simple linear regression model between flood inundation frequency and NDVI showed no relation between the two. This observation of no relation was consistent in both vegetation types under three different flood scenarios (5-year, 10-year and 37- year recurrence interval). This indicates that the inundation frequency doesn't play a role in spatial variability of NDVI in either of the vegetation types in the study area. The reason behind

observing no relation between NDVI and inundation frequency could be due to the length of time considered for flood simulation. Because of the computationally complicated and time-consuming nature of the CAESAR model (Coulthard, 2001), floods (5-year, 10-year, and 37-year) were simulated for a shorter period (20 days). The shorter simulation could have missed the recession of the floodwater and retention of standing water in low lying areas and secondary channels. Had there been longer simulations of each flood, there may have been some correlation with the vegetation productivity. Therefore, simulation period was not sufficient for the floods to show noticeable impacts on the vegetation indices. Further research is needed to analyze the long-term impact of floods and their roles in regulating the vegetation productivity.

Flooding has been demonstrated to affect the ability of plants to maintain the store reserves that are crucial for their survival. This phenomenon drives a difference between productivity among mature trees and thereby affects forest composition along the floodplains forests (Townsend 2001). This study did not look at the forest composition due to flooding but expected to see variations in the NDVI due to flooding in the two vegetation types in the floodplain. In fact, this study expected to find a decreasing trend of NDVI with increasing flood inundation frequency because, from an ecological point of view, flooding could kill the seedlings by creating anaerobic conditions and thereby affect the NDVI pattern.

My results contrasted with other studies conducted in similar areas, which have found that the frequency of flooding was among the strongest hydrological predictor of vegetation productivity. Cecilia et al. (2016) found that in the hardwood swamps of the Apalachicola delta, fewer inundation events tend to increase the NDVI. Sims and Thoms (2002) also reported that floodplains that were less frequently inundated had more vigorous vegetation (and hence higher NDVI) due to oxygenated soil and less disturbance affecting seedling survival. However, it is

important to note that these studies were based on flood simulations for longer period while my study considered only 20-day simulations due to computational limitations of the model. In addition, growth and survival of hardwood swamp trees are dependent on the wide range of hydrologic conditions. Study conducted by Rypel (2009) in the Sipsey watershed found that high flows replenished the nutrients along the floodplain and positively affected the growth of bald cypress trees (hardwood swamp tree). While Keeland et al. (1995) found that the germination of the bald cypress seeds was poor during long standing water and successful germination occurred only during the dry years when seeds fall into non-inundated floodplain soil (Keeland et al., 1995). Therefore, future research is also needed to examine the impact of flooding at different stages of the tress regeneration.

There were several limitations to this analysis. The first was analyzing the two rasters of different spatial resolution. This analysis required resampling of the flood inundation raster from 10 m to 30 m; which could have lost the information from inundated pixels and vegetation associated with it. Secondly, the small areal coverage or AOI (area of interest) of the study area could have several mixed pixels of vegetation and water. These mixed pixels might have dampened the values of NDVI associated with the pixels. Therefore, in the future, better delineation of water and vegetation pixels could improve the results.

Swamps such as the ones created by the Sipsey River are dynamic systems due to annual and seasonal variation in timing, depth, and duration of flooding (Heitmeyer eta l., 1991). In such systems, inundation frequency and wetting patterns are often the known mechanisms that select which species develop and where. Field observations during this study provided the evidence that most of the hardwood swamp species (water tupelo and bald cypress), which are more flood tolerant grow nearest to the channel and along the lowest elevation. Therefore, incorporating

high resolution DEM data (e.g, <0.2m vertical and 5m horizontal) along the floodplain topography in combination with high resolution (spatial and temporal) satellite image, would strengthen the analysis to quantify the effects of floods on the vegetation productivity. Studying these eco-hydrological relationships in the watersheds like Sipsey River becomes more important as it is one of the few remaining free flowing rivers in Alabama and supports a variety of biologically diverse flora and fauna. Hence, collection and documentation of such relationships would help make more informed decisions in floodplain management projects in the future.

5. CONCLUSIONS

Unsupervised classification and SI identification techniques successfully identified three dominant vegetation types in the study area; with overall medium accuracy. While unsupervised classification showed higher accuracy for water and pinelands, the SI showed higher accuracy in identifying the hardwood swamp and bottomland hardwood vegetation.

Normalized Difference Vegetation Index, used as a proxy of vegetation productivity, successfully captured the changes occurred in the vegetation types driven by seasonality and elevation. The distribution of the vegetation and their associated NDVI was found to be changing along different elevations in the study area. While pinelands were found to be situated along the highest elevation; hardwood swamps were present along the lowest elevation. The field survey to identify vegetation also proved this distribution, as hardwood swamps were limited along the lowest elevation and pinelands were along the highest elevation.

Change detection by both methods showed that there has been a decrease of hardwood swamp vegetation over the study period. Investigation of seasonal and annual water levels over the period found that there has not been any trend in the decrease or increase of water level. This confirmed that the change in vegetation cover was not due to change in water level. The possible reason of decreasing hardwood swamp could be due to the replacement of floodplain vegetation for agricultural purposes, species replacement and commercial plantation over the period. Further study is needed to verify what factors led to this decrease in hardwood swamp and increase in pine trees in the study site.

For two vegetation types, hardwood swamp and bottomland hardwoods, NDVI values showed high correlation coefficients with the climate variables such as maximum, minimum and average monthly temperature; weak negative correlation with the monthly rainfall variable; and medium negative correlation with hydrological variable such as weekly streamflow.

The temporal variability in the NDVI determined by the partial least square regression modeling approach found that the NDVI variability is predominantly regulated by the climate variables instead of hydrological variables. The most important variables in both models were, average monthly temperature, average monthly temperature of antecedent two months, followed by the monthly maximum temperature. Monthly average temperature, and its time lag playing the most important factor in temporal variability of NDVI supports several previous investigations of impact of climate variables on the vegetation productivity in the deciduous forests. Both model showed a negative correlation with the minimum temperature. Partial least square regression models for summer and winter seasons separately were unable to be produced with the datasets used in this study. Which suggests that seasonal NDVI could be more complex and there might be additional factors that regulates the seasonal NDVI.

Spatial variability in NDVI determined by linear regression found that there is no relationship between flood inundation frequency and NDVI. The result was identical in case of all the floods of 5-year, 10-year and 37-year recurrence interval. This analysis identified that spatial variability in NDVI due to inundation frequency could be detected if the floods are simulated for a longer period which would capture the recession of the flood water and the retention of water in secondary channels.

My study successfully identified three different vegetation types and found that vegetation distribution is driven by seasonality and elevation. Hydrological parameters such

streamflow and water level were found to have no relation with the vegetation productivity and change in areal coverage over the period. Limited studies have been conducted to analyze the regulatory effects of climate variables on the floodplain forests like the one in the study area. While there were several limitations to the study, results of this study serve as a background on how natural ecosystems work along floodplain forests created by unregulated rivers in the southeastern US.

My study also demonstrated that by providing the information related to NDVI, the 30-year archive of Landsat data has the potential to significantly improve understanding of how climate controls forest phenology. Utilizing two methods of vegetation identification, it was realized that techniques to combine the two methods in future research would enhance the classification accuracy for each vegetation type. However, from a purely empirical perspective, the combination of long-term field observations and higher-resolution (both temporal and spatial) satellite images should be used to understand the species-specific phenology and their response to the climate and hydrological variables. Considering the smaller time lags of 7, 10 or 15 days might affect or enhance the results of model predictions of temporal variability in NDVI. In addition, incorporating high resolution DEMs in the floodplain modeling, combined with high resolution aerial images could help to establish an improved eco-hydrological relationship.

REFERENCES

Alabama Department of Conservation and Natural Resources. 2016. 2016 Annual Report. Montgomery.

Alabama Department of Conservation and Natural Resources. 2012. Fisheries section, Division of Wildlife and Freshwater Fisheries. Montgomery.

Alabama Department of Conservation and Natural Resources Lands Division. 2009. Restoration and enhancement of the Pine ecosystem and mixed forest floodplain in applicable Forever Wild Land Trust Lands. Montgomery.

Anchang, J.Y., Ananga, E.O., Pu, R. 2016. An efficient unsupervised index-based approach for mapping urban vegetation from IKONOS imagery. *International Journal of Applied Earth Observation and Geoinformation.* 50, 211-220.

Apalachicola National Estuarine Research Reserve. 2013. Management Plan, Tallahassee, Fl.

Asner, G.P., Martin, R.E. 2008. Spectral and chemical analysis of tropical forests: scaling from leaf to canopy levels. *Remote Sensing of Environment*, 112 (10), 3958-3970.

Baker, W.L. 1989. Macro-and Micro-scale influences on Riparian Vegetation in Western Colorado. *Annals of the Association of American Geographers banner*, 79 (1), 65-78.

Barbosa, H.A. Huete, A.R., Baethgen, W.E. 2006. A 20-year study of NDVI variability over the northeast region of Brazil. *Journal of Arid Environment*, 67 (2), 288-307.

Barr, A.G., Black, T.A., Hogg, E.H., Kljun, N., Morgenstern, K., Nesic, Z. 2004. Inter-annual variability in the leaf area index of a boreal aspen-hazelnut forest in relation to net ecosystem production. *Agricultural and Forest Meteorology*, 126 (3–4), 237–255.

Battaglia, L.L., Minchin, P.R., Pritchett, D.W. 2002. Sixteen years of old-filed succession and reestablishment of a bottomland hardwood forest in the Lower Mississippi Alluvial Valley. *Wetlands* 22 (1), 1-17.

Beedlow, P.A., Lee, E.H., Tingey, D.T., Waschmann, R.S., Burdick, C.A. 2013. The importance of seasonal temperature and moisture patterns on growth of Douglas-fir in western Oregon, USA. *Agricultural and Forest Metereology*, 169, 174–185.

Benke, A.C. 1990. A perspective on America's vanishing streams. *Journal of North American Benthological Society*, 9, 77-88.

Benke, A.C., Chaubey, I., Milton Ward, G., Dunn, El. L. 2000. Flood pulse dynamics of an unregulated river floodplain in the southeastern U.S coastal plain. *Ecology* 81, 2730-2741.

Bledsoe, B.P., Shear, T.H. 2000. Vegetation along hydrologic and edaphic gradients in a North Carolina coastal plain creek bottom and implications for restoration. *Wetlands*, 20 (1), 126–47.

Brauman, K.A., Daily, G.C., Duarte, T.K., Mooney, H.A. 2007. The nature and values of ecosystem services: An overview highlighting hydrologic services. *Annual Review of Environmental Resources,* 32, 67-98.

Brooks, R.T. 2002. Weather related effect on woodland vernal pools hydrology and hydroperiod. *Wetlands*, 1 (24), 104-114.

Brinson, M.M., Lugo, A.E., Brown, S. 1981. Primary productivity, decomposition and summer activity in freshwater wetlands. *Annual Review of Ecology, Evolution and Systemics*, 12, 123-161.

Bulcock, H.H., Jewitt, G.P. 2010. Spatial mapping of leaf area index using hyperspectral remote sensing for hydrological applications with a particular focus on canopy interception. *Hydrology and Earth System Science,* 14, 383-392.

Cain, M.D., Shelton, M. 2001. Secondary forest succession following reproduction cutting on the upper coastal plain of southeast Arkansas, USA. *Forest Ecology and Management,*146, 222-238.

Calzada, A., Barquin, J., Huszar, V., Mazzeo, N., Mendex, F., Martinez, M. 2017. Long-term dynamics of a floodplain shallow lake in the Pantanal wetland: Is it all about climate? *Science of Total Environment*, 605-606, 527-540.

Cecilia, D., Toffolon, M., Woodcock, C.E, Fagherazzi, S. 2016. Interaction between river stage and wetland vegetation detected with Seasonality Index derives from LANDSAT images in the Apalachicola delta, Florida. *Advances in Water Resources*, 89, 10-23.

Chen, Y., Xue, Y., Hu, Y. 2018. How multiple factors controls evapotranspiration in North America evergreen needle leaf forests. *Science of Total Environment,* 622-623, 1217-1224.

Chuai, X., Huang, X., Wang, W., Bao, G. 2013. NDVI, temperature and precipitation changes and their relationship with different vegetation types during 1998-2017 in Inner Mongolia, China. *International Journal of Climatology*, 33, 1696-1706.

Cissell. J.R., Delgado, A.M., Sweetman, B.M., Steinberg, M.K. 2018. Monitoring mangrove forest dynamics in Campeche, Mexico, using Landsat satellite data. *Remote Sensing Applications: Society and Environment*, 9, 60-68.

Coppin, P., Jonckheere, I., Nackaerts, K., Muys, B. 2004. Digital change detection methods in ecosystem monitoring: a review. *International Journal of Remote Sensing*, 25 (9), 1565-1596.

Coulthard, T.J., Kirkby, M.J., Macklin, M.G. 1998. Non-linearity and spatial resolution in a cellular automaton model of a small upland basin. *Hydrology and earth System Sciences*, 2 (2-3), 257-264.

Coulthard, T.J., Macklin, M.G., Kirkby, M.J 2002. A cellular model of Holocene upland river basin ad alluvial fan evolution. *Earth Surface Processes Landforms*, 27 (3), 269-288.

Coulthard, T.J., Macklin, M.G., Kirkby, M.J. 2001. A cellular model of Holocene uplands river basin and alluvial fan evolution. *Earth Surface Processes and Landforms*, 27, 269-288.

Dahl, T.E., Johnson, C.E. 1991. Status and trends of wetlands in the conterminous United States.: Mid 1970s to mid-1980s. *US Department of Interior Fish and Wildlife Services*, Washington DC.

Dalrymple, T. 1960. United State Geological Survey. Flood frequency analyses, Manual of hydrology: Part-3. Washington DC.

Darvishzadeh, R., Skidmore, A., Atzberger, C., Wieren, S. 2008. Estimation of vegetation LAI from hyperspectral reflectance data: Effects of soil type and plant architecture. *International Journal of Applied Earth Observation and Geoformation*, 10 (3), 358-373.

Day Jr., J.W., Shaffer, G.P., Britsch, L.D., Reed, D.J., Hawes, S.R., Cahoon, D.R. 2000. Pattern and process of land loss in the Mississippi Delta: a spatial and temporal analysis of wetland habitat change. *Estuaries* 23 (4), 425–438.

De Steven, D. & Sharitz, R.R. 1997. Differential recovery of a deep-water swamp forest across a gradient of disturbance intensity. *Wetlands*, 17 (4), 476–484.

Dudek, D.M., Mccleanahen, J.R., Mitsch, W.J. 1998. Tree growth response of populous deltoids ad *Juglans nigra* to streamflow and climate in bottomland hardwood forest in Central Ohio. *The American Midland Naturalist*, 140 (2), 233-244.

Duncan, R.S. & Linhos, J.E. 2005. Regeneration of Virginia pine (*Pinus virginiana*) following southern pine beetle (*Dendroctonus frontalis*) outbreak in the Sipsey Wilderness, Alabama. *Forest Ecology and Management*, 212 (1-3), 65-74.

Ersnt, K.A. & Brooks, J.R. 2001. Prolonged flooding decreased stem density, tree size and shifted composition towards clonal species in a central Florida hardwood swamp. *Forest Ecology and Management*, 173 (1-3), 261-279.

Farjat, A., Reich, B.J., Guinness, J., Whetten, R., McKeand, S., Isik, F. 2017. Optimal Seed Deployment Under Climate Change Using Spatial Models: Application to Loblolly Pine in the Southeastern US. *Journal of American Statistical Association*, 112, 909-920.

Feister, U., Junk, J., & Woldt, M. (2008). Long-term solar UV radiation reconstructed by Artificial Neural Networks (ANN). *Atmospheric Chemistry and Physics Discussions*, 8 (1), 453-488.

Frensholt, R. & Rasmussen, K. 2011. Analysis of trends in Sahelian "rain-use efficiency" using GIMMS NDVI, RFE and GPCP rainfall data. *Remote Sensing of Environment*, 115 (2), 438-451.

Gitelson, A.A., Y.J. Kaufman, and M.N. Merzlyak, 1996. Use of a green channel in remote sensing of global vegetation from EOS-MODIS. *Remote Sensing of Environment*, 58, 289–298.

Haag, W.R. & Warren, M.L. 2010. Diversity, abundance, and size structure of bivalve assemblages in the Sipsey River, Alabama. *Aquatic Conservation Marine and Freshwater Ecosystems*, 20 (6), 655-667.

Hall, T.F. & Smith, G.E. 1955. Effects of flooding on woody plants, West Sandy dewatering project, Kentucky Reservoir. *Journal of Forestry*, 53 (4), 281-285.

Harvey., K.R, Hill., J.E. 2001. Vegetation mapping of a tropical freshwater swamp in the Northern Territory, Australia: a comparison of aerial photography, Landsat TM and SPOT satellite imagery. *Remote Sensing of Environment*, 22, 2911–2925.

Hasenauer, H., Nemani, R., Schadauer, K., Running, S. 1999. Forest growth response to changing climate between 1961 and 1990 in Austria. *Forest Ecology and Management*, 122 (3), 209-219.

Heitmeyer, M.E., Fredrickson, L.H., Krause, G.F. 1991. Water relationships among wetland habitat types in the Mingo Swamp, Missouri. *Wetlands*, 11 (1), 55-66.

Hillard, E.M., Nielson, C.K., Groninger, J.W. 2017. Swamp rabbits as indicators of wildlife habitat quality in bottomland hardwood forest ecosystems. *Ecological Indicators*, 79, 47-53.

Hodges, J.D. 1997. Development and ecology of bottomland hardwood sites. *Forest Ecology and Management*, 90, 117-125.

Hoeppner, S.S., Rose, K.A. 2011. Individual-based modeling of flooding and salinity effects on a coastal swamp forest. *Ecological Modelling*, 222, 3541-3558.

Hoeppner, S.S., Shaffer, G.P., Perkins, T.E. 2008. Through droughts and hurricanes: Tree mortality, forest structure, and biomass production in a coastal swamp targeted for restoration in the Mississippi River Deltaic Plain. *Forest Ecology and Management*, 256, 937-948.

Hook, D.D. 1984. Waterlogging tolerance of lowland tree species of the south. *Southern Journal of Applied Forestry,* 8 (3), 136–49.

Hook, D.O., De Bell. D.S., Askew, J.L. 1983. Response of loblolly pine (mesophyte) and swamp tupelo (hydrophyte) seedling to soil flooding and phosphorous. *Plant and Soil*, 71 (1-3), 387-394.

Hopper, J., Huryn, A. & Schuster, G. 2012. The Sipsey River, Alabama: A crayfish diversity "hotspot"? *Southeastern Naturalist,* 11 (3), 405-414.

Huang, K. 2002. Synergistic Automatic clustering techniques for multispectral image analysis. *Photogrammetric Engineering and Remote Sensing*, 68(1), 33-40.

Huang, C., Chen, Y., Wu. J. 2014. Mapping spatio-temporal flood inundation dynamics at large river basin scale using time-series and MODIS imagery. *International Journal of Applied Earth Observation and Geoformation*, 26, 350-362.

Ichii, K., Kawabata, A., Yamaguchi, Y. 2002. Global correlation analysis for NDVI and climatic variables and NDVI trends, 1982-1990. *International Journal of Remote Sensing*, 23 (18), 3873-3878.

Jensen, J.R. 2016. Introductory digital image processing: A Remote Sensing Perspective. Upper Saddle River, NJ: Pearson.

Jeong, S., David Schimel, D., Frankenberg, C., Drewry, D.T., Fisher, J.B., Verma, M., Berry, J.A., Lee, J., Joiner, J. 2017. Application of satellite solar-induced chlorophyll fluorescence to understanding large-scale variations in vegetation phenology and function over northern high latitude forests. *Remote Sensing of Environment*, 190, 178-187.

Jones, T.G., Ratsimba, H.R, Ravaoarinorotsihoarana L., Cripps, G., Bey, A. 2014. Ecological variability and carbon stock estimates of mangrove ecosystems in northwestern Madagascar. *Forests* 5(1), 177-205

Jones, J.A., Post, D.A. 2004. Seasonal and successional streamflow responses to forests cutting and regrowth in the northwest and eastern United States. *Water Resources Researches*, 5 (40), 1-19.

Jones, R.H., Sharitz, R.R., Dixon, P.M., Segal, D.S., Schneider, R.I. 1994. Woody plant regeneration in four floodplain forests. *Ecological Monographs,* 64 (3), 345-67.

Junk, W.J., Bayley, P.B., Sparks, R.E. 1989. The flood pulse concept in river-floodplain systems, p. 110-127. Proceeding of the International Large River Symposium. *Canadian Special Publications of Fisheries and Aquatic Sciences*, 106, 110-127.

Karl, T.T., Melillo, J.M., Peterson, T.C., Hassol, S.J. 2009. Global climate change impacts in the United States. US Global Change Research Program, 13-26.

Kaszta, Ż., Van De Kerchove, R., Ramoelo, A., Cho, M.A., Madonsela, S., Mathieu, R., Wolff, E. 2016. Seasonal separation of African savanna components using worldview 2 imagery:

a comparison of pixel-and object-based approaches and selected classification algorithms. *Remote Sensing*, 8 (9), 763.

Keddy, P. 2000. Wetland Ecology Principles and Conservation. Cambridge University Press, Cambridge.

Keeland, B.D., Sharitz, R.R. 1995. Seasonal growth patterns of *Nyssa sylvatica var biflora*, *Nyssa aquatica*, and *Taxodium distichum* as affected by hydrologic regime. *Canadian Journal of Forest Resource*, 25 (7), 1084–1096.

Kaller, M.D., Kelso, W.E. 2006. Swine activity alters invertebrate and microbial communities in coastal plain watershed. *American Midland Naturalist*, 156, 784-799.

Kellison, R.C., Young, M.J. 1997. The bottomland hardwood forest of the southern United States. *Forest Ecology and Management*, 90 (2-3), 101-115.

Kokaly, R.F., Despain, D.G., Clark, R.N., Livo, K.E. 2003. Mapping vegetation in Yellowstone National Park using spectral feature analysis of AVIRIS data. *Remote Sensing of Environment*, 84(3), 437-456.

Kolka, R.K., Singer, Coppock, C.R., Casey, W.P., Trettin, C.C. 2000. Influence of restoration and succession on bottomland hardwood hydrology. *Ecological Engineering*, 15, 131-140**.**

Kovacs, J.M., Wang, J., Blanco-Correa, M. 2001. Mapping disturbance in a mangrove forest using multi-date Landsat imagery. *Environment Management*, 27 (5), 763-776.

Kikuzawa, K., 2003. Phenological and morphological adaptations to the light environment in two woody and two herbaceous plant species. *Functional Ecology*, 17 (1), 29–38.

Kirkman, L.K., Brown, C.L., Leopald, D.J. 2007. Native trees of Southeast, an identification guide. Portland, Oregon: Timber press.

Klostermana, S., Melaas, E., Wang, J.A, Martinezc, A., Frederickc, S., Keefec, J.O., Orwigc, D.A., Wang, Z., Sund, Q., Schaafd, C., Friedl, M., Richardson, A.D. 2018. Fine-scale perspectives on landscape phenology from unmanned aerial vehicle (UAV) photography. *Agricultural and Forest Meteorology*, 248 (15), 397-407.

Kroschel, W.A., King, S.L., Keim, R.F. 2016. Tree regeneration by seed in bottomland hardwood forests: a review. *Proceeding of the 6th Big thickest science conference: watersheds and waterflow southeastern naturalist 15* (Special issues 9), 42-60.

Lazaridis, D.C., Verbesselt, J., Robinson, A.P. 2011. Penalized regression techniques for prediction: a case study for predicting tree mortality using remotely sensed vegetation indices. *Canadian Journal of Forest Resources*, 41 (1), 24-34.

Lillesand, T. & Kiefer, R. 2000. Remote sensing and Image Interpretation. Fourth Edition, New York: John Wiley & Sons.

Linderholm, H.W., 2006. Growing season changes in the last century. *Agriculture and Forest Meteorology*, 137 (1–2), 1–14.

Liu, Z.J., Wu, C.Y., Liu, Y.S., Wang, X.Y., Fang, B., Yuan, W.P., Ge, Q.S., 2017. Spring green-up date derived from GIMMS3g and SPOT-VGT NDVI of winter wheat cropland in the North China plain. *Journal of Photogrammetry and Remote Sensing*, 130, 81–91.

Long JB, Giri C (2011) Mapping the Phillippines' mangrove forests using Landsat imagery. Sensors 11(3):2972-2981

Los, S.O., Justice, C.O., Tucker, C.J. 1994. A global 1*1-degree NDVI data set for climate studies derived from the GIMMS continental NDVI data. *International Journal of Remote Sensing*, 15 (17), 3493-3518.

Mao, D., Wang, Z., Luo, L., Ren, C. 2012. Integrating AVHRR and MODIS data to monitor NDVI changes and their relationships with climatic parameters in Northeast China. *International Journal of Applied Earth Observation and Geoinformation*, 18, 528-536.

Marchetti, Z.Y., Minotti, P.G., Ramonell, C.G., Schivo, F., Kandus, P. 2016. NDVI patterns as indicator of morpho dynamic activity in the middle Parana River floodplain. *Geomorphology*, 253, 146-158.

Marques, M.C., Roper, J.J., Salvalaggio, A.P.B. 2004. Phonological patterns among plant life forms in a subtropical forest in southern Brazil. *Plant Ecology*, 13, 203-213.

Martens, H., Hoy, M., Westad, F., Folkenberg, D., Martens, M. 2001. Analysis of designed experiment by stabilized PLSR regression and jack-knifing. *Chemometric and Intelligence Laboratory Systems*, 58 (2), 151-170.

Maxwell, J.T., Knapp, P.A. 2012. Reconstructed tupelo-honey yield in northwest Florida inferred from *Nyssa ogeche* tree ring data: 1850-2009. *Agriculture Ecosystem and Environment*, 149, 100-108.

McCarthy, J., Gumbricht, T., McCarthy, T.S. 2005. Ecoregion classification in the Okavango Delta, Botswana from multitemporal remote sensing. *International Journal of Remote Sensing*, 26, 4339–435.

McCarthy, S.E., Evans, J.P. 2000. Population dynamics of Overcup Oak (*Quercus lyrate*) in a seasonally flooded karst deposition. *Journal of the Torrey Botanical Society*, 127 (1), 9-18.

McCullagh, W., Williams, J., McGregor, S., Pierson, J., Lydeard, C. 2002. The unionid (Bivalia) fauna of the Sipsey River in northwestern Alabama, an aquatic hotspot. *American Malacological Bulletin*, 17 (1-2), 1-15.

MEA (Millennium Ecosystem Assessment). 2005. Ecosystem and Human Well Being-Synthesis. Washington: Island Press.

Megonigal, J.P. and Day, F.P. 1992. Effects of flooding on root and shoot production of bald cypress in large experimental enclosures, *Ecology*, 73, 1182--1193.

Meitzen, K.M. 2009. Lateral channel migration effects on riparian forest structure and composition, Congaree River, South Carolina, USA. *Wetlands*, 29 (2), 465-475.

Melaas, E.K., Friedl, M.A., Zhu, Z. 2013. Detecting interannual variation in deciduous broadleaf forest phenology using Landsat TM/ETM+ data. *Remote Sensing of Environment,* 132, 176–185.

Mevik, B.H., Wehrens, R. 2007. Principal component and Partial least square regression model in R. *Journal of Statistical Software,* 18 (2), 1-23.

Middelton, B.A., McKee, K.L. 2004. Use of latitudinal gradient in bald cypress (*Taxodium distichum*) production to examine physiological controls of biotic boundaries and potential response to environmental changes. *Global Ecology and Biogeography,* 13, 247-258.

Milzow, C., Burg, V., Kinzelbach, W. 2010. Estimating future ecoregion distributions within the Okavnago Delta Wetlands based on hydrological simulations and future Climate and development scenarios. *Journal of Hydrology,* 381 (1-2), 89-100.

Nabavi, M., Dahlen, J., Schimleck, L., Eberhardt, T.L., Montes, C. 2018. Regional calibration models for predicting loblolly pine tracheid properties using near-infrared spectroscopy. *Wood Science Technology*, 52 (2), 445-463.

Nicholsan, S.E., Davenport, M.L., A.R. 1990. A comparison of the vegetation response to rainfall in the Sahel and East Africa, using normalized difference vegetation index from NOAA AVHHR. *Climate Change*, 17 (2-3), 209-241.

Otto, M., Scherer, D., Richters, J. 2011. Hydrological differentiation and spatial distribution of high altitude wetlands in a semi- arid Andean region derived from satellite data. *Journal of Hydrology and Earth System Sciences*, 15 (5), 1713.

Onoz, B. and Bayazit, M.2003. The Power of Statistical Tests for Trend Detection. Turkish *Journal of Engineering & Environmental Sciences*, 27, 247 – 251.

Pasher J, King DJ. 2010. Multivariate forest structure modelling and mapping using high resolution airborne imagery and topographic information. *Remote Sensing of Environment,* 114, 1718-1732.

Pezeshki, S. R. 1994. Responses of bald cypress seedlings to hypoxia: leaf protein content, ribulose-1, 5-biphosphate carboxylase/oxygenase activity and photosynthesis. *Photosynthetica*, 30, 59-68.

Piao, S., Mohammat, A., Fang, J., Cai, Q., Feng, J. 2006. NDVI-based increase in growth of temperate grasslands and its responses to climate changes in China. *Global Environmental. Change,* 16 (4), 340–348.

Piao, S.L., Fang, J.Y., Zhou, L., Guo, Q.H., Mark, H., Ji, W., Li, Y., Tao, S. 2003. Inter-annual variations of monthly and seasonal normalized difference vegetation index (NDVI) in China from 1982 to 1999. *Journal of Geophysical Research*, 108 (14), 1-12.

Poff, N.L., Allan, J.D., Bain, M.B., Karr, J.R. 1997. The natural flow regime, paradigm for river conservation and restoration. *Bioscience*, 47 (11), 769-784.

Praskievicz, S. 2016. Modeling hillslope sediment yield using rainfall simulator field experiments and partial least square regression: Cahaba River watershed, Alabama (USA). *Environmental Earth Science*, 75, 75-1324.

Qi, Y. 1999. The effects of climate change on vegetation at high latitudes of the northern hemisphere, a functional analysis. *Acta Ecologica Sinica*, 19 (4), 474-477.

Ramoelo, A., Cho, M.A., Mathieu, R., Madonsela, S., Van De Kerchove, R., Kaszta, Z., Wolff, E. 2015. Monitoring grass nutrients and biomass as indicators of rangeland quality and quantity using random forest modelling and WorldView-2 data. *International Journal of Applied Earth Observation and Geoinformation*, 43, 43–54.

Rajan, P., Shukla, S., Bajpai, D. 2015. Assessment of natural resources in part of Lucknow, district Uttar Pradesh using unsupervised classification. *Procedia Computer Science*, 57, 1440-1445.

Rouse, J. W., R. H. Haas, J. A. Schell, and D. W. Deering, 1973. Monitoring vegetation systems in the Great Plains with ERTS, Third ERTS Symposium, NASA SP-351 I, 309-317.

Reid, M.L., S.R. Allen., Bhattacharjee, J. 2014. Patterns of spatial distribution and seed dispersal among bottomland hardwood tree species. Southern Appalachian Botanical Society. *Castanea*, 79 (4), 255-265.

Renza, D., Martinez, E., Molina, I., Ballesterso, D.M. 2017. Unsupervised change detection vegetation land cover type using spectral angle mapper. *Advances in Space research*, 59, 2019-2031.

Rypel, A. L., W. R. Haag, and R. H. Findlay. 2009. Pervasive hydrologic effects on freshwater mussels and riparian trees in southeastern floodplain ecosystems. *Wetlands*, 29, 497-504.

Schneider, R. L. & Sharitz, R.R. 1988. Hydrochory and regeneration in a bald cypress-water tupelo swamp forest. *Ecology*, 69 (4), 1055–1063.

Seyednasrollaha, B., Swensonb, J.J., Domec, J.C., James, S., Clark, J.S. 2018. Leaf phenology paradox: Why warming matters most where it is already warm. *Remote Sensing of Environment*, 209, 446-455.

Shen, M., Piao, S., Cong, N., Zhang, G., Jassens, I.A. 2015. Precipitation impacts on vegetation spring phenology on the Tibetan Plateau. *Global Change Biology*, 21 (10), 3647–3656.

Shi, Z.H., Ai, L., Li, X., Huang, X.D., Wu, G.L., Liao, W. 2013. Partial least square regression for linking land cover patterns to soil erosion and sediment yield in watersheds. *Journal of Hydrology*, 498, 165-176.

Siemann, E., Carrillo, C.A., Gabler, R., Rogers, W.E. 2009. Experimental test of the impacts of feral hogs on forest dynamics and processes in the southeastern US. *Forest Ecology and Management*, 258 (5), 546-553.

Sims N.C., Thoms, M.C. 2002. What happens when floodplains wet themselves: vegetation response to inundation in lower Balonne floodplains. *International Association of Hydrological Science*, 276, 195 - 202.

Singer, F.J., Swank, W.T., Clebsch, E.E.C. 1984. Effects of wild pig rooting in a deciduous forest. *Journal of Wildlife Management*, 48 (2), 464–473.

Smith, M.C., Stallins, J.A., Maxwell J.T., Van, D.C. 2013. Hydrological shifts and tree growth responses to river modification along the Apalachicola River, Florida. *Physical Geography*, 34 (5), 491-511.

Intergovernmental Panel on Climate Change. 2007. Climate change 2007: the physical sciences basis. Working group contribution to the fourth assessment report of the IPCC. New York, Cambridge: Cambridge University Press.

Stallins, J.A., Nesius, M., Smith, M., Watson, K. 2010. Bio geomorphic characterization of floodplain forest change in response of reduced flows along the Apalachicola River, Florida. *River Research Applications*, 26, 242-260.

Stanturf, J.A., E.S. Gardiner, P.B. Hamel, M.S. Devall, T.D. Leininger, and M.E. Warren Jr. 2000. Restoring bottomland hardwood ecosystems in the Lower Mississippi Alluvial Valley. *Journal of Forestry*, 98 (8), 10–16.

Tabari, H., Marofi, S., Aeini, A., Talaee, P.H. and Mohammadi, K.2011. Trend Analysis of Reference Evapotranspiration in the Western half of Iran. *Agricultural and Forest Meteorology*, 151, 128-136.

Tewari, S., Kulhavy, J., Rock B.N., Hadas, P. 2003. Remote monitoring of forest response to changed soil moisture regime due to river regulation. *Journal of Forest Science*, 49, 429-438.

Thomey, M.L., Collins, S.L., Vargas, R., Johnson, J.E., Brown, R.F., Natvig, D.O., Friggens, M.T. 2011. Effect of precipitation variability on net primary production and soil respiration in a Chihuahuan desert grassland. *Global Change Biology*, 17, 1505–1515.

Tomlinson, K.W., Poorter, L., Sterck, F.J., Borghetti, F., Ward, D., Bie, S., Langevelde, F. 2013. Leaf adaptations of evergreen and deciduous trees of semi-arid and humid savannas on three continents. *Journal of Ecology*, 101 (2), 430–440.

Townsend, P.A. 2001. Relationships between Vegetation patterns and Hydro period on the Roanoke River Floodplain, North Carolina. *Plant Ecology*, 156, 43-58.

Tronstad, L., Tronstas, B., Benke, A. 2005. Invertebrate responses to decreasing water levels in a subtropical river floodplain wetland. *Wetlands*, 25 (3), 583-593.

Tucker, Compton J., 1979. Red and photographic infrared linear combinations for monitoring vegetation. *Remote Sensing of Environment*, 8, 127-150.

Udelhoven, T., Stellmes, M., Barrio del, G., Hill, J. 2009. Assessment of rainfall and NDVI anomalies in Spain (1989-1999) using distributed lad models. *International Journal of Remote Sensing*, 30, 1961-1976.

Wang, H., Liu, G.H., Li, Z.S., Ye, X., Wang, M., Gong, L. 2016. Driving force and changing trends of vegetation phenology in the Loess Plateau of China from 2000 to 2010. *Journal of Mountain Science*, 13 (5), 844–856.

Wang, S., Fu, Z.Y., Chen, H.S., Nie, Y.P., Wang, K.L. 2016. Modeling daily reference ET in the karst area of northwest Guangxi (China) using gene expression programming (GEP) and artificial neural network (ANN). *Theoretical and Applied Climatology*, 126 (3-4), 1–12.

Wen, L., Yang, X., Saintilan, N. 2012. Local climate determines the NDVI-based primary productivity and flooding creates heterogeneity in semi-arid floodplain ecosystem. *Ecological Modelling*, 242, 116-126.

William, G.P. 1978. Bank-Full Discharge of Rivers. *Water Resource Research*, 14 (6).

Wolski, P., Savenije, H.H.G. 2006. Dynamics of floodplain-island groundwater flow in the Okavango Delta, Botswana. *Journal of Hydrology*, 320 (3-4), 283-301.

Xie, Yichun., Sha, Zongyao., Yu, Mei. 2008. Remote sensing imagery in vegetation mapping: a review. *Journal of Plant Ecology*, 1 (1), 9-23.

Yang, X., Tang, J., Mustard, J.F., Lee, J.-E., Rossini, M., Joiner, J. 2015. Solar-induced chlorophyll fluorescence that correlates with canopy photosynthesis on diurnal and seasonal scales in a temperate deciduous forest. *Geophysical Research Letter*, 42, 2977–2987.

Yeniay, O. & Goktass. 2002. A comparison of partial least square regression with other prediction methods. *Hacettepe Journal of Mathematics and Statistics*, 31, 99-111.

Yousfi, N., Saidi, I., Slama, I., Abdelly, C. 2015. Phenology, leaf gas exchange, growth and seed yield in *Medicago polyrnorpha* L. populations affected by water deficit and subsequent recovery. *Flora Morphology, Distribution, Functional Ecology of Plants*, 214, 50–60.

Zellou, B., Rahali, H. 2017. Assessment of reduced complexity landscape evolution model suitability to adequately simulate flood events in complex flow conditions. *Natural Hazards*, 86 (1), 1-29.

Zha, T., Li, C., Kellomäki, S., Peltola, H., Wang, K.Y., Zhang, Y. 2013. Controls of evapotranspiration and CO_2 fluxes from scots pine by surface conductance and abiotic factors. *PLOS One*, 8 (7), e69027.

Zhao D., Kane, M.B., Teskey, R.O., Fox, T.R., Albaugh, T.J., Allen, H.L., Rubilar, R.A. 2016. Maximum response of loblolly pine plantations to silvicultural management in the southern United States. *Forest Ecological Management*, 375, 105–111.

Zhou, L., Tucker, C., Kaufmann, R., Slayback, D., Shabanov, N., Myneni, R. 2001. Variation in northern vegetation activity inferred from satellite data of vegetation index from 1981-1999. *Journal of Geophysical Research*, 106, 20069-2008.

APPENDIX

Table 1. Number of bands and wavelengths of the bands in different sensors used in the study.

Landsat 5	Bands	Wavelength (micrometers)	Resolution (meters)
Thematic Mapper (TM)	Band 1 - Blue	0.45-0.52	30
	Band 2 - Green	0.52-0.60	30
	Band 3 - Red	0.63-0.69	30
	Band 4 - Near Infrared (NIR)	0.76-0.90	30
	Band 5 - Shortwave Infrared (SWIR) 1	1.55-1.75	30
	Band 6 - Thermal	10.40-12.50	120* (30)
	Band 7 - Shortwave Infrared (SWIR) 2	2.08-2.35	30
Landsat 7 Enhanced Thematic Mapper Plus (ETM)	Band 1 - Blue	0.45-0.52	30
	Band 2 - Green	0.52-0.60	30
	Band 3 - Red	0.63-0.69	30
	Band 4 - Near Infrared (NIR)	0.77-0.90	30
	Band 5 - Shortwave Infrared (SWIR) 1	1.55-1.75	30
	Band 6 - Thermal	10.40-12.50	60 * (30)
	Band 7 - Shortwave Infrared (SWIR) 2	2.09-2.35	30
	Band 8 - Panchromatic	.52-.90	15

Table 2A. List of Landsat images downloaded for this study (Path 21/Row 37).

S.No	Date of acquisition	Sensor	Spatial resolution
1	1/10/1990	LANDSAT_5 TM	30 m
2	6/19/1990	LANDSAT_5 TM	30 m
3	1/16/1992	LANDSAT_5 TM	30 m
4	6/24/1992	LANDSAT_5 TM	30 m
5	11/15/1992	LANDSAT_5 TM	30 m
6	12/1/1992	LANDSAT_5 TM	30 m
7	2/3/1993	LANDSAT_5 TM	30 m
8	6/11/1993	LANDSAT_5 TM	30 m
9	7/29/1993	LANDSAT_5 TM	30 m
10	10/1/1993	LANDSAT_5 TM	30 m
11	1/21/1994	LANDSAT_5 TM	30 m
12	5/29/1994	LANDSAT_5 TM	30 m
13	6/30/1994	LANDSAT_5 TM	30 m
14	1/24/1995	LANDSAT_5 TM	30 m
15	2/25/1995	LANDSAT_5 TM	30 m
16	4/14/1995	LANDSAT_5 TM	30 m
17	6/17/1995	LANDSAT_5 TM	30 m
18	9/5/1995	LANDSAT_5 TM	30 m
19	10/7/1995	LANDSAT_5 TM	30 m
20	11/8/1995	LANDSAT_5 TM	30 m
21	12/1/1995	LANDSAT_5 TM	30 m
22	1/27/1996	LANDSAT_5 TM	30 m

Table 2A. List of Landsat images downloaded for this study (Path 21/Row 37).

S.No	Date of acquisition	Sensor	Spatial resolution
23	2/12/1996	LANDSAT_5 TM	30 m
24	4/16/1996	LANDSAT_5 TM	30 m
25	5/2/1996	LANDSAT_5 TM	30 m
26	7/21/1996	LANDSAT_5 TM	30 m
27	9/7/1996	LANDSAT_5 TM	30 m
28	10/9/1996	LANDSAT_5 TM	30 m
29	5/5/1997	LANDSAT_5 TM	30 m
30	8/28/1997	LANDSAT_5 TM	30 m
31	8/25/1998	LANDSAT_5 TM	30 m
32	8/28/1998	LANDSAT_5 TM	30 m
33	10/15/1998	LANDSAT_5 TM	30 m
34	12/2/1998	LANDSAT_5 TM	30 m
35	1/19/1999	LANDSAT_5 TM	30 m
36	2/20/1999	LANDSAT_5 TM	30 m
37	8/15/1999	LANDSAT_5 TM	30 m
38	9/16/1999	LANDSAT_5 TM	30 m
39	10/18/1999	LANDSAT_5 TM	30 m
40	11/3/1999	LANDSAT_5 TM	30 m
41	1/6/2000	LANDSAT_5 TM	30 m
42	5/29/2000	LANDSAT_5 TM	30 m
43	7/16/2000	LANDSAT_5 TM	30 m
44	8/17/2000	LANDSAT_5 TM	30 m

Table 2A. List of Landsat images downloaded for this study (Path 21/Row 37).

S.No	Date of acquisition	Sensor	Spatial resolution
45	9/20/2000	LANDSAT_5 TM	30 m
46	10/4/2000	LANDSAT_5 TM	30 m
47	11/21/2000	LANDSAT_5 TM	30 m
48	12/7/2000	LANDSAT_5 TM	30 m
49	3/13/2001	LANDSAT_5 TM	30 m
50	5/16/2001	LANDSAT_5 TM	30 m
51	6/17/2001	LANDSAT_5 TM	30 m
52	8/20/2001	LANDSAT_5 TM	30 m
53	9/21/2001	LANDSAT_5 TM	30 m
54	10/7/2001	LANDSAT_5 TM	30 m
55	11/7/2001	LANDSAT_5 TM	30 m
56	12/16/2001	LANDSAT_5 TM	30 m
57	2/12/2002	LANDSAT_5 TM	30 m
58	5/19/2002	LANDSAT_5 TM	30 m
59	7/6/2002	LANDSAT_5 TM	30 m
60	8/7/2002	LANDSAT_5 TM	30 m
61	12/29/2002	LANDSAT_5 TM	30 m
62	1/14/2003	LANDSAT_5 TM	30 m
63	6/23/2003	LANDSAT_5 TM	30 m
64	8/26/2003	LANDSAT_5 TM	30 m
65	9/11/2003	LANDSAT_5 TM	30 m
66	10/29/2003	LANDSAT_5 TM	30 m

Table 2A. List of Landsat images downloaded for this study (Path 21/Row 37).

S.No	Date of acquisition	Sensor	Spatial resolution
67	4/6/2004	LANDSAT_5 TM	30 m
68	5/8/2004	LANDSAT_5 TM	30 m
69	9/29/2004	LANDSAT_5 TM	30 m
70	10/15/2004	LANDSAT_5 TM	30 m
71	12/18/2004	LANDSAT_5 TM	30 m
72	5/19/2005	LANDSAT_5 TM	30 m
73	9/18/2005	LANDSAT_5 TM	30 m
74	10/26/2005	LANDSAT_5 TM	30 m
75	11/11/2005	LANDSAT_5 TM	30 m
76	2/7/2006	LANDSAT_5 TM	30 m
77	6/15/2006	LANDSAT_5 TM	30 m
78	7/1/2006	LANDSAT_5 TM	30 m
79	8/18/2006	LANDSAT_5 TM	30 m
80	9/3/2006	LANDSAT_5 TM	30 m
81	10/5/2006	LANDSAT_5 TM	30 m
103	12/27/2010	LANDSAT 7 ETM	30 m
104	3/17/2011	LANDSAT 7 ETM	30 m
105	4/2/2011	LANDSAT 7 ETM	30 m
106	5/20/2011	LANDSAT 7 ETM	30 m
107	8/24/2011	LANDSAT 7 ETM	30 m
108	9/9/2011	LANDSAT 7 ETM	30 m
109	8/29/2013	LANDSAT 7 ETM	30 m
110	9/14/2013	LANDSAT 7 ETM	30 m

Table 2B. Images used for pre and post vegetation classification using unsupervised classification (Path 21/Row 37).

S.No	Date of acquisition	Sensor	Spatial resolution
1	6/19/1990	LANDSAT_5 TM	30 m
2	5/19/2008	LANDSAT_5 TM	30 m

Table 2C. Image used for vegetation identification by Seasonality Index method.

S.No	Date of acquisition	Sensor	Spatial resolution
1	1/10/1990	LANDSAT_5 TM	30 m
2	6/19/1990	LANDSAT_5 TM	30 m
14	1/24/1995	LANDSAT_5 TM	30 m
21	12/1/1995	LANDSAT_5 TM	30 m
41	1/6/2000	LANDSAT_5 TM	30 m
42	5/29/2000	LANDSAT_5 TM	30 m
95	5/19/2008	LANDSAT_5 TM	30 m
98	12/29/2008	LANDSAT_5 TM	30 m

Table 3. Sets of predictor variables used in PLSR model for each vegetation class.

Climatological datasets	
Maximum temperature	running average of monthly maximum up to antecedent 6 months
Minimum temperature	running average of monthly minimum up to antecedent 6 months
Average temperature	running monthly average up to antecedent 6 months
Precipitation	running average of up to antecedent 6 months
Hydrological datasets	
Streamflow	discharge followed by running average up to antecedent 6 weeks

Table 4. Error matrix of accuracy assessment performed on 2008 unsupervised classification. Each row contains the type of vegetation as visually identified by reference image and each column contains vegetation types classified by unsupervised classification.

		Reference Image (Google Earth Image, May 2006)						
		Water/unclassified	Hardwood swamp	Bottomland hardwood	Pineland	Row total	Producer's accuracy (%)	User accuracy (%)
Unsupervised classification	Water/unclassified	61	10	7	8	86	71	87
	Hardwood swamp	6	50	25	5	86	58	40
	Bottomland hardwood	10	64	100	15	189	52	57
	Pineland	10	2	42	85	139	61	75
	Column total	87	126	174	113	500		
	Overall accuracy	60.00%						
	Kappa coefficient	0.47						

Table 5. Error matrix of accuracy assessment for 2008 image-for vegetation identification by SI. Each row contains the type of vegetation as visually identified by reference image and each column contains vegetation types identified by SI.

		Reference Image (Google Earth Image, May 2006)						
		Water/unclassified	Hardwood swamp	Bottomland hardwood	Pineland	Row total	Producer's accuracy (%)	User accuracy (%)
Identified vegetation (by Seasonality Index)	Water/unclassified	20	6	8	15	49	40	35
	Hardwood swamp	4	140	20	5	169	82	86
	Bottomland hardwood	8	15	127	22	173	79	74
	Pineland	15	5	20	69	109	54	60
	Column total	57	161	185	97	500		
	Overall accuracy	71.20%						
	Kappa coefficient	0.59						

Table 6. SI thresholds for forest classification; dominant tree species are listed for each class.

Class	Types	Species	SI thresholds
Class 1	Pineland forest (PF)	Loblolly pine (*Pinus taeda*)	SI>0.8
Class 2	Bottomland hardwood forest (BHF)	Southern red oak (*Quercus falcata*)	
		White oak (*Quercus alba*)	
		Sweetgum (*Ulnus americana*)	
		Yellow poplar (*Liridendron tulipefera*)	0.5<SI<0.8
		American beech (*Fagus grandifolia*)	
		Swamp cottonwood (*Populus heterophylla*)	
		Overcup oak (*Quercus lirata*)	
Class 3	Hardwood swamp (HS)	Baldcypress tupelo (*Taxodium distichum*)	0<SI<0.5
		Tupelo gum trees (*Nyssa aquatica, Nyssa biflora, Oegeche sylvatica*)	
Class 4	Water and Unclassified (W-N)		SI<0

Table 7. Change detection in vegetation cover types determined by unsupervised classification (unit in km^2).

	1990	2008	Change	% increase or decrease
Hardwood swamp	23.3	15.5	7.9	33% decrease
Bottomland hardwood	18.5	26.8	8.3	45% increase
Pineland	5.8	7.3	1.5	26%increase

Table 8. Change detection of vegetation types in the study period as identified by Seasonality Index (unit in km^2).

	1990	1995	2000	2008	Change (1990- 2008)	% increase or decrease
Hardwood swamp	27.3	18.98	24.7	21.84	5.46	20% decrease
Bottomland hardwood	22.1	30.42	25.1	26.26	4.16	15.3% increase
Pineland	3.9	4.94	4.2	6.24	2.34	60% increase
Total	53.3	54.34	54	54.08	0.78	1.5% increase

Table 9. Results of Mann-Kendall test on water level variation (1977-2008).

Annual		Winter		Summer	
S'	6	S'	2	S'	4
Var(S')	12	Var(S')	12	Var(S')	12
p-value	0.083	p-value	0.564	p-value	0.248
alpha	0.05	alpha	0.05	alpha	0.05

Table 10A. Comparison of accuracy assessments of two vegetation identification techniques.

	Unsupervised classification		(SI)	
	Producer' acc (%)	User's acc (%)	Producer's acc (%)	User's acc(%)
Water/unclassified	71	87	40	35
Hardwood swamp	58	40	82	86
Bottomland hardwood	52	57	79	74
Pinelands	61	75	54	60

Acc-accuracy

Table 10B. SI versus unsupervised classification (% percentage).

	1990-UNS(sq-km)	1990-SI(sq-km)	% difference	2008-UNS(sq-km)	2008-SI(sq-km)	%difference	Change-UNS(sq-km)	Change-SI(sq-km)	% difference
Hardwood swamp	23	27	-17	16	22	-41	8	5	31
Bottomland hardwood	19	22	-19	27	26	2	8	4	50
Pineland	6	4	33	7	6	15	2	2	-56

UNS-Unsupervised classification

SI-Seasonality Index

Negative numbers indicate SI predicted higher than unsupervised

Table 11A. Descriptive Statistics of variables for summer months (1990-2013).

	N	Range	Minimum	Maximum	Mean	Std. Deviation
NDVI-HS	37	0.33	0.47	0.8	0.75	0.07
NDVI BH	37	0.16	0.66	0.82	0.77	0.04
Ave temp	37	16.25	67.65	83.9	77.24	4.82
Max temp	37	16.7	80.1	96.8	88.81	4.88
Min temp	37	17.3	54.95	72.25	65.67	5.17
Ave precip	37	10.24	0.12	10.36	3.98	2.32
Discharge_weekly	37	57.99	1.19	59.18	12.3	14.68
N	37					

Table 11B. Descriptive Statistics of variables for the winter months (1990-2013).

	N	Range	Minimum	Maximum	Mean	Std. Deviation
NDVI-HS	30	0.4	0.38	0.79	0.49	0.1
NDVI-BH	30	0.19	0.26	0.45	0.35	0.05
Ave temp	30	12.95	38.4	51.35	45.8	3.33
Max temp	30	14.45	48.6	63.05	57.11	3.62
Min temp	30	12.85	27.8	40.65	34.48	3.46
Ave precip	30	9.81	1.09	10.89	5.08	2.37
Discharge_weekly	30	160.3	3.94	164.24	42.43	41.57
N	30					

NDVI-HS=NDVI for Hardwood swamp

NDVI-BH=NDVI for Bottomland hardwood

Ave temp=Average monthly temperature

Max temp=Maximum monthly temperature

Min temp=Minimum monthly temperature

Ave precip=Average monthly precipitation

Table 12. Spearman's rho correlation matrix for mean NDVI for each vegetation types and hydrological and climatological variables.

	Bottomland hardwood mean	Hardwood swamp mean	Ave temp	Max temp	Min temp	Ave precip	Discharge-week
Bottomland hardwood mean	1	.839**	**.712****	**.712****	**.705****	-0.137	-.351**
Hardwood swamp mean		1	**.825****	**.824****	**.823****	-.186*	-.461**
Ave temp			1	.993**	.994**	-.200*	-.578**
Max temp				1	.977**	-.247**	-.604**
Min temp					1	-0.148	-.545**
Ave precip						1	.551**
Discharge-weak							1

** Significant at the 0.01 level

* Significant at 0.05 level.

Bold numbers are representing strong positive correlation

Table 13A. Results of PLSR models- temporal variability in NDVI for hardwood swamp, and bottomland hardwood in the study period of 1990-2013.

	NDVI for Hardwood swamp				NDVI for Bottomland hardwood			
PRESS	0.45				0.71			
Cumulative Q square	0.96				0.53			
Cumulative R square	0.83				0.58			
Number of factors	2				1			
Variable	**VIP**	**Coefficient**	**Intercept**	**p**	**VIP**	**Coefficient**	**Intercept**	**p**
Average Temp	1.02	0.009	-0.38	<0.001	1.04	0.006	0.15	<0.001
Average Temp (Ant 2 months)	0.99	0.009			0.99	0.0005		
Min Temp (month)	1	-0.006			0.98	-0.0002		
Max Temp (monthly)	0.98	0.002			0.99	0.0013		

PRESS- Predicted Residual sum of squares
VIP-Variable Importance for projection
Ant - Antecedent

Table 13B. PLSR models estimating winter NDVI for each vegetation class for the study period 1990-2013.

	winter NDVI for hardwood swamp			winter NDVI for bottomland hardwood		
PRESS	1.099			1.09		
Cumulative Q square	0.004			0		
Cumulative R	0.08			0.08		
Number of factors	1			0		
Variable	**VIP**	**Coefficients**	**p**	**VIP**	**Coefficients**	**p**
Max temp (antecedent 5 months)	0.5	<-0.0002	-	-	-	-
Min temp (antecedent 4 months)	0.5	<-0.0002	-	-	-	-
Avge temp (antecedent 5 months)	0.57	<-0.0002	-	-	-	-
Discharge weekly	0.44	<-0.0001	-	-	-	-

Table 13C. PLSR models estimating summer NDVI for each vegetation type for the study period 1990-2013.

	summer NDVI for hardwood swamp			summer NDVI for bottomland hardwood		
PRESS	1.01			0.99		
Cumulative Q square	0.11			0.3		
Cumulative R	0.14			0.05		
Number of factors	5			2		
Variable	**VIP**	**Coefficients**	**p**	**VIP**	**Coefficients**	**p**
min temp (antecedent 7 months)	0.7	-	-	-	-	-
avg temp (antecedent 7 months)	0.6	-	-	-	-	-
avg temp (antecedent 5 months)	0.5	-	-	-	-	-
max temp (antecedent 4 months)	0.7	-	-	-	-	-
avg temp (antecedent 3 months)	1	-	-	-	-	-
min temp (antecedent 3months)	0.7	-	-	-	-	-
min temp (antecedent 2 months)	0.5	-	-	-	-	-
avg temp (antecedent 2 months)	0.4	-	-	-	-	-
Rainfall (antecedent 3 months)	0.5	-	-	-	-	-

Table 14A. Results of linear regression performed between NDVI of hardwood swamp and flood inundation frequency.

Variables	5-year	10- year	37-year
Intercept	0.86	0.78	0.82
Coefficients	-0.0023	0.0002	-0.0003
R- square value	0.0046	0.00026	0.0005
F significance	0.14	0.2	0.3

Table 14B. Results of linear regression performed between NDVI of bottomland hardwood and flood inundation frequency.

Variable	5-years	10-year	37-year
Intercept	0.725	0.8	0.86
Coefficients	-0.002	-0.0003	-0.0004
R-square	0.012	0.002	0.002
F-significance	0.14	0.06	0.023

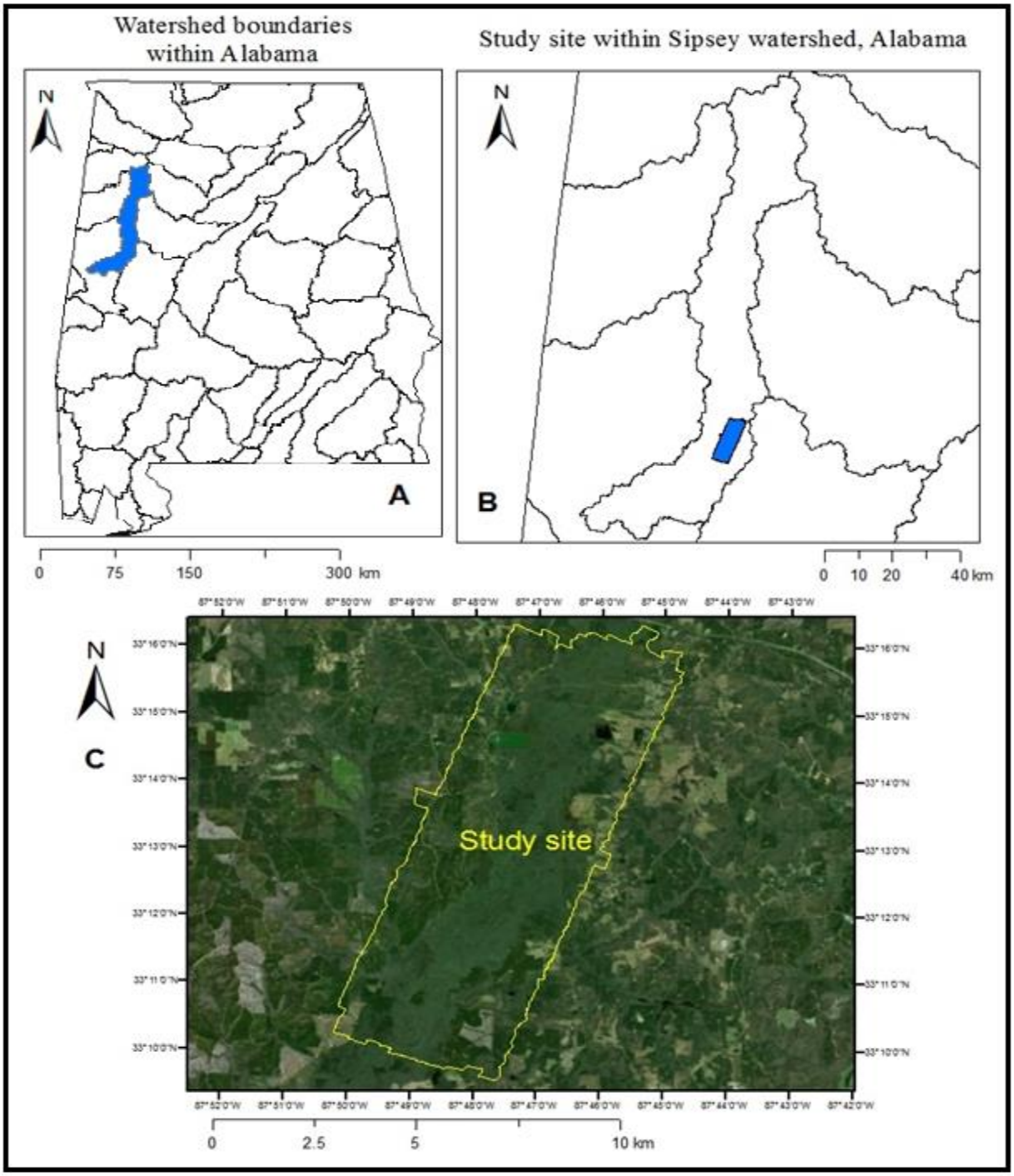

Figure 1. Study area: A) Watershed boundaries in Alabama in the state of Alabama, B) study site in the Sipsey watershed, and C) exact location of study site within the watershed.

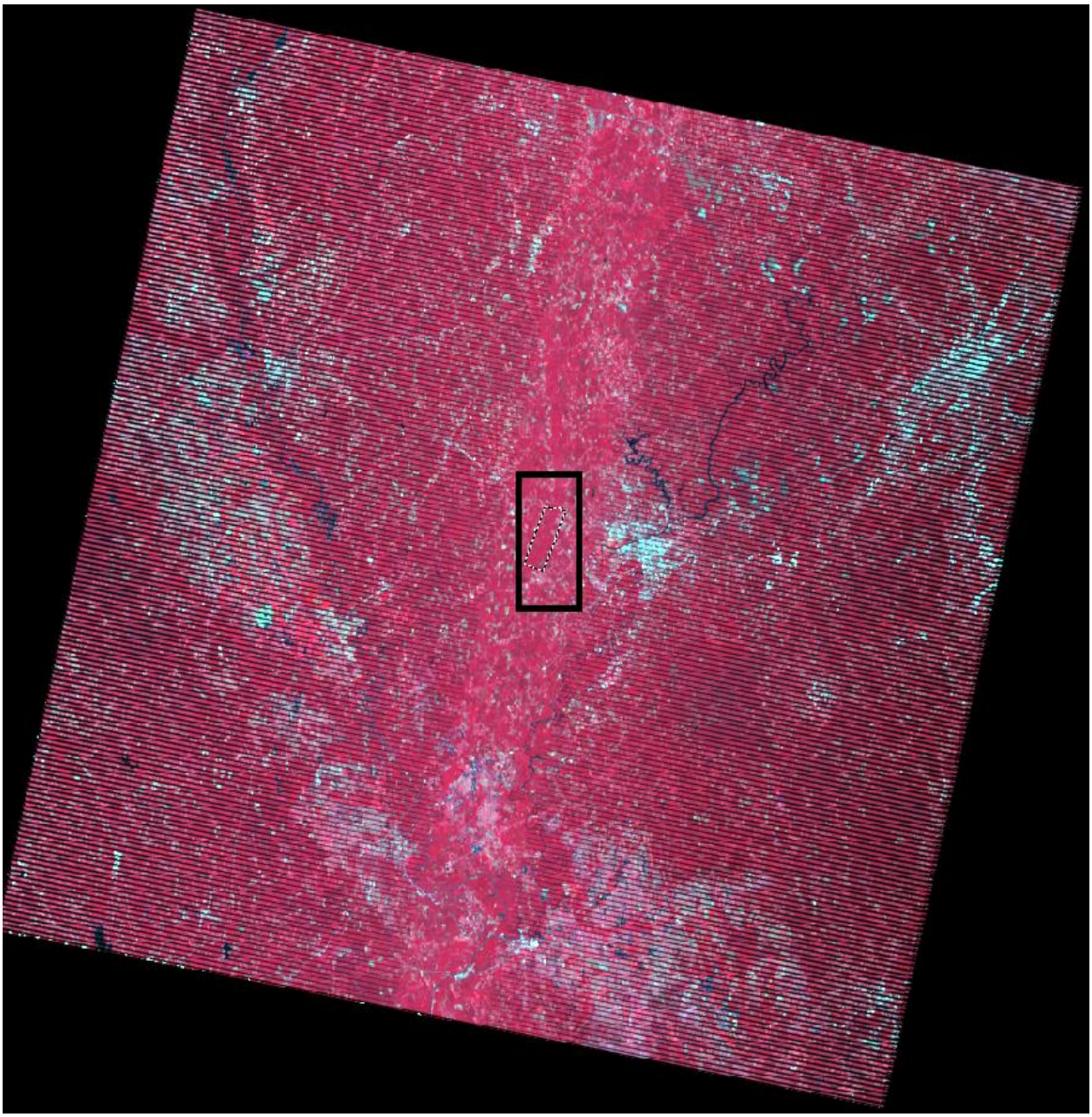

Figure 2. An image of date 5/8/2009 showing a highlighted portion of the study area that was unaffected by the scan line failure of Landsat ETM.

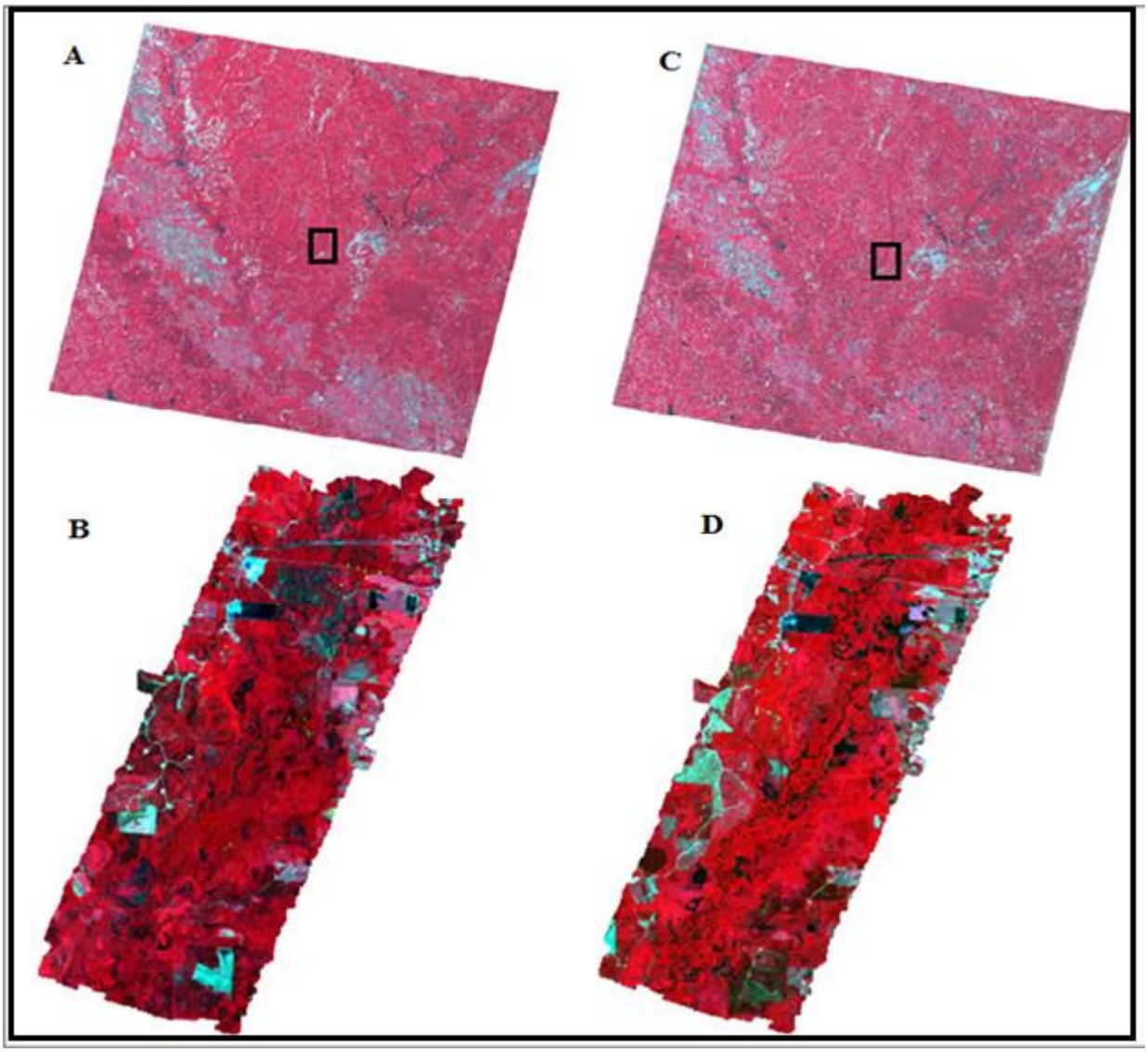

Figure 3. A) Top left corner image is full scene of Landsat TM of date 6/19/1990 and B) down left corner is the subset of study area. C) Top right corner image is full scene of Landsat TM of date 5/19/2008 and D) down right corner image is the subset of study area (size =54.5 km^2).

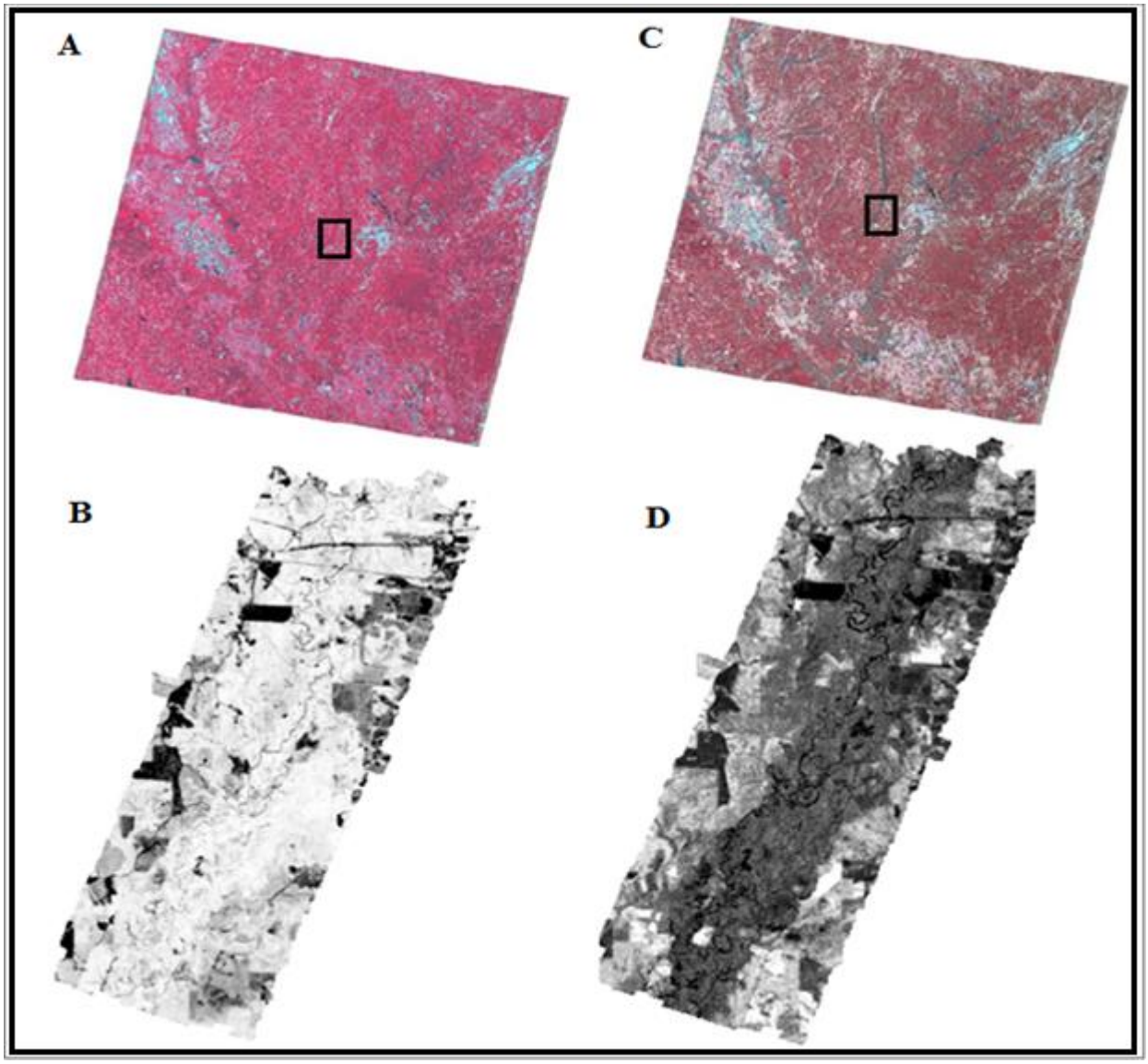

Figure 4. A) Top left corner image is full scene of Landsat TM of date 6/19/1990 and B) down left is the NDVI of the study area. C) Top right corner image is full scene of Landsat TM of date 1/10/1990 and D) down right corner image is the NDVI of the study area (size= 54.5 km^2).

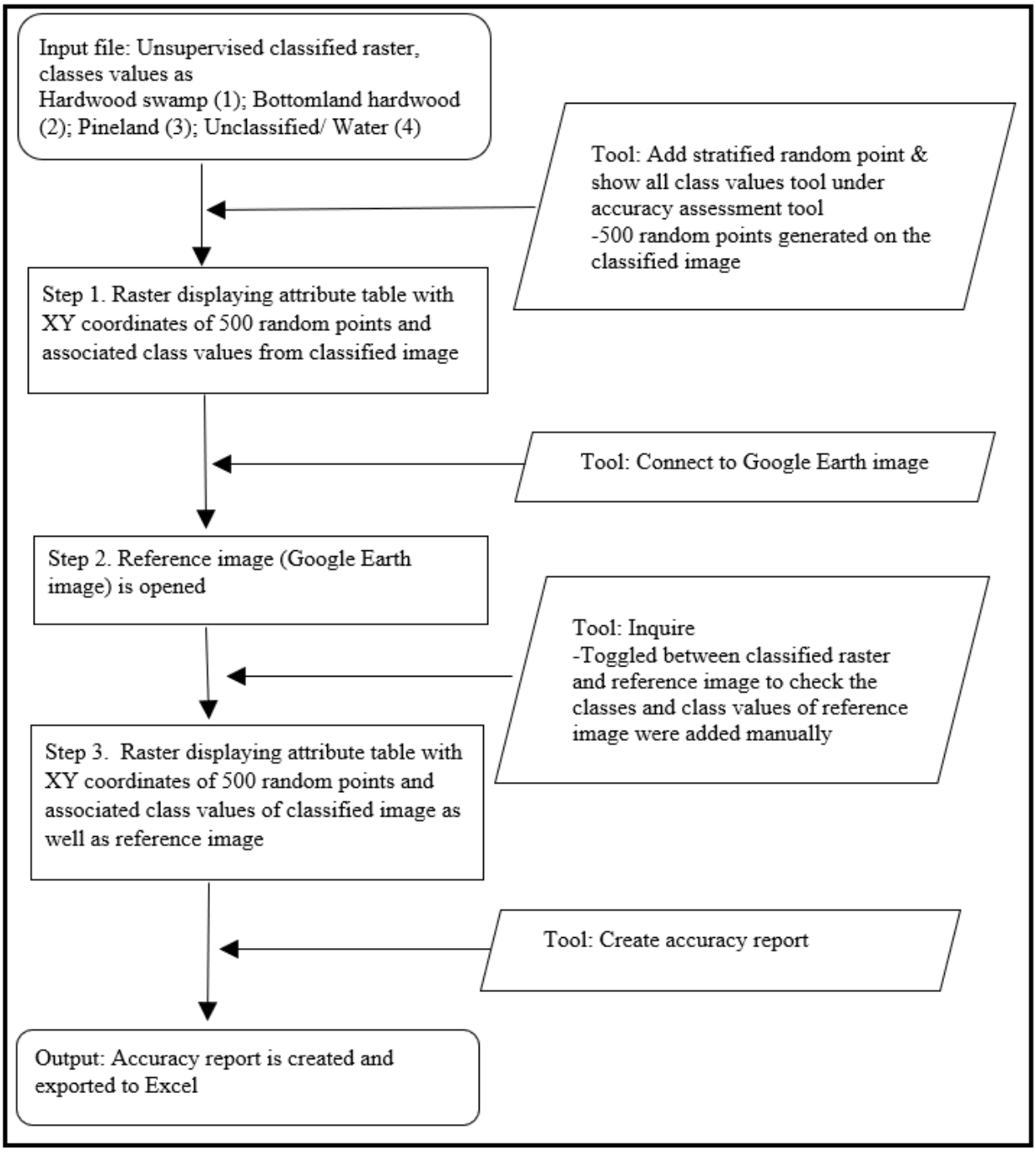

Figure 5A. Flow chart describing the steps and tools used in accuracy assessment of vegetation identification by Unsupervised classification for year 2008. All the steps were conducted in ERDAS Imagine. Reference image-Google Earth image of May 2006.

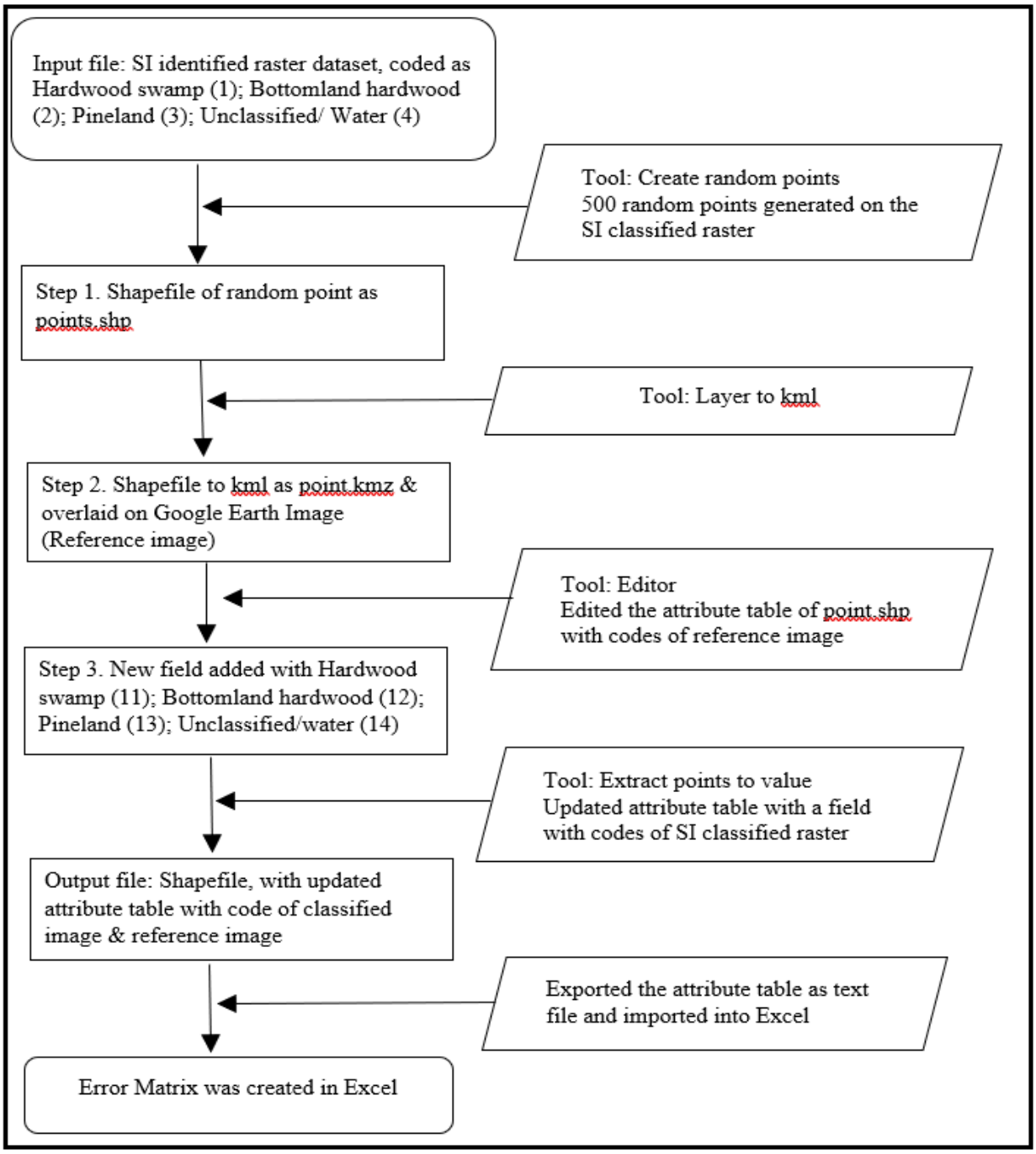

Figure 5B. Flow chart describing the steps and tools used in accuracy assessment of vegetation identification by Seasonality Index for year 2008.
All the steps were conducted in ArcMap 10.4. Reference image-Google Earth image of May 2006.

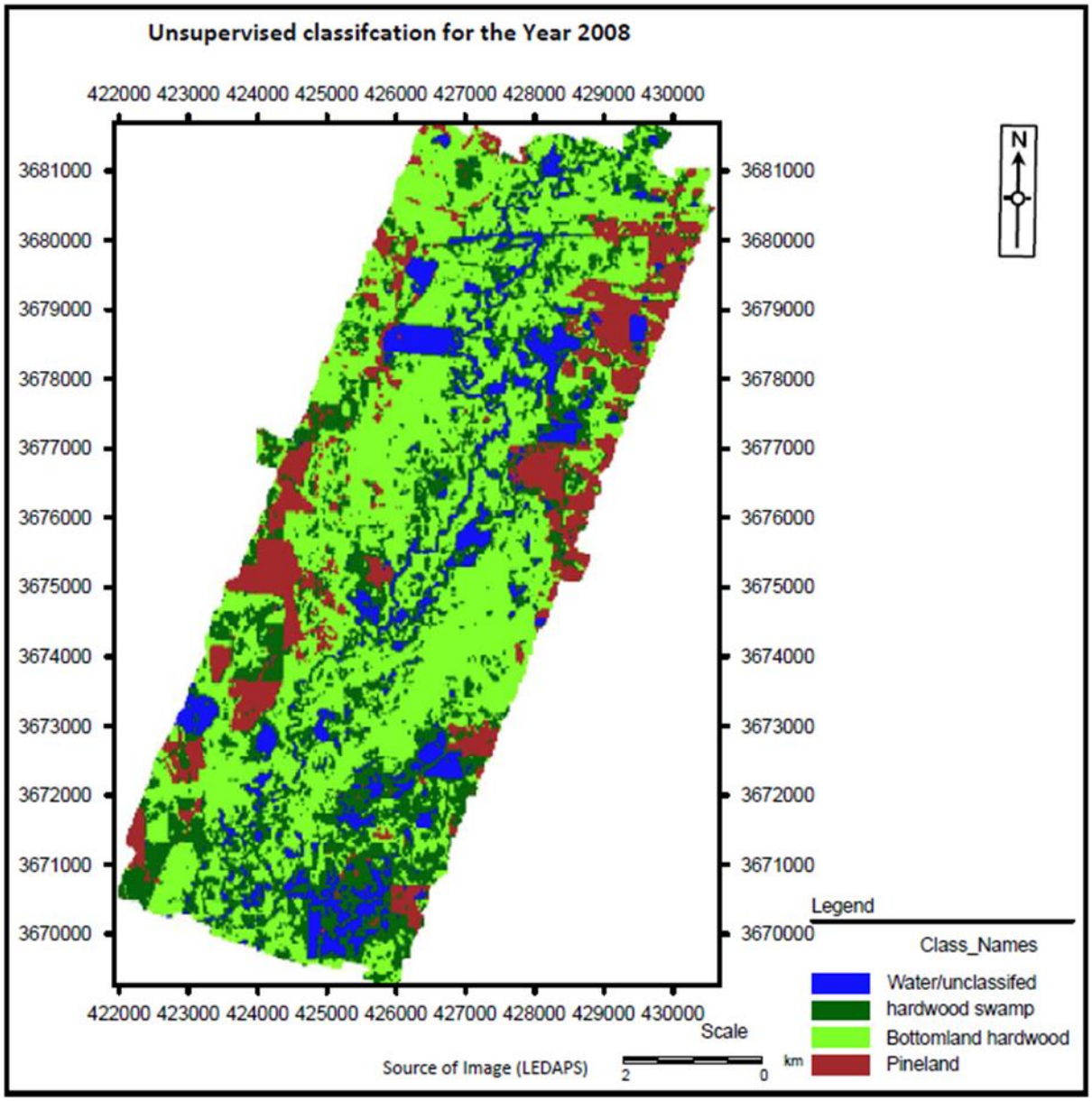

Figure 6. Vegetation types determined by unsupervised classification for the Year 2008.

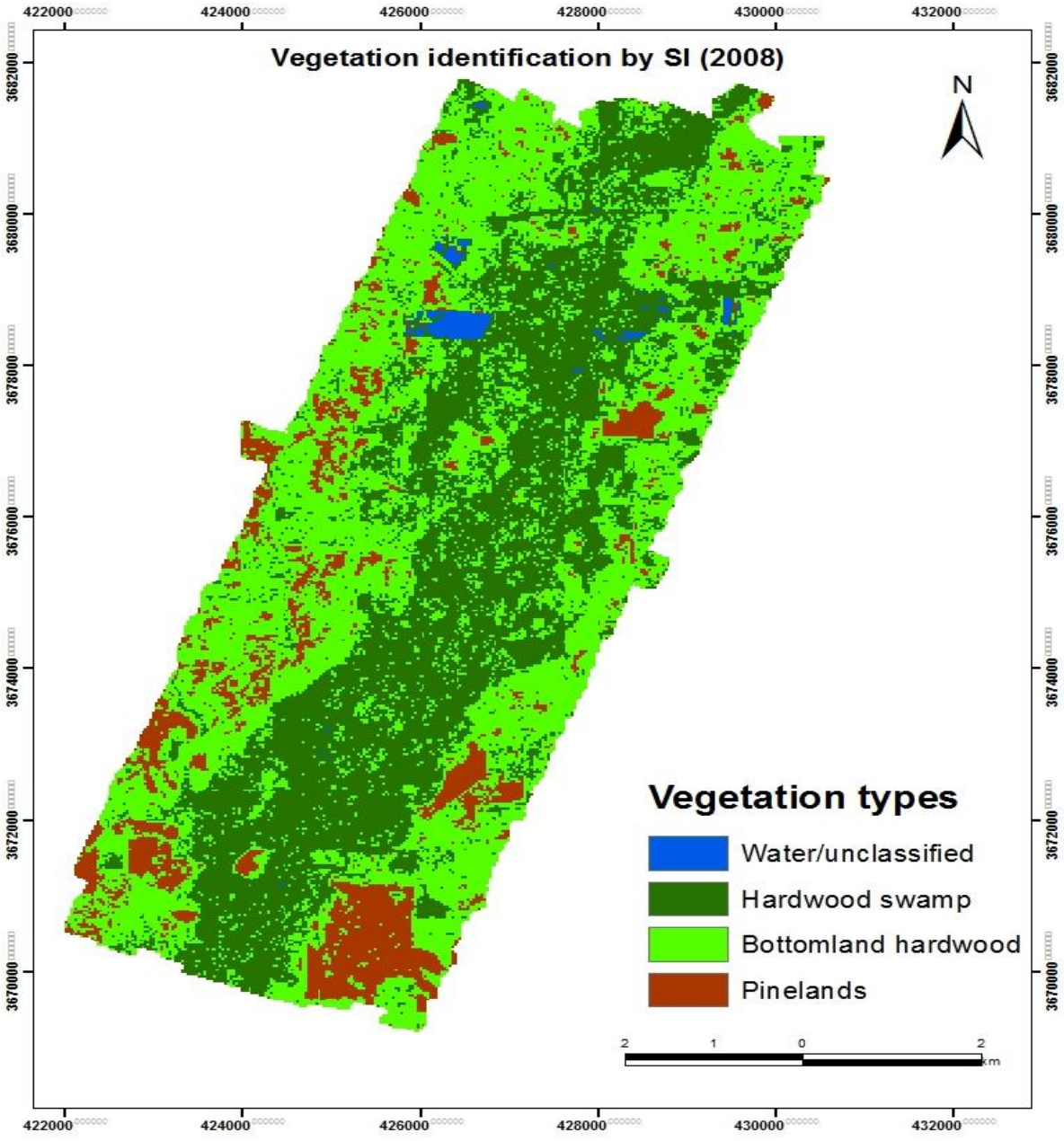

Figure 7. Vegetation identification by Seasonality Index for the year 2008.

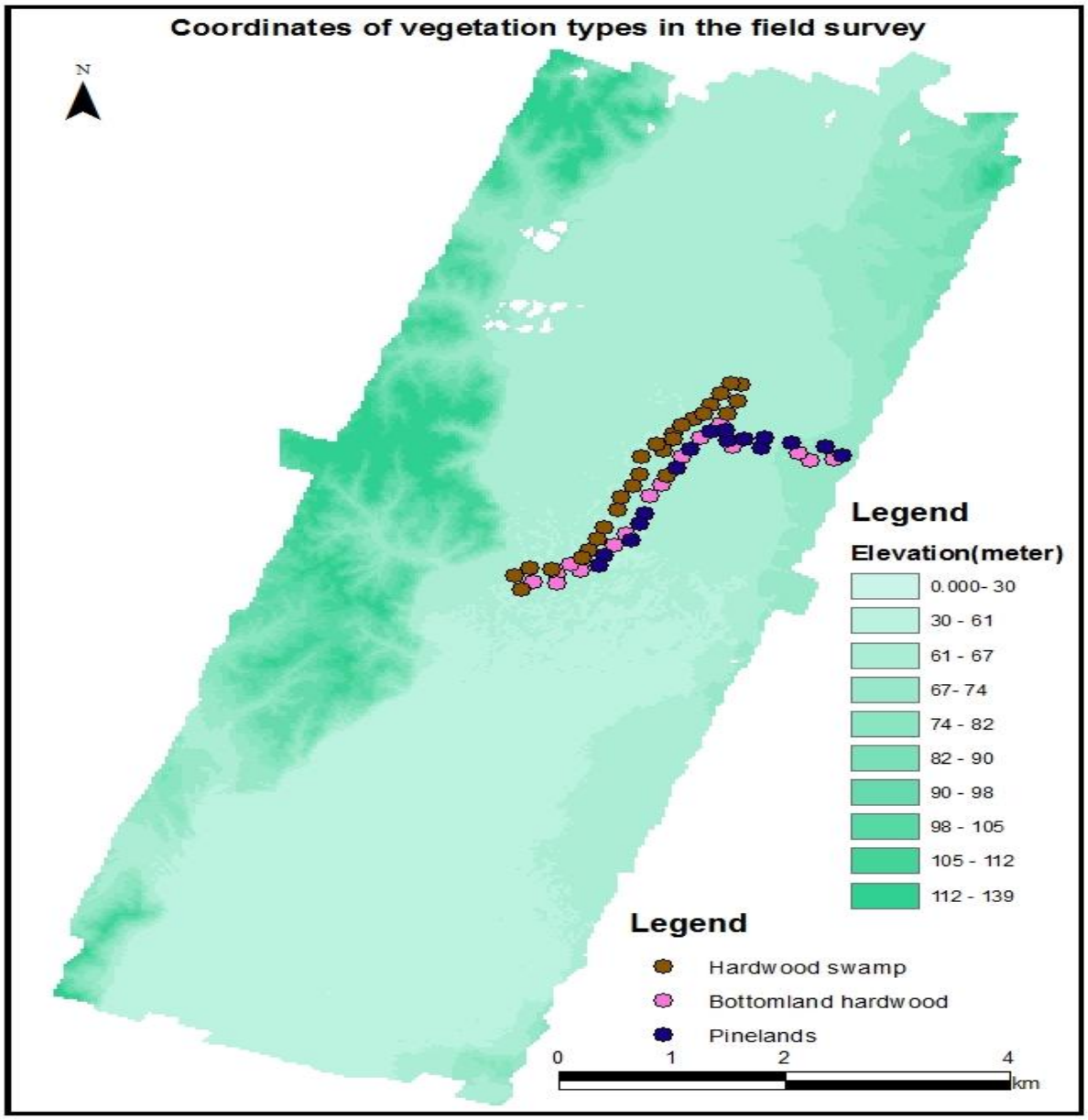

Figure 8. Field survey conducted in August 2018. 60 GPS locations were recorded across 3 km stretch of the road.

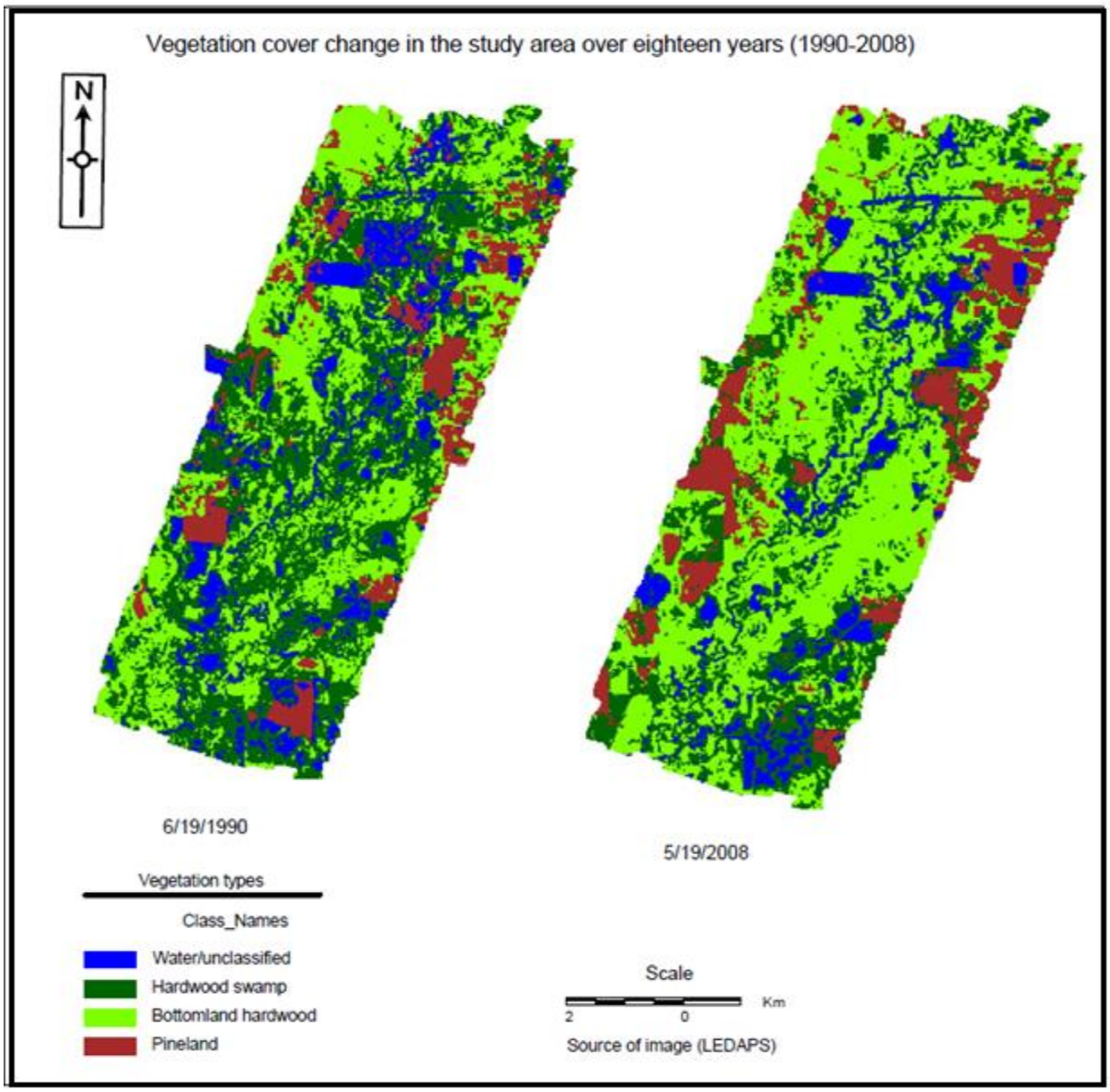

Figure 9. Change detection in vegetation cover between 1990 and 2008, performed as result of unsupervised classifications.

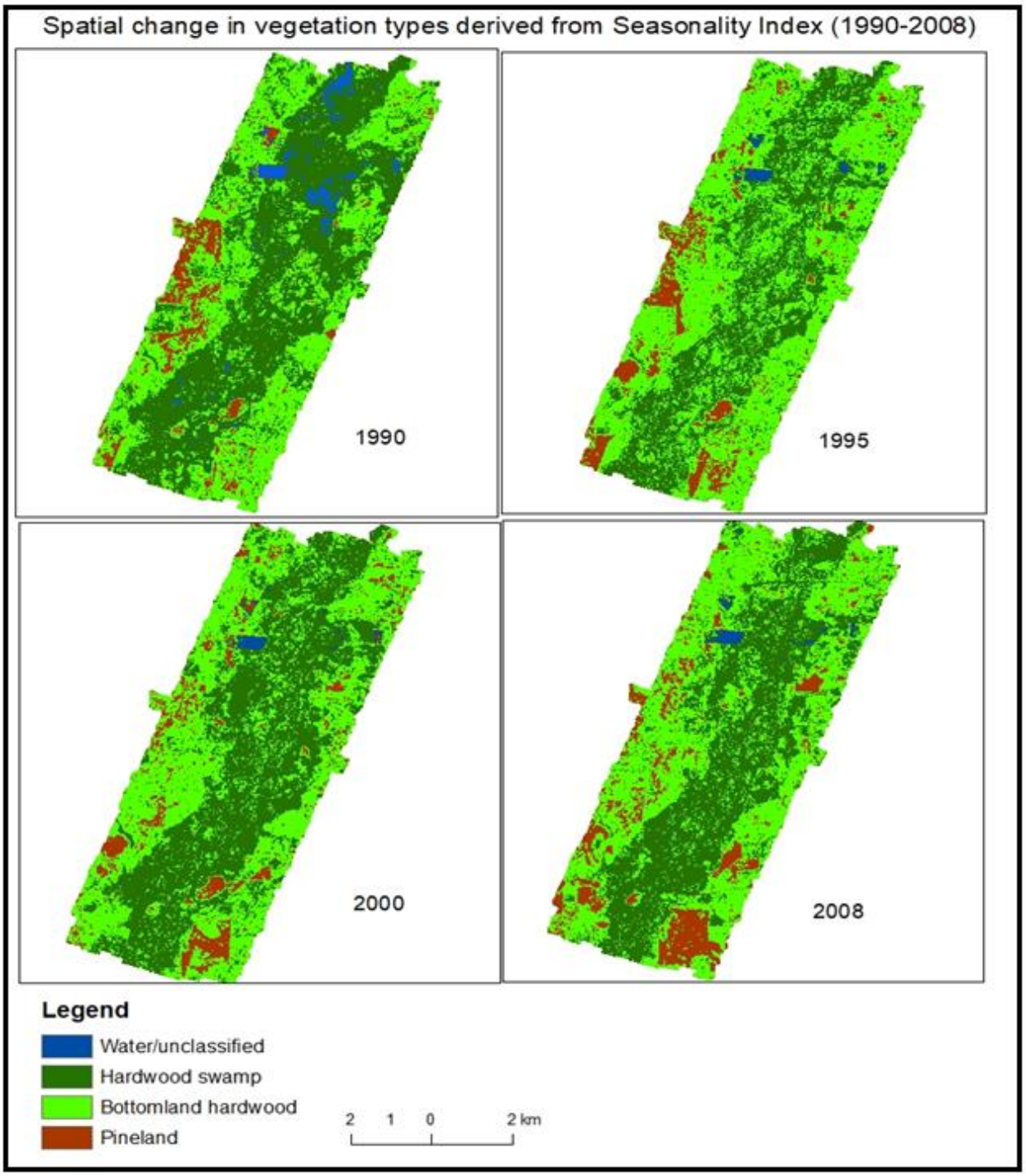

Figure 10. Change detection in vegetation cover between 1990 and 2008, performed as a results of vegetation identifcation by SI.

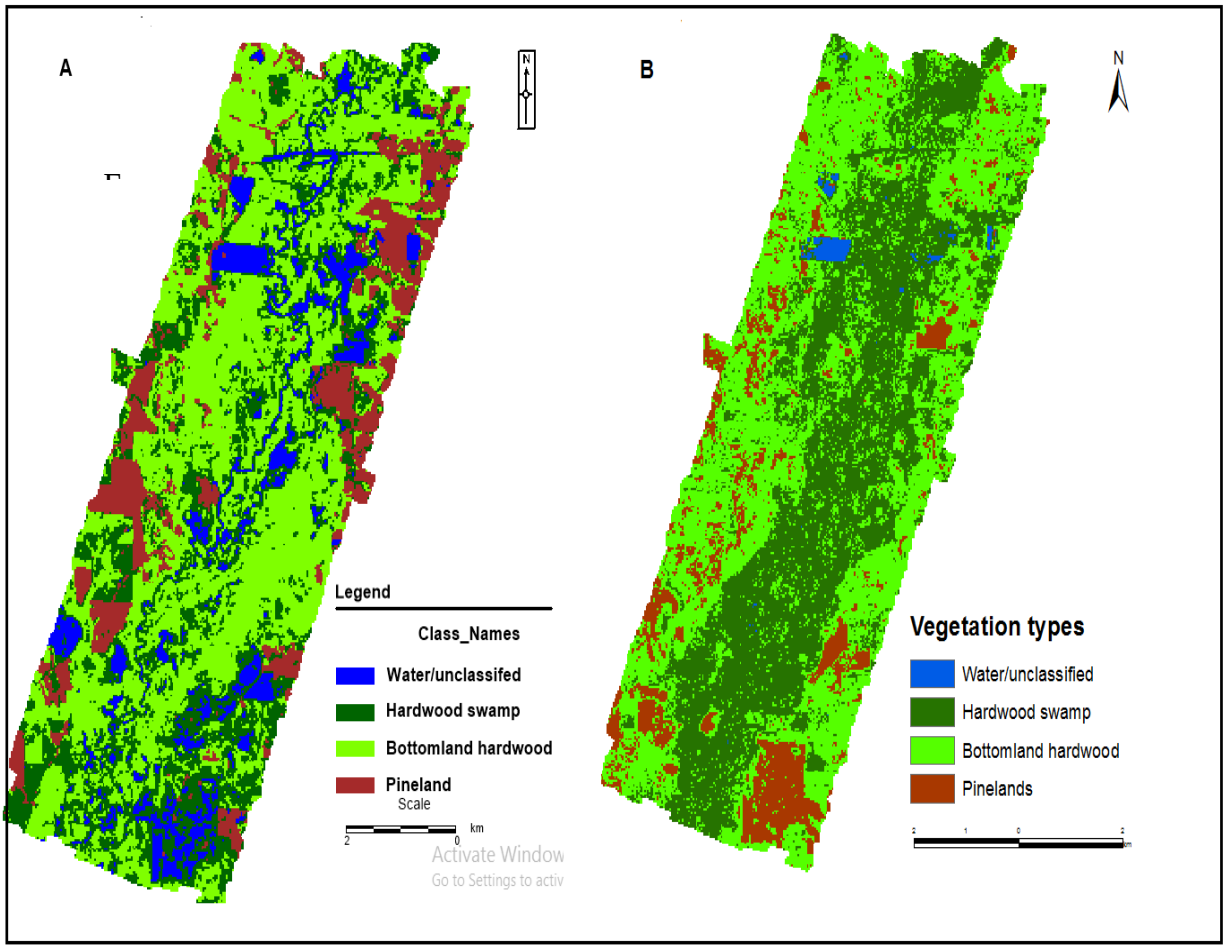

Figure 11. Vegetation classification by unsupervised classification for the year 2008. B) Vegetation types identified by SI for the year 2008.

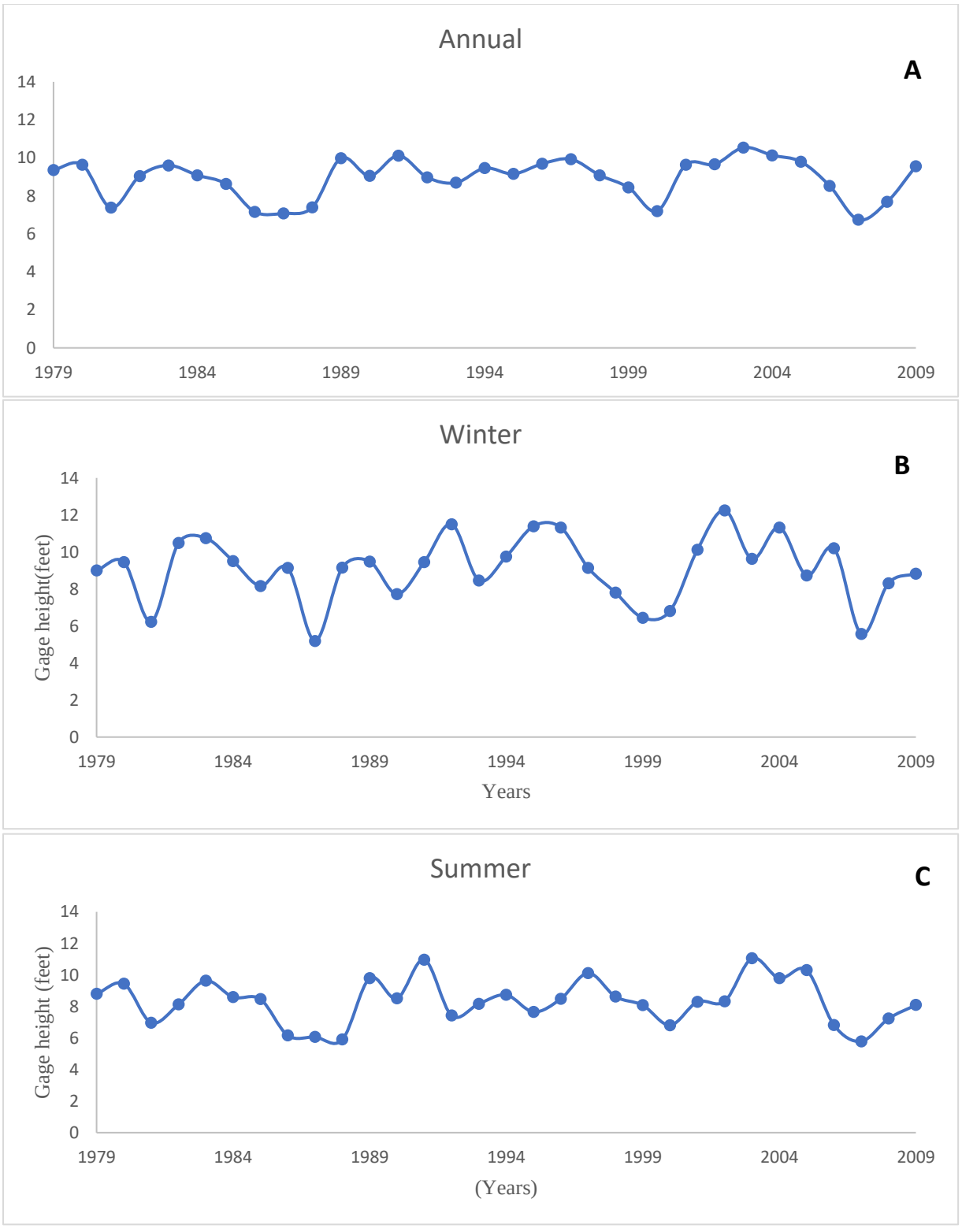

Figure 12. Results of Mann-Kendall test showing no significant trend in A) annual water level, B) winter water level and C) summer water level.

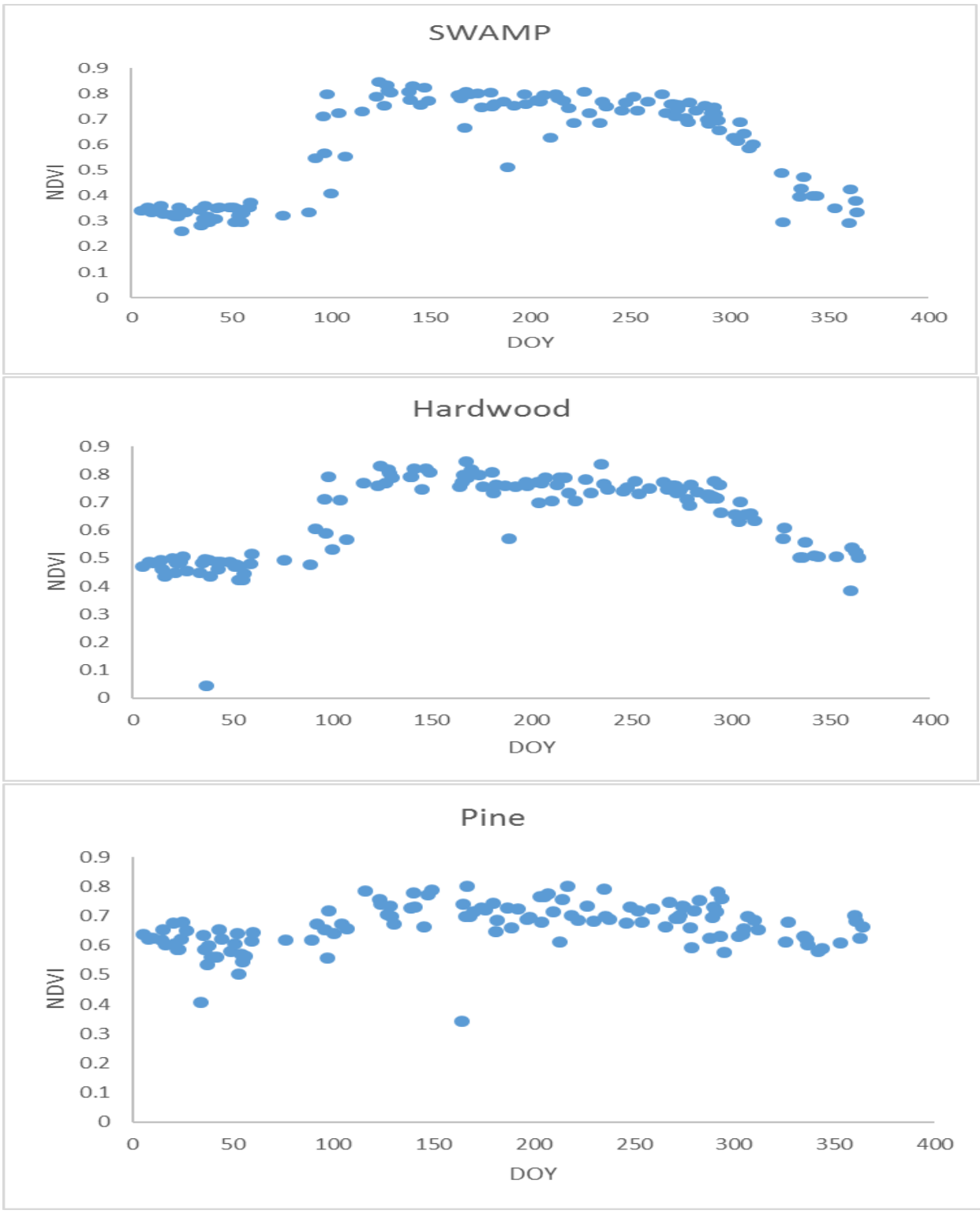

Figure 13. NDVI for typical year (NTY) for swamp, hardwood, and pine. Typical year shows the points (NDVI), ordered by calendar day of the year when image was collected. Each point is the mean NDVI for that day in the calendar vear.

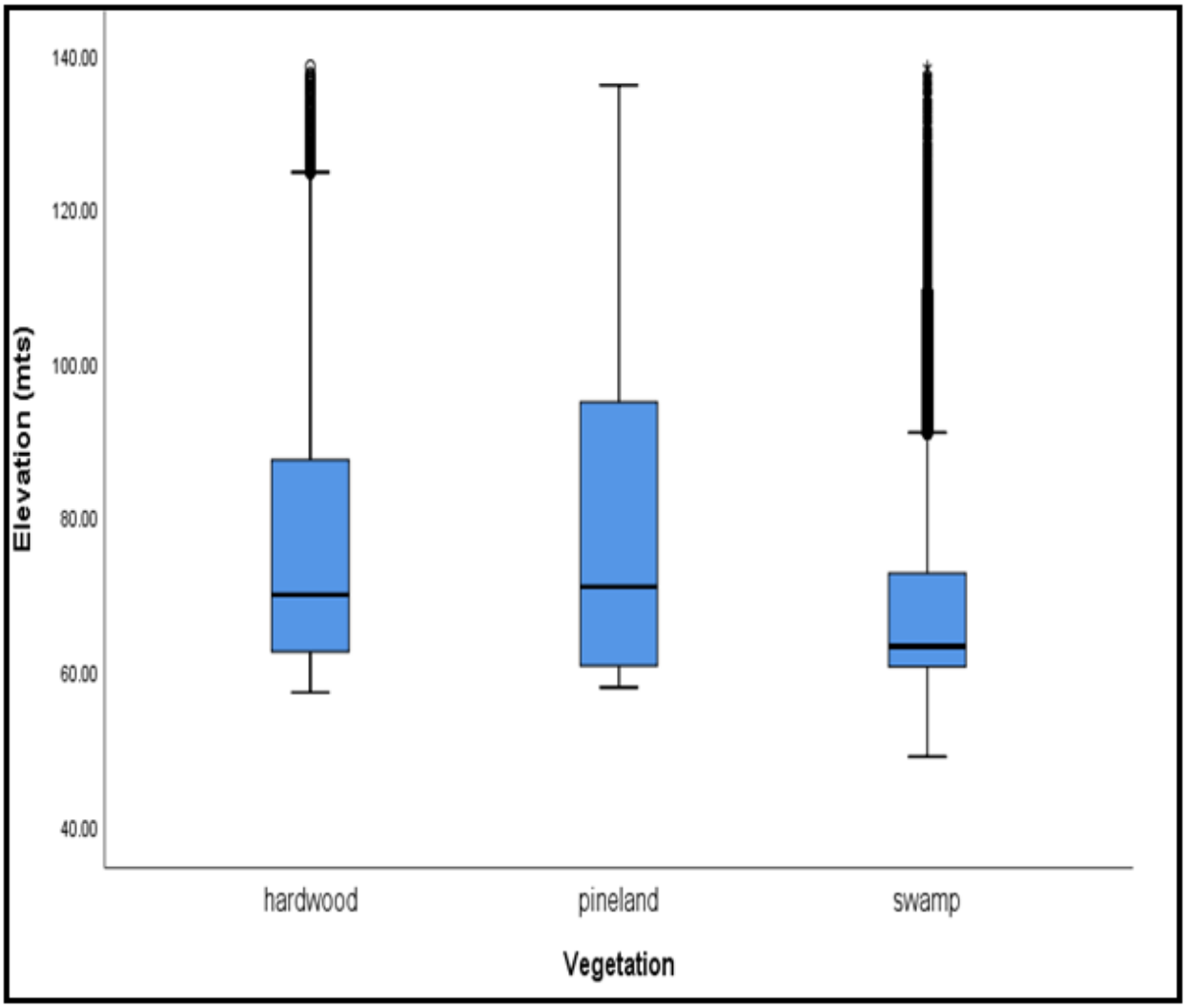

Figure 14. Box and whisker plot showing the vegetation distribution as a function of elevation.

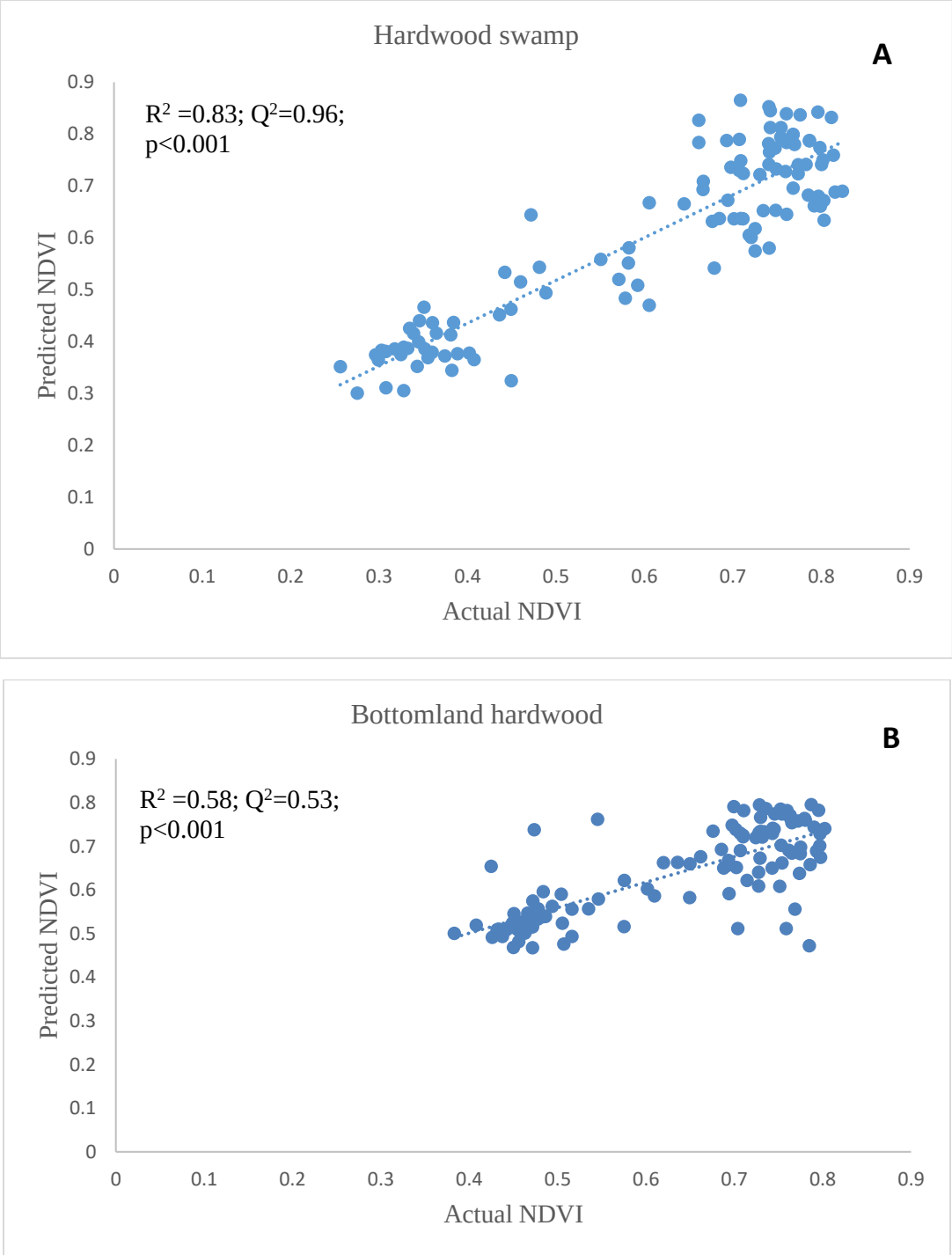

Figure 15. PLSR model outputs: A) scatter plot between Predicted NDVI and actual NDVI for Hardwood swamp. B) Scatter plot between Predicted NDVI and actual NDVI for bottomland hardwoods.

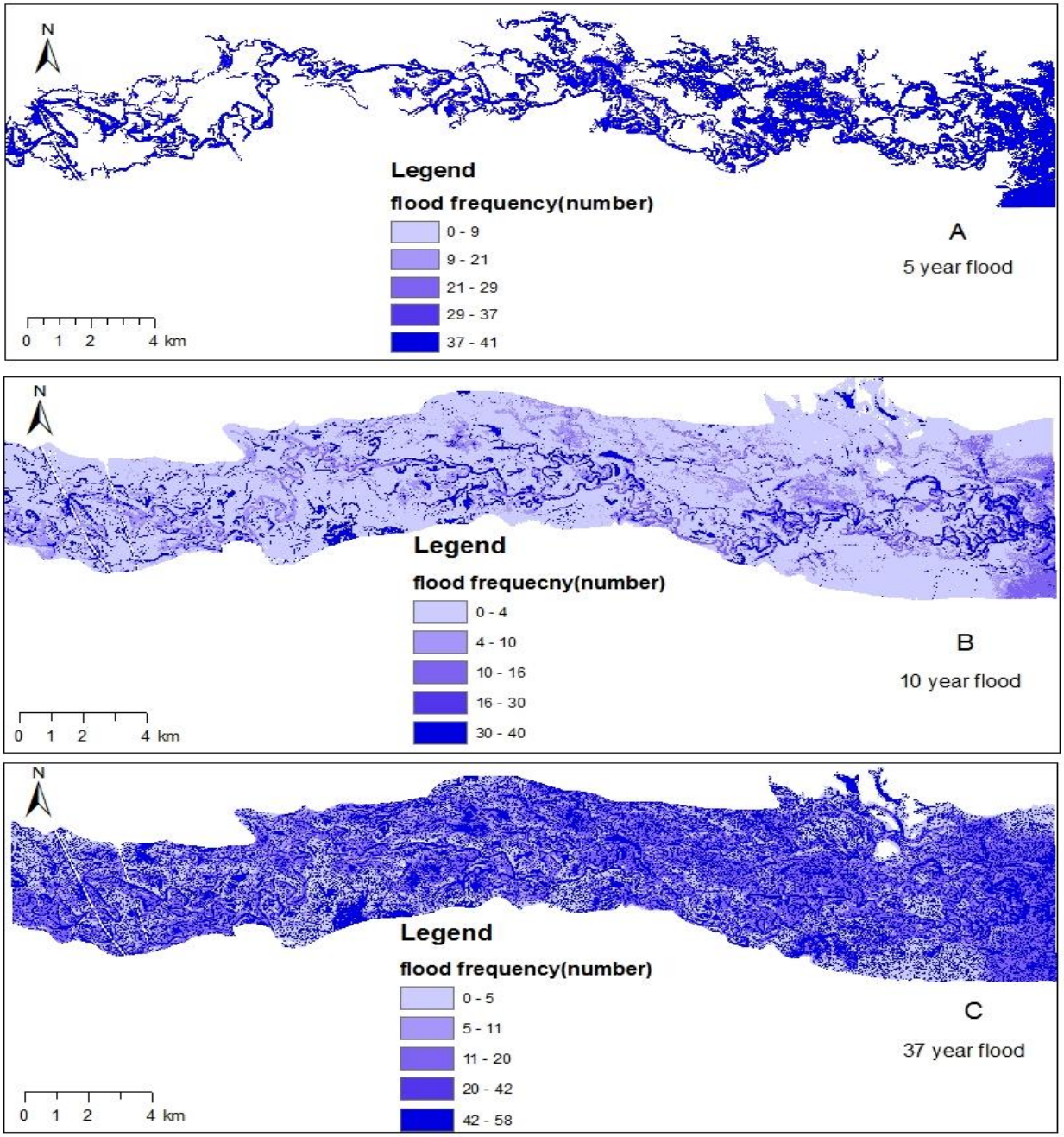

Figure 16. Flood inundation frequency maps for A) 5-year recurrence interval flood B) 10-year recurrence interval flood and C) 37- year recurrence interval flood.

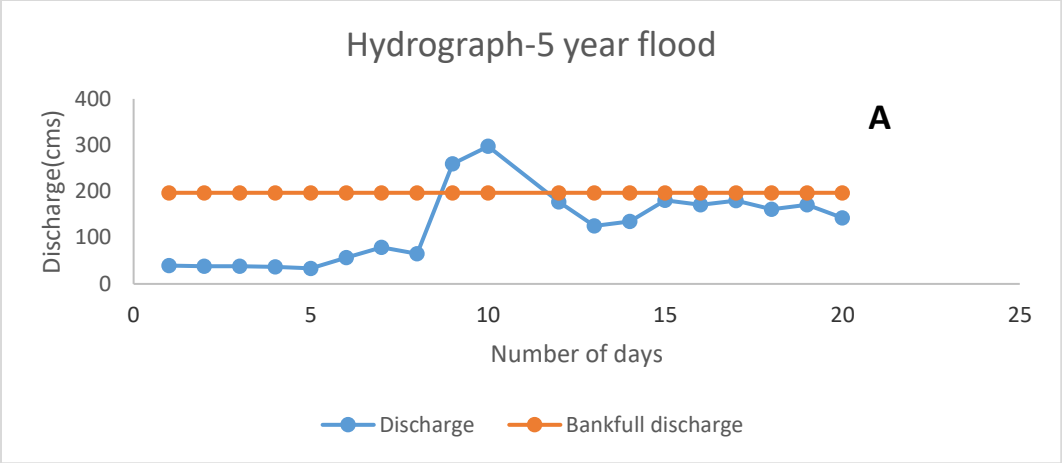

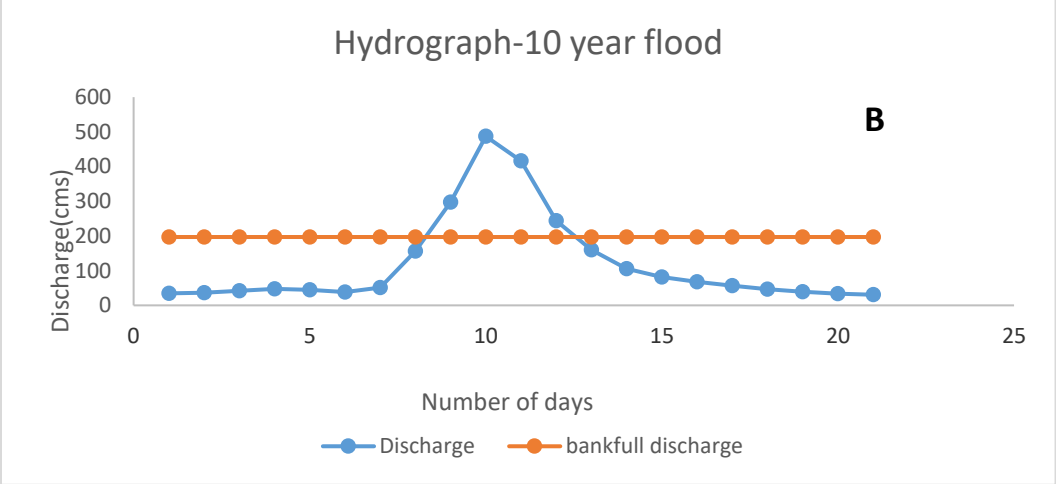

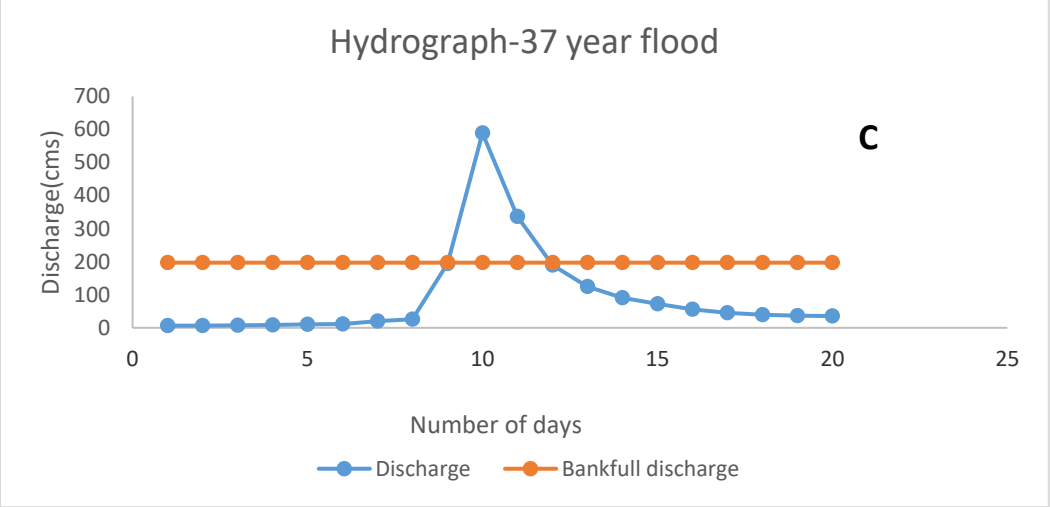

Figure 17. Hydrograph of 20 days, showing number of days that exceeds bankfull flow A) 2 days in 5-year recurrence interval flood B) 4 days in 10-year recurrence interval flood C) 2 days in 37-year recurrence interval flood.

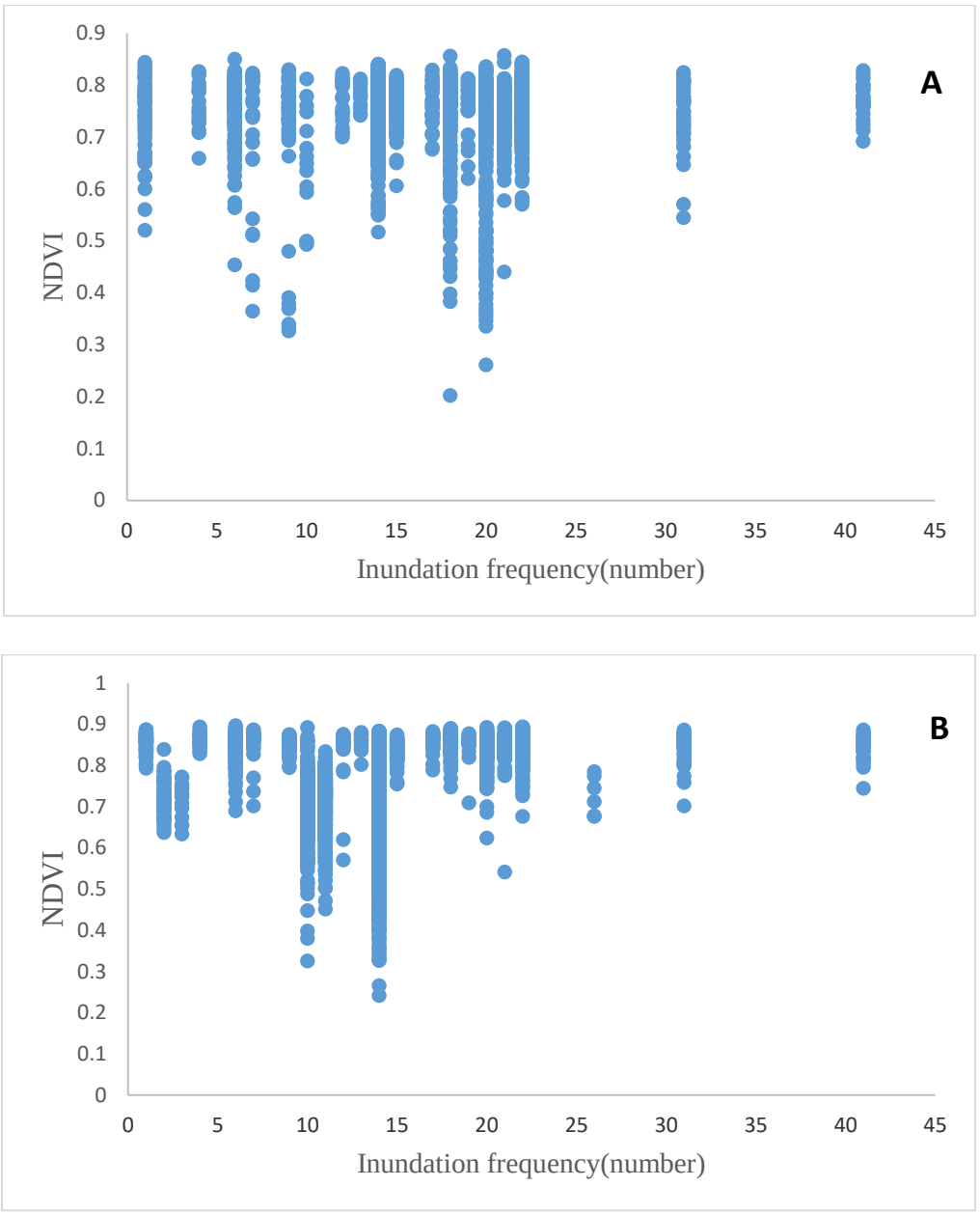

Figure 18. Scatter plot, drawn in Excel, showing no relationship between inundation frequency created by 5-year recurrence interval flood in A) Hardwood swamps and B) Bottomland hardwoods cover.

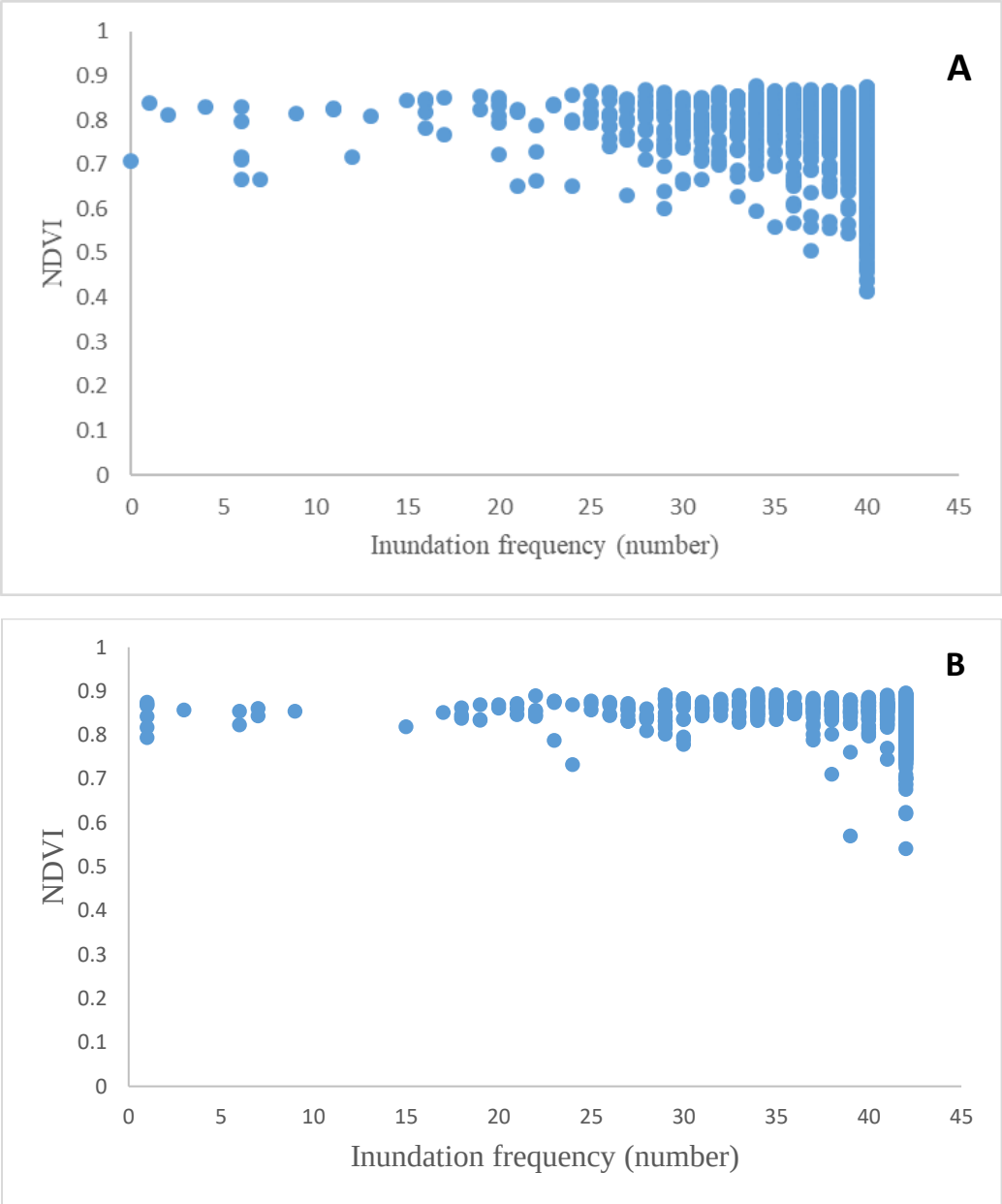

Figure 19. Scatter plot, drawn in Excel, showing no relationship between inundation frequency created by 10-year recurrence interval flood in A) Hardwood swamps and B) Bottomland hardwoods cover.

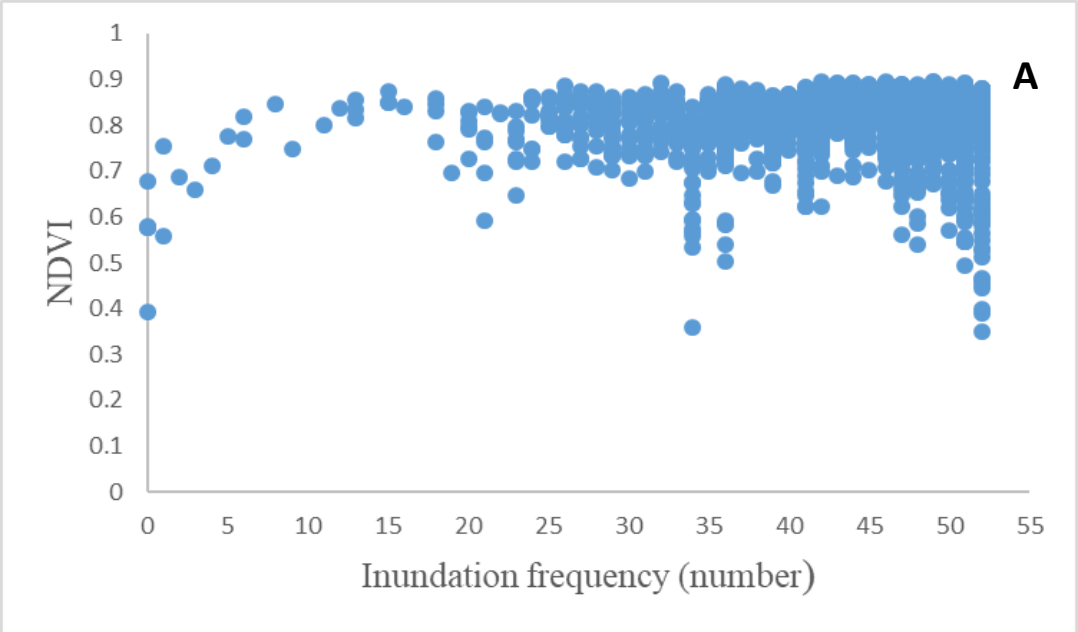

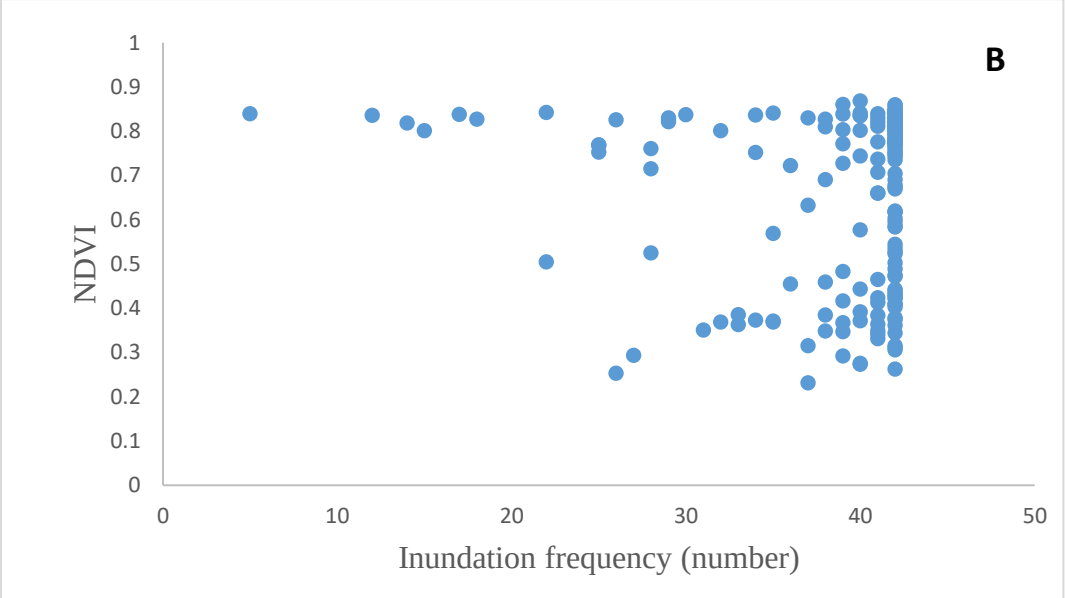

Figure 20. Scatter plot, drawn in Excel, showing no relationship between inundation frequency created by 37-year recurrence interval flood in A) Hardwood swamps and B) Bottomland hardwoods cover.